

Stability of Single layer and Two layer fluid flow past a deformable wall

**A thesis submitted
in partial fulfillment of the requirements
for the degree of
Master of Technology**

by

Lalit Kumar



**To the
Department of Chemical Engineering
Indian Institute of Technology, Kanpur
July, 2004**

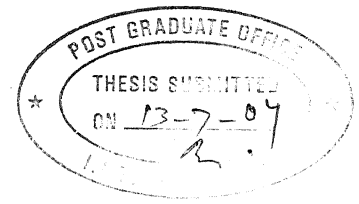
TH
CHE/2004/10
K 98 A

4 OCT 2004

मुकेशचंद्र — ज्ञान कैलकर पुस्तकालय
भारतीय प्रौद्योगिकी संस्थान कोलकोता
अवधि क्र० A...148883...



A148883



CERTIFICATE

This is to certify that the present research work entitle 'STABILITY OF SINGLE LAYER AND TWO LAYER FLUID FLOW PAST A DEFORMABLE WALL' has been carried out by Mr. Lalit Kumar under my supervision and that this has not been submitted elsewhere for a degree.

A handwritten signature in dark ink, appearing to read 'V. Shankar', written over a horizontal line.

(Dr. V. SHANKAR)

Assistant Professor,

Department of Chemical Engineering,

Indian Institute of Technology,

Kanpur-208016.

July, 2004

ACKNOWLEDGEMENT

I am deeply indebted to Dr. V. Shankar, my thesis supervisor, whose expert guidance and valuable suggestions was the prime motivation behind the successful completion of this work.

I would like to thank my lab mates Sameer, Ram Singh, Bhanu Pratap, Chetan Verma, Akhilesh and Pavan for providing help and excellent environment in the lab work.

I pay my deepest respect to all my teachers.

Finally, I am indebted to my parents and other family members for their love and tangible support and encouragement throughout my life. I would not have been able to do this research without their unshakable confidence on me.

Lalit Kumar

ABSTRACT

In this thesis, we have studied two different problems in the area of stability of fluid flow past a deformable solid. First we studied the stability of Newtonian fluid flow past a deformable wall using a combination of asymptotic and numerical methods for the case of Couette flow as well as Poiseuille flow past a deformable wall. The fluid has viscosity μ thickness R supported by a viscoelastic medium of elasticity G and viscosity μ_g and having thickness $H R$. We have shown that 'wall mode instability' predicted by the asymptotic analysis is also captured by numerical methods for both Couette flow as well as Poiseuille flow past a deformable wall. Although in Couette flow the coupling between mean flow and fluctuations is only via an additional term in the boundary condition for the tangential velocity at the interface, as compared to Poiseuille flow where other than this one extra term in Orr-Sommerfeld equation which is responsible for the coupling. Further we have shown that there exists a mode in Couette flow which has scaling as $\Gamma \sim O(Re^{-1})$, ($\Gamma = \mu U^*/GR$, $Re = U^*R\rho/\mu$) as compare to wall modes where $\Gamma \sim O(Re^{-1/3})$ and further we confirm that this mode is also present in the case of Poiseuille flow. To examine the nature of the modes, we calculated the scaling of boundary layer thickness, velocity and velocity derivatives as a function of Reynolds number (Re) for both the cases and we find that new modes are indeed inviscid modes. Further we find the boundary layer thickness as a function of Reynolds number and this also indicates that the new mode is an inviscid mode. Other than these, the distribution of the perturbation velocity field also confirms validity of our results.

The second problem we studied concerns the stability of two-layer Newtonian fluids flow past a deformable for the case of plane Couette flow. The fluids have viscosities μ_1, μ_2 thickness $\beta R, (1 - \beta) R$ and densities ρ_1, ρ_2 respectively supported by a viscoelastic medium of elasticity G and viscosity μ_g and having thickness $H R$. Here, the idea is to explore the possibility of using deformable solid layers to suppress two-fluid interfacial instability due to viscosity stratification. We have shown that deformable wall could have both stabilizing and destabilizing effect on the two-layer flow past a deformable solid wall, depending on the arrangement of the two fluids and their relative thicknesses. Further we have shown that deformable wall has an effect on long and

intermediate waves but it does not have any effect on short wave perturbations. Since short wave perturbations are confined near the interfaces, therefore there is no possibility of interference in the case of short waves. However, by ensuring sufficient interfacial tension between the two fluids, it is shown that it is possible to suppress two-fluid interfacial instabilities at all wavelengths by the deformable solid layer.

Contents

List of figure	(i)
List of Tables	(vii)
Nomenclature	(viii)
CHAPTER 1	
Introduction	1
CHAPTER 2 Single layer fluid flow past a deformable wall	
2.0 Introduction	6
2.1 Problem formulation	7
2.2 Governing equations	
2.2.1 Governing equations in Dimensional form	8
2.2.2 Governing equation in non-dimensional form	10
2.2.3 Base state calculation for both Poiseuille and Couette flow	12
2.3 Linear stability analyses	
2.3.1 General equation for linear stability analysis	13
2.3.2 Numerical method for solving characteristic equations	16
2.3.3 Validation of numerical method	18
2.4 Results and Discussions	
2.4.1 Couette flow past a deformable wall	19
2.4.2 Poiseuille flow past a deformable wall	31
2.5 Conclusion and future work	36
CHAPTER 3 Two-layer fluid flow past a deformable wall	
3.0 Introduction	38
3.1 Problem formulation	40
3.2 Governing equations	
3.2.1 Governing equations in non-Dimensional form	41
3.2.2 Base state calculation for both Poiseuille and Couette flow:	43
3.3 Linear stability analyses	
3.3.1 General equation for linear stability analysis	43
3.3.2 Numerical method for solving characteristic equations;	47

3.4 Results and discussions	
3.4.1 Numerical validation and results for Rigid channel	49
3.4.2 Asymptotic results	52
3.4.3 Fluid flow past a rigid wall is unstable and deformable wall has stabilizing effect	53
3.4.4 Fluid flow past a rigid wall is stable and deformable wall has destabilizing effect.	59
3.4.5 Neutral stability curves (Γ vs. k)	63
3.4.6 Effect of various parameters on the stability	68
3.5 Conclusion and future work	70
CHAPTER 4	
Conclusion and future work	72
Bibliography	74

List of figures

- Fig 2.1** Schematic diagram of plane Couette flow past a deformable wall. *pp7*
- Fig 2.2** Schematic diagram of plane Poiseuille flow past a deformable wall. *pp8*
- Fig.2.3** Schematic diagram of plane Couette flow past a deformable wall after applying perturbations. *pp13*
- Fig. 2.4** Schematic diagram for numerical calculation. *pp16*
- Fig. 2.5** Γ vs. Re in Couette flow past a deformable wall: Data from numerical solution for $H = 2$, $k = 0.5$, $\eta_r = 0$ for first two modes. The two dotted lines are asymptotic results. *pp18*
- Fig. 2.6** Γ vs. Re in Couette flow past a deformable wall: Data from numerical solution for $H = 1$, $k = 1$, $\eta_r = 0$ for first two modes. The two dotted lines are asymptotic results. *pp19*
- Fig.2.7** Γ vs. Re for Couette flow past a deformable wall with $H = 1$, $k = 1$, $\eta_r = 0$. *pp20*
- Fig.2.8** Γ vs. Re in case of Couette flow past a deformable wall for $H = 2$, $k = 0.5$, $\eta_r = 0$: Data from full numerical solution. *pp20*
- Fig.2.9** Γ vs. Re in case of Couette flow past a deformable wall for $H = 1$, $k = 1$, $\eta_r = 0$ from full numerical solution corresponding to second asymptotic wall mode. *pp21*

- Fig.2.10** Γ vs. Re in case of Couette flow past a deformable wall for $H = 1$, $k = 1$, $\eta_r = 0$ from full numerical solution corresponding to second asymptotic wall mode. *pp22*
- Fig.2.11** Γ vs. Re in case of plane Couette flow past a deformable wall for $H = 1$, $k = 1$, $\eta_r = 0$ for second wall mode and their extension. *pp23*
- Fig. 2.12** Variation of the absolute value of velocity field and their derivative in the fluid with Reynolds number for wall mode with $H = 1$, $k = 1$, $\eta_r = 0$. The two dotted lines are reference line with slopes $1/3$ and $2/3$. *pp24*
- Fig. 2.13** Variation of the absolute value of displacement field and their derivative in the fluid with Reynolds number for wall mode with $H = 1$, $k = 1$, $\eta_r = 0$. The three dotted lines are reference line with slopes $1/3$, $1/2$ and $1/3$. *pp25*
- Fig. 2.14** Variation of the absolute value of velocity field and their derivative in the fluid with Reynolds number for lower curve with $H = 1$, $k = 1$, $\eta_r = 0$. *pp25*
- Fig. 2.15** Variation of the absolute value of velocity field and their derivative in the fluid with Reynolds number for the lowest curve with $H = 1$, $k = 1$, $\eta_r = 0$. *pp26*
- Fig. 2.16** Variation of the absolute value of displacement field and their derivative in the fluid with Reynolds number for lower curve with $H = 1$, $k = 1$, $\eta_r = 0$. *pp26*
- Fig. 2.17** Variation of the absolute value of displacement field and their derivative in the fluid with Reynolds number for the lowest curve with $H = 1$, $k = 1$, $\eta_r = 0$. The three dotted lines in Fig 2.16 and 2.17 are reference line with slope 0. *pp27*

- Fig. 2.18** Variation of thickness of wall layer (Boundary layer) with Reynolds number for plane Couette flow with $H = 1$, $k = 1$, $\eta_r = 0$. The three dotted lines have slope $-1/3$, $-1/2$ and $-1/2$. *pp28*
- Fig. 2.19** The amplitude of velocity $|v_z|$ vs. z in case of Couette flow for $H = 2$, $k = 0.5$, $\eta_r = 0$ at Reynolds number 3000 corresponding to all the curve of mode 2. *pp29*
- Fig. 2.20** The amplitude of velocity $|v_x|$ vs z in case of Couette flow for $H = 2$, $k = 0.5$, $\eta_r = 0$ at Reynolds number 3000 corresponding to all the curve of mode 2. *pp30*
- Fig. 2.21** Gamma vs. Re in case of Poiseuille flow past a deformable wall for $H = 1$, $k = 1$, $\eta_r = 0$: Data from full numerical solution. *pp31*
- Fig. 2.22** Variation of the absolute value of velocity field and their derivative in the fluid with Reynolds number for the wall mode Poiseuille flow with $H = 1$, $k = 1$, $\eta_r = 0$. The two dotted lines in are reference line with slope $1/3$ and $2/3$. *pp32*
- Fig. 2.23** Variation of the absolute value of displacement field and their derivative in the fluid vs. Reynolds number for wall mode Poiseuille flow with $H = 1$, $k = 1$, $\eta_r = 0$. *pp33*
- Fig. 2.24** Variation of the absolute value of velocity field and their derivative in the fluid with Reynolds number for inviscid mode Poiseuille flow with $H = 1$, $k = 1$, $\eta_r = 0$. *pp33*
- Fig. 2.25** Variation of the absolute value of displacement field and their derivatives vs. Reynolds number for the inviscid mode in Poiseuille flow with $H = 1$, $k = 1$, $\eta_r = 0$. *pp34*

- Fig. 2.26** Variation of thickness of wall layer (Boundary layer) with Reynolds number for Poiseuille flow with $H = 1$, $k = 1$, $\eta_r = 0$. The two dotted lines have slope $-1/3$ and $-1/2$. *pp34*
- Fig. 2.27** The amplitude of velocity $|v_z|$ vs. z in case of Poiseuille flow for $H = 1$, $k = 1$, $\eta_r = 0$ at Reynolds number 1000. *pp35*
- Fig. 2.28** The amplitude of velocity $|v_x|$ vs. z in case of Poiseuille flow for $H = 1$, $k = 1$, $\eta_r = 0$ at Reynolds number 1000. *pp36*
- Fig. 2.29** The amplitude of velocity $|u_z|$ vs. z in case of Poiseuille flow for $H = 1$, $k = 1$, $\eta_r = 0$ at Reynolds number 1000. *pp36*
- Fig. 2.30** The amplitude of velocity $|u_x|$ vs. z in case of Poiseuille flow for $H = 1$, $k = 1$, $\eta_r = 0$ at Reynolds number 1000. *pp37*
- Fig. 3.1** Schematic diagram of two layers plane Couette flow past a deformable wall. *pp40*
- Fig. 3.2** Schematic diagram of two layers plane Couette flow past a deformable wall in perturbed state. *pp44*
- Fig. 3.3** Schematic diagram for numerical calculation. *pp47*
- Fig. 3.4** Fluid-fluid interface instability in rigid channel ($\Gamma = 0$): c_i vs. k for different values of thickness ratio β , interfacial tension $= 0$, $\mu_r = 0.5$ and $Re = 1$. *pp49*
- Fig. 3.5** Fluid-fluid interface instability in rigid channel ($\Gamma = 0$): c_r vs. k for different values of thickness ratio β , interfacial tension $= 0$, $\mu_r = 0.5$ and $Re = 1$. *pp50*

- Fig. 3.6** Fluid-fluid interface instability in rigid channel ($\Gamma = 0$): variation of with k for different value of β , interfacial tension = 0.01, $\mu_r = 0.5$, $H = 0.5$ and $Re = 1$. *pp51*
- Fig. 3.7** Fluid-fluid interface instability in rigid channel ($\Gamma = 0$): variation of c_r with k for different value of β , interfacial tension = 0.01, $\mu_r = 0.5$, $H = 0.5$ and $Re = 1$. *pp51*
- Fig. 3.8** Variation of c_i with k for different value of Γ , $\beta = 0.4$, interfacial tension = 0.0, $\mu_r = 0.5$, $H = 0.5$ and $Re = 1$. *pp54*
- Fig. 3.9** Variation of c_r with k for different value of Γ , $\beta = 0.4$, interfacial tension = 0.0, $\mu_r = 0.5$, $H = 0.5$ and $Re = 1$. *pp55*
- Fig. 3.10** Variation of c_i with k for different value of Γ , $\beta = 0.4$, interfacial tension = 0.01, $\mu_r = 0.5$, $H = 0.5$ and $Re = 1$. *pp56-57*
- Fig. 3.11** Variation of c_r with k for different value of Γ , $\beta = 0.4$, interfacial tension = 0.01, $\mu_r = 0.5$, $H = 0.5$ and $Re = 1$. *pp57*
- Fig. 3.12** Variation of c_i with k for different value of Γ , $\beta = 0.4$, interfacial tension = 0.05, $\mu_r = 0.5$, $H = 0.5$ and $Re = 1$. *pp58*
- Fig. 3.13** Variation of c_r with k for different value of Γ , $\beta = 0.4$, interfacial tension = 0.05, $\mu_r = 0.5$, $H = 0.5$ and $Re = 1$. *pp59*
- Fig. 3.14** Variation of c_i vs. k for $\Gamma = 0.0$, $\beta = 0.8$, $\mu_r = 0.5$, $H = 2.0$ and $Re = 1$. *pp60*
- Fig. 3.15** Variation of c_i vs. k for different values of Γ , $\beta = 0.8$, interfacial tension = 0.0, $\mu_r = 0.5$, $H = 2.0$ and $Re = 1$. *pp61*
- Fig. 3.16** Variation of c_i vs. k for different values of Γ , $\beta = 0.8$, interfacial tension = 0.05, $\mu_r = 0.5$, $H = 2.0$ and $Re = 1$. *pp62*

- Fig. 3.17** Neutral stability curves (Γ vs. k) for fluid-fluid interfacial mode (Model1) and Fluid- deformable wall mode (Mode 2) for parameter $\beta = 0.4$, interfacial tension = 0.00, $\mu_r = 0.5$, $H = 0.5$ and $Re = 1$. *pp63*
- Fig. 3.18** Neutral stability curves (Γ vs. k) for Model1 and Mode 2 for parameter $\beta = 0.4$, interfacial tension = 0.01, $\mu_r = 0.5$, $H = 0.5$ and $Re = 1$. *pp64*
- Fig. 3.19** Neutral stability curves (Γ vs. k) for Model1 and Mode 2 for parameter $\beta = 0.4$, interfacial tension = 0.05, $\mu_r = 0.5$, $H = 0.5$ and $Re = 1$. *pp64*
- Fig. 3.20** Neutral stability curves (Γ vs. k) for Model1 and Mode 2 for parameter $\beta = 0.4$, interfacial tension = 0.01, $\mu_r = 0.5$, $H = 4$ and $Re = 1$. *pp65*
- Fig. 3.21** Neutral stability curves (Γ vs. k) for Model1 and Mode 2 for parameter $\beta = 0.6$, interfacial tension = 0.01, $\mu_r = 2.0$, $H = 0.1$ and $Re = 1$. *pp65*
- Fig. 3.22** Neutral stability curves (Γ vs. k) for Model1 and Mode 2 for parameter $\beta = 0.2$, interfacial tension = 0.01, $\mu_r = 0.5$, $H = 0.5$ and $Re = 1$. *pp66*
- Fig. 3.23** Neutral stability curves (Γ vs. k) for Model1 and Mode 2 for parameter $\beta = 0.8$, interfacial tension = 0.01, $\mu_r = 2.0$, $H = 0.1$ and $Re = 1$. *pp66*
- Fig. 3.24** Neutral stability curves (Γ vs. k) for Model1 and Mode 2 for parameter $\beta = 0.8$, interfacial tension = 0.01, $\mu_r = 0.25$, $H = 2.0$ and $Re = 1$. *pp67*
- Fig. 3.25** Neutral stability curves (Γ vs. k) for Mode 2 for the parameter $\beta = 0.4$, interfacial tension = 0.0, $H = 5.0$ and $Re = 1$. *pp68*
- Fig. 3.26** Variation of Γ vs. k for different values of densities ratio, $\beta = 0.6$, interfacial tension = 0.01, $\mu_r = 0.5$, $H = 2.0$ and $Re = 1$. *pp69*
- Fig. 3.27** Neutral stability curves (Γ vs. k) for Mode 2 for the parameter $\beta = 0.4$, interfacial tension = 0.0, $H = 5.0$ and $Re = 1$. *pp69*

List of Tables

- Table1. Scaling of different quantities in fluid as a function of Reynolds number for $H = 1$, $k = 1$, $\eta_r = 0$. Obtained from our numerical code. *pp24*
- Table2. Scaling of different parameters in deformable wall vs Reynolds number for $H = 1$, $k = 1$, $\eta_r = 0$. *pp27*
- Table3. Scaling of different parameters in the fluid past a deformable wall with Poiseuille base velocity profile flow vs Reynolds number for $H = 1$, $k = 1$, $\eta_r = 0$. *pp35*
- Table4. Scaling of different parameters in the deformable wall with Poiseuille base velocity profile flow vs Reynolds number for $H = 1$, $k = 1$, $\eta_r = 0$. *pp35*

Nomenclature

Symbol	Description
$c = c_r + ic_i$	Complex wave speed
k	wave number
μ	Viscosity of the fluid
μ_g	Viscosity of the wall
G	Shear modulus of the solid
R	Dimensional thickness of fluid
U^*	Dimensional velocity of the top plate
H	Nondimensional thickness of the wall
γ^*	Dimensional interfacial tension
$\eta_r = \mu_g / \mu$	Ratio of Wall to fluid viscosity
$\Gamma = V\mu / (GR)$	Nondimensional velocity of top plate
$Re = \rho VR / \mu$	Reynolds number
$\gamma = \gamma^* / (\mu_1^* U^*)$	Nondimensional surface tension between fluid-fluid interface.
$\rho^{*\alpha}$	Densities of two fluids as $\alpha = 1, 2$
μ^α	Viscosities of two fluids
$\mu_r^{(1)} = \mu_1 / \mu_1 = 1$	Ratio of fluid1 to fluid 1 viscosity
$\mu_r^{(2)} = \mu_2 / \mu_1$	Ratio of fluid 2 to fluid 1 viscosity
β	Fluid thickness ratio

CHAPTER 1

1.1 Introduction

Fluid flows are ubiquitous in the technological and the natural world. Their importance and abundant use in science and technology result in a long list of areas that are used every day. Recently, one of the important areas of study in fluid mechanics is fluid flow past a deformable solid wall. The stability of fluid flow near a deformable wall is of interest in diverse applications such as marine and aerospace propulsion, biotechnology and polymer processing applications. The flow of blood and other fluids in the body takes place through deformable tubes, and the separation and purification processes in biotechnological processes often involve flow in a tube and channels made up of polymeric materials. Apart than these situations, it is also very important in polymer processing applications such as multilayer co-extrusion, where there is need to control flow in such a way that there is no possibility of mixing between the layers, so as to enhance the product quality.

From a technological viewpoint, the presence of instability has two effects: it increases the drag force and the power consumption, and it also enhances mixing and heat and mass transfer. In processes where it is advantageous to have lower drag force, the wall and fluid properties could be adjusted so that the flow is stable and remains in the laminar regime. Alternatively, in situations where greater mixing and heat or mass transfer are desirable, the fluid and wall properties could be suitably chosen to make the flow unstable. Therefore, a detailed understanding of the mechanism(s) responsible for destabilizing the flow could be used in biotechnology applications. Other than this, we know from the past studies of Yih [1967] and Hooper & Boyd [1983] that multilayer flows of Newtonian fluids are unstable even in the limit of small (but finite) Reynolds number. Thus by delaying the instability of multi-layer fluid flows at finite Reynolds number, we can reduce the mixing during multi-layer extrusion of polymers. For that purpose, we explore the possibility of using a deformable wall and we will show further in Chapter 3 that it has the ability to suppress the interfacial instability. Thus, an

understanding of the stability of flow past a deformable wall is often crucial in order to obtain the desired results.

There is a significant difference between instability criteria for the fluid flow in a rigid channel and fluid flow through deformable wall. In a rigid channel for the high Reynolds number flow, the fluid inertia plays an important role in destabilizing the flow. However, the inertial effects are absent in a low Reynolds number flow, and instabilities have to be driven by a different mechanism in this case. The low Reynolds number flow of a Newtonian fluid past a rigid surface is always stable because the Stokes equations are not explicitly dependent on time, but the flow of viscoelastic liquids could become unstable due to the time dependence of the elastic terms in the momentum equations. When a fluid flows past a deformable wall, the dynamics of elastic wall and fluid get coupled and cause an additional time dependence via the deformable wall, which causes instability at very low Reynolds number as shown in the experiment of Krindel & Silberberg [1979]. Hence an anomalous drag force is observed when the fluid velocity is increased beyond a critical value, which depends on the fluid viscosity and the wall elasticity, in addition to the usual dimensionless groups characterizing the fluid domain. The nature of the instability observed is also different in a deformable wall channel; there is a gradual increase in the drag force as the Reynolds number is increased, in the contrast to the sharp (nearly discontinuous) jump in the drag force in the rigid channel at the critical Reynolds number. In the case of two-layer fluid flow in a rigid channel, the flow is unstable even in the range of very small Reynolds number but we will show in our results in Chapter 3 that it is possible to stabilize this type of flow by making solid layer deformable.

The study of high Reynolds number flow of a fluid past a deformable wall has been motivated by the desirability of drag reduction in marine and aerospace propulsion. There have been many papers after the first significant study done by Kramer [1957, 1960]. In this thesis, we consider the stability of single layer fluid past a deformable wall at moderate and high Reynolds number, and this is an extension of the work of Kumaran, Shankar, Srivatsan and Carpenter for flow past a deformable solid wall (their works are discussed in an appropriate place). Here we briefly discuss their previous work

related to our present work. The stability of Couette flow past a deformable wall first studied by Kumaran *et.al* [1994] in the zero Reynolds number limit and they found that flow is unstable even for vanishing Reynolds number. Later this zero Reynolds number viscous mode was numerically continued to intermediate and high Reynolds number by Srivatsan and Kumaran [1997]. They found that this mode of instability is present for intermediate and high Reynolds number. Shankar and Kumaran [2002] studied Couette flow past a deformable wall, but they carried out an asymptotic analysis at high Reynolds number for wall modes. They refer the above modes as ‘wall modes’ since the vorticity for this mode is confined only in a region of thickness δ near the fluid-solid interface, here $\delta \sim O(Re^{-1/3})$ is the boundary layer thickness, which is small compared to thickness of the fluid. In that study they found that there are many modes of instability corresponding to the same class of wall modes. Further they continued the lowest mode (i.e. wall mode with the lowest numerical value of c_r) numerically to intermediate and low Reynolds number. While doing so, they found that the first wall mode is the same mode as that of Srivatsan and Kumaran who continued the low Reynolds number instability of Kumaran *et.al* [1994]. Before these studies, Kumaran [1995] predicted that inviscid mode is always stable for plane Couette flow past a deformable wall. Kumaran referred to the above modes as ‘inviscid mode’ because boundary layer thickness $\delta \sim O(Re^{-1/2})$. Apart from the study of single layer Couette flow past a deformable wall, we also study the stability of Poiseuille flow past a deformable wall in a channel in order to examine whether all the modes found in Couette flow are present in Poiseuille flow or not. This problem had not studied extensively other than the study of Davis and Carpenter [1997], but they did not discuss all class of modes. Besides that motivation, the stability of Poiseuille flow is significantly different from that of Couette flow since it has singularities at high Reynolds number, which gives rise to a critical layer, similar to Shankar and Kumaran [1999, 2000].

The other problem we intend to study in the thesis is the stability of two layer flows past a deformable wall. The first significant study had been done by Yih [1967] for the stability analysis of two-layer flow. Yih did an asymptotic analysis of the interfacial mode for long waves and shows that jump in viscosity across the interface can lead to

long wave instability, even in the low Re limit. Later Hooper and Boyd [1983] solved the linear stability problem for two-dimensional plane Couette flow. They showed that this flow is unstable for short waves, and there is no instability in the long-wave limit. The asymptotic expression for the growth rate of the interfacial mode for short wave is essentially a sum of three terms. The term associated with surface tension, which is always stabilizing. The next term depends on gravity and the ratio of the densities and third term depends on ratio of viscosities: the last term is always destabilizing if the densities are equal.

We now give an overview of the present thesis. In this thesis, we first intend to study the problem of single layer Couette as well as Poiseuille flow past a deformable wall in Chapter 2. For these problems, we would like to determine the nature of instability at intermediate and low Reynolds number corresponding to the wall modes present at high Reynolds number. Other than this, we are also interested to observe the effect of singularities present in Poiseuille flow past a deformable wall.

For the above mentioned purpose, we first wrote the governing equation for mass and momentum conservation with the required boundary conditions. Then we non-dimensionalise the governing equations by using dimensional quantities: thickness of fluid, velocity of upper plate, viscosity of the fluid and density of deformable solid wall in such that the non-dimensional velocity gradient of fluid at fluid-deformable wall interface remains same. By doing so we ensure that boundary condition and Orr-Sommerfeld equations are equally valid for Couette flow as well as Poiseuille flow. For solving Orr-Sommerfeld equation numerically we used the principle of expansion of the solution as a linear combination of orthogonal solutions. But to solve Orr-Sommerfeld equation by mentioned method we need to know sufficiently close initial guess. Thus we perform asymptotic analysis for high Reynolds number limit and the results of asymptotic analysis we used as an initial guess in the numerical code. First of all we calculated and presented the result of Shankar and Kumaran [2002] at high Reynolds number to verify the code. Further we calculated neutral stability curve and found a new mode. After examination of velocity field for the fluid, displacement field for deformable wall and scaling of all the quantities for the fluid as well as deformable wall. We concluded that this new mode is

nothing other than inviscid mode. Finally we tried for Poiseuille flow and found that all modes those are present in Couette flow is also in Poiseuille flow.

Then further we studied the stability of two-layer Newtonian fluids past a deformable wall in Chapter 3. For this problem we are first looking for constant density ratio equal to one and further we will show the effect on density difference on the stability. Hence out of the three terms (mentioned above) for short wave as shown by Hooper and Boyd only first and third are valid for equal fluid densities as mentioned by Joseph and Renardy [1993]. The case of equal densities of the fluid there exist some rules of thumb, which tells that we can stabilize long waves by placing the less viscous fluid in a thin layer, and stabilize the short waves by ensuring sufficiently high surface tension.

In present study our aim is to show that:

- I. Two layer flows past a rigid wall is unstable and it is possible to stabilize with the help of deformable wall,
- II. Two layer flow past a rigid wall is stable and it is possible to destabilize the flow with help of deformable wall and finally,
- III. Effect of various parameters on the stability of our system of flows.

For this analysis all the governing equation, non-dimensionalisation and numerical methods are same as in Chapter 2. But here we perform long wave and low Reynolds number asymptotic analysis as compare to high Reynolds number asymptotic analysis for single layer flow to find initial guess of numerical code. To check to validity of numerical code we recaptured the results for rigid wall case. Then first, we discuss the case where fluid flow in rigid channel is unstable ($\mu_r > 1$ & $\beta > 1/2$ or $\mu_r < 1$ & $\beta < 1/2$) and deformable wall has stabilizing effect on the flow. Again we discuss the case where fluid flow in a rigid channel is stable ($\mu_r > 1$ & $\beta < 1/2$ or $\mu_r < 1$ & $\beta < 1/2$) and deformable wall has destabilizing effect on the system of flow. Although from above cases we are able to know that deformable wall has stabilizing as well as destabilizing ability. But to calculate the range of elastic properties of deformable wall we need to know the neutral stability curve between gamma ($\Gamma = \mu U^*/G R$) vs. k . Thus we plotted neutral stability curve for both the above cases. In this Chapter we finally discuss the effect of various quantities on the stability of two-layer fluid flow.

CHAPTER 2

Linear stability analysis of high Reynolds number Poiseuille flow and Couette flow past a deformable wall.

2.0 Introduction

We first started with an asymptotic analysis in the limit of high Reynolds number to find the instability for Couette flow past a deformable wall, which is equally valid for Poiseuille flow. This is because, for both the cases non-dimensionalisation had been done in such a way that velocity gradients are same near the wall (V. Shankar, personal communication). The stability of Couette flow past a deformable wall first studied by Kumaran *et.al* (1994) for zero Reynolds number limit and they found that flow is unstable even for vanishing Reynolds number. Later this, zero Reynolds number viscous mode was numerically continued to intermediate and high Reynolds number by Srivatsan and Kumaran (1997). They found that this mode of instability is present for intermediate and high Reynolds number. Shankar and Kumaran (2002) studied Couette flow past a deformable wall, but this time they did asymptotic analysis at high Reynolds number for wall modes. They refer the above modes as wall modes since the vorticity for this mode is confined only in a region of thickness δ . Here $\delta \sim O(Re^{-1/3})$ is the boundary layer thickness, which is small compared to thickness of the fluid and is confined near the fluid-solid interface. In that study they found that there are many modes of instability corresponding to the same class of wall modes. Further they continued the lowest mode (i.e. wall mode with the lowest numerical value of c_r) numerically to intermediate and low Reynolds number. While doing so, they found that first wall mode is the same mode as that of Srivatsan and Kumaran when they continued the low Reynolds number instability of Kumaran *et.al* (1994). Before these studies, Kumaran (1995) predicted that inviscid mode is always stable for plane Couette flow past a deformable wall. They called above modes inviscid mode because boundary layer thickness $\delta \sim O(Re^{-1/2})$.

In this present study, our first aim is to know the nature of neutral stability curves at intermediate as well as low Reynolds number corresponding to wall modes for Couette flow. Then further we intend to study the effect of base velocity profile on the Couette

flow stability modes by changing base velocity profile to Poiseuille flow. Further we would like to check critical layer thickness as suggested by Orr-Sommerfeld equation since second derivative in the case of Poiseuille base velocity profile is non zero, which reveals the possibility of critical layer singularity at high Reynolds number. Finally, we would like to explain nature and causes of the entire class of modes those are present in above plane Couette and Poiseuille flow past a deformable wall. Besides these things, it is important to study Poiseuille flow past a deformable wall in a channel on its own right. Since there is little information available in literature, mainly by Davis and Carpenter (1997) but they did not study the problem extensively.

2.1 Problem formulation

The problem consists of fluid layer of thickness R with base velocity profile as plane Couette and Poiseuille flow, base is supported by a viscoelastic solid of thickness H and upper layer is bounded by a rigid wall. The fluid is assumed to be an incompressible, Newtonian fluid with constant viscosity and interfacial tension. Here our aim is to examine the wall mode instability for plane Couette and Poiseuille channel flow and to determine the effect of base velocity profile on wall mode instability. Although we examine instability for both viscous and inviscid limit, we extend our solution to moderate Reynolds number using a numerical method with the asymptotic solution as initial guess. Governing equations for both fluid and viscoelastic solid for mass and momentum transfer in the bulk phases are the continuity equations and the Navier-Stokes equation.

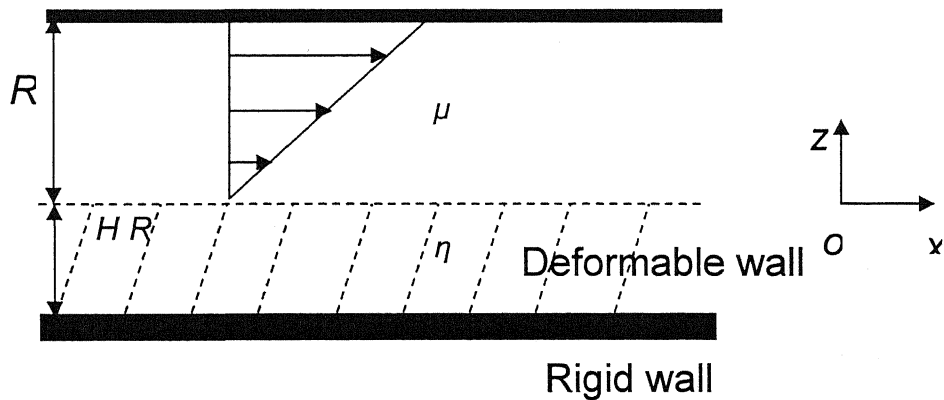


Fig 2.1 Schematic diagram of plane Couette flow past a deformable wall

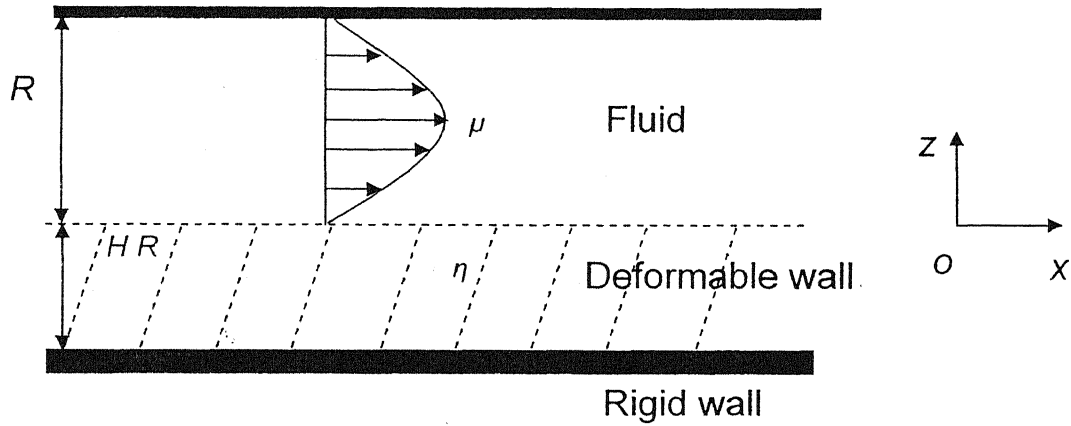


Fig 2.2 Schematic diagram of plane Poiseuille flow past a deformable wall

2.2 Governing equations

2.2.1 Governing equations in Dimensional form

This system consists of a single layer of fluid flowing past deformable solid as shown in Fig 2.1 and 2.2. The governing mass and momentum conservation equations with required boundary conditions can be written as follows.

Mass balance for fluid:

$$\partial_i v_i = 0, \quad (2.1)$$

Mass balance for deformable wall:

$$\partial_i u_i = 0, \quad (2.2)$$

The indices $i, j = x$ and z .

The momentum balances in the fluid and in the deformable wall are given by:

$$\rho(\partial_t + v_j \partial_j) v_i = -\partial_i p + \mu \partial_j^2 v_i, \quad (2.3)$$

$$\rho(\partial_t^2 u_i) = -\partial_i p_g + (G + \mu_g \partial_i) \partial_j^2 u_i. \quad (2.4)$$

Here we have assumed the density of both fluid and deformable wall to be the same for the sake of simplicity. Here repeated indices are summed over and single index means component of a vector. Here v , u , p_f and p_g represents velocity of fluid, deformation in viscoelastic wall, pressure inside fluid and pressure inside deformable wall respectively, ρ , μ , μ_g and G represents density of fluid and deformable wall, viscosity of fluid, viscosity and coefficient of elasticity of the deformable wall respectively.

Now for solving equations from 2.1 to 2.4 we need boundary conditions at upper wall and deformable wall-solid interface and matching conditions at fluid-deformable wall interface.

The no slip condition at rigid solid and fluid interface is (at $z = R$):

$$v_x = 0, \quad (2.5)$$

The impermeability condition at the solid surface is (at $z = R$):

$$v_z = 0, \quad (2.6)$$

The tangential and normal velocity balance at fluid-deformable wall interface:

$$v_x = \partial_t u_x, \quad (2.7)$$

$$v_z = \partial_t u_z, \quad (2.8)$$

The shear stress balance at fluid-deformable wall interface can be given as:

$$t_i T_{ij} n_j = t_i \sigma_{ij} n_j, \quad (2.9)$$

The normal stress balance at fluid-deformable wall interface can be given as:

$$n_i T_{ij} n_j = n_i \sigma_{ij} n_j, \quad (2.10)$$

The no slip condition at rigid solid surface is (at $z = -H R$):

$$u_x = 0, \quad (2.11)$$

The impermeability condition at solid surface is (at $z = -H R$):

$$u_z = 0, \quad (2.12)$$

For fluid stress can be represented written as:

$$T_{ij} = -p_f \delta_{ij} + \mu (\partial_i v_j + \partial_j v_i),$$

For deformable wall stress can be represented written as

$$\sigma_{ij} = -p_g \delta_{ij} + (G + \mu_g \partial_t) (\partial_i u_j + \partial_j u_i).$$

The dimensional stress ' σ_{ij} ' consists term ' $G (\partial_i u_j + \partial_j u_i)$ ' the elastic stress due to the strain in an incompressible deformable wall and the terms ' $\mu_g \partial_t (\partial_i u_j + \partial_j u_i)$ ' is the viscous stress due to the gradients in the velocity in deformable wall.

2.2.2 Governing equation in non-dimensional form

Before starting non-dimensionalisation we want to mention that in above section namely in 2.1 even though we did not put * anywhere, all the expressions represents dimensional quantities. But in this section dimensional quantities are represented by * superscript and non-dimensional quantities are represented without * superscript. The dimensional equations from 2.1 to 2.12 can be non-dimensionalised by using the following expressions:

$$\begin{aligned} x &= x^*/R, & z &= z^*/R, \\ t &= t^* U^*/R, \\ v &= v^*/U^*, & \mu_r &= \mu_g/\mu, \\ P &= P^*/(\mu U^*/R), & \Gamma &= \mu U^*/GR, \\ Re &= U^* R \rho / \mu, & \Sigma &= \rho G R^2 / \mu^2, \\ T_{ij} &= T_{ij}^*/(\mu U^*/R), & \sigma_{ij} &= \sigma_{ij}^*/(\mu U^*/R). \end{aligned}$$

Where x , z , t and v has obvious meanings as mentioned above. Here we represent dimensional velocity ' U^* ' for non-dimensionalisation of other quantities. Where $U^* = v_{max}$ for Couette flow and $U^* = 4v_{max}$ for Poiseuille flow. We choose above method for non-dimensionalisation velocity in order to keep the non dimensional gradient of velocity at the interface of fluid and deformable wall to be the same for both flows. Here v_{max} represents maximum velocity for the case of Couette flow as well as Poiseuille flow, Γ is the non-dimensional strain rate and Re represents Reynolds number.

Thus non-dimensional equations corresponding to equations 2.1 to 2.12 can be written as follows.

Mass balance for fluid:

$$\partial_i v_i = 0, \quad (2.13)$$

Mass balance for deformable wall:

$$\partial_i u_i = 0, \quad (2.14)$$

Momentum balance for fluid and deformable wall can be written as:

$$\text{Re} (\partial_i + v_j \partial_j) v_i = -\partial_i P_f + \partial_j^2 v_i. \quad (2.15)$$

$$\text{Re} (\partial^2 u_i) = -P_g \delta_{ij} + \left(\frac{1}{\Gamma} + \mu_r \partial_i \right) \partial_j^2 u_i. \quad (2.16)$$

The no slip condition at rigid solid and fluid interface is (at $z=1$):

$$v_x = 0, \quad (2.17)$$

The impermeability condition at the solid surface is (at $z=1$):

$$v_z = 0, \quad (2.18)$$

The tangential and normal velocity balance at the fluid-deformable wall interface:

$$v_x = \partial_i u_x, \quad (2.19)$$

$$v_z = \partial_i u_z, \quad (2.20)$$

The shear stress balance at fluid- deformable wall interface:

$$t_i T_{ij} n_j = t_i \sigma_{ij} n_j, \quad (2.21)$$

The normal stress balance at fluid- deformable wall interface:

$$n_i T_{ij} n_j = n_i \sigma_{ij} n_j, \quad (2.22)$$

The no slip condition at rigid solid surface is (at $z=-H$):

$$u_x = 0, \quad (2.23)$$

The impermeability condition at solid surface is (at $z = -H$):

$$u_z = 0, \quad (2.24)$$

Non-dimensional stresses in liquid and deformable wall can be given respectively as follows:

$$T_{ij} = -p_f \delta_{ij} + (\partial_i v_j + \partial_j v_i),$$

$$\sigma_{ij} = -\partial_i p_g + \left(\frac{1}{\Gamma} + \mu_r \partial_i\right)(\partial_j u_i + \partial_i u_j).$$

2.2.3 Base state calculation for both Poiseuille and Couette flow

After solving two-dimensional Navier-Stokes equation in non-dimensional form for fig.

2.1 we are able to get base velocity profile as follows:

$$\bar{v}_x = z,$$

$$\bar{v}_z = 0,$$

Base state deformation for the deformable solid in non-dimensional form is:

$$\bar{u}_x = \Gamma (z + H),$$

$$\bar{u}_z = 0.$$

After solving two-dimensional Navier-Stoke equation in non-dimensional form for fig.

2.2 we are able to get base velocity profile as follows:

$$\bar{v}_x = z (1-z),$$

$$\bar{v}_z = 0,$$

Base state deformation for the deformable solid in non-dimensional form is:

$$\bar{u}_x = \Gamma (z + H), \quad \bar{u}_z = 0.$$

2.3 Linear stability analyses

2.3.1 General equation for linear stability analysis

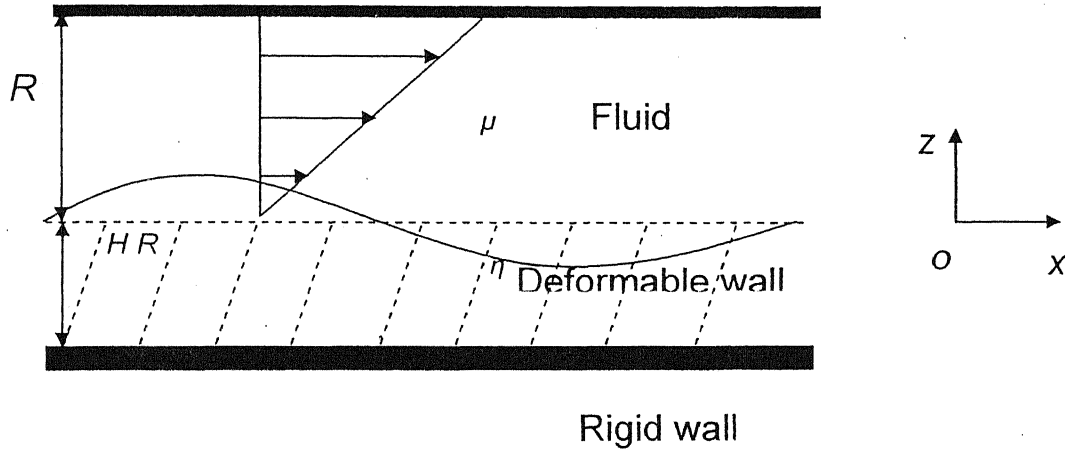


Fig 2.3 Schematic diagram of plane Couette flow past a deformable wall with perturbation.

Linear stability analysis predicts the length scale and the sufficient condition for instability. The objective of this analysis is to determine the stability of the fluid motion by applying infinitesimal perturbations to basic laminar flows. For simplicity we assume two-dimensional perturbations.

The base states for Couette flow as well as Poiseuille flow are given in section 2.2.3. So now we add perturbations to the base profiles to find instability of flow.

Thus perturbed quantities can be represented as follows;

$$[v_x - \bar{v}_x, v_z - \bar{v}_z, u - \bar{u}, p_f - p_0, p_g - p_0] = [\tilde{v}_x, \tilde{v}_z, \tilde{u}, \tilde{p}_f, \tilde{p}_g] \exp\{ik(x - ct)\}.$$

Where, c and k are the growth velocity and the wave number of the instability respectively and base state condition is given in section 2.2.3.

Applying this perturbation state to equation 2.13 to 2.24 and equating linear term on both the sides, we obtain:

$$d_z \tilde{v}_z + ik \tilde{v}_x = 0, \quad (2.25)$$

$$\text{Re}\{ik(\bar{v}_x - c)\tilde{v}_x + (d_z^2 \bar{v}_x)\tilde{v}_z\} = -ik\tilde{P}_f + [d_z^2 - k^2]\tilde{v}_x, \quad (2.26)$$

$$\text{Re}\{ik(\bar{v}_x - c)\tilde{v}_z\} = -d_z^2 \tilde{P}_f + [d_z^2 - k^2]\tilde{v}_z. \quad (2.27)$$

For deformable wall continuity equation, x and z component momentum balance for perturbed states are respectively:

$$d_z \tilde{u}_z + ik\tilde{u}_x = 0, \quad (2.28)$$

$$-\text{Re } k^2 c^2 \tilde{u}_x = -ik\tilde{p}_g + \left(\frac{1}{\Gamma} - \eta_r\right) ikc [d_z^2 - k^2] \tilde{u}_x, \quad (2.29)$$

$$-\text{Re } k^2 c^2 \tilde{u}_z = -d_z^2 \tilde{p}_g + \left(\frac{1}{\Gamma} - \eta_r\right) Ikc [d_z^2 - k^2] \tilde{u}_z. \quad (2.30)$$

After combining above equations 2.25 to 2.27 for fluid and 2.28 to 2.30 for deformable wall we get a standard equation, which is known as Orr- Sommerfeld equation for fluid and deformable wall respectively.

For deformable wall:

$$-\text{Re } k^2 c^2 [d_z^2 - k^2] \tilde{u}_z = \left(\frac{1}{\Gamma} - \eta_r\right) ikc [d_z^2 - k^2]^2 \tilde{u}_z, \quad (2.31)$$

$$\tilde{p}_g = (1/(ik)) \{ \text{Re } k^2 c^2 \tilde{u}_x + \left(\frac{1}{\Gamma} - \eta_r\right) ikc [d_z^2 - k^2] \tilde{u}_x \}. \quad (2.32)$$

For fluid:

$$\text{Re } ik \{ (\bar{v}_x - c) [d_z^2 - k^2] + (d_z^2 \bar{v}_x) \} \tilde{v}_z = [d_z^2 - k^2]^2 \tilde{v}_z, \quad (2.33)$$

$$\tilde{p}_f = (1/(ik)) \{ -\text{Re}\{ik(\bar{v}_x - c)\tilde{v}_x + (d_z^2 \bar{v}_x)\tilde{v}_z\} + [d_z^2 - k^2]\tilde{v}_x \}. \quad (2.34)$$

Boundary conditions for both Couette flow as well as Poiseuille flow in term of perturbed quantities are given below:

At fluid solid interface (at $z = 1$):

$$\tilde{v}_z = 0, \quad (2.35)$$

$$\tilde{v}_x = 0, \quad (2.36)$$

At fluid-deformable wall interface (at $z = 0$):

For Couette flow $\bar{v}_x = z$ and for Poiseuille flow $\bar{v}_x = z(1-z)$, the second term of left hand side of the tangential velocity condition given below is obtained by linearizing the x -component interface velocity about the unperturbed interface at $z = 0$:

$$\tilde{v}_z = -ikc\tilde{u}_z, \quad (2.37)$$

$$\tilde{v}_x + (d_z \bar{v}_x)_{z=0} \tilde{u}_z = -ikc\tilde{u}_x, \quad (2.38)$$

$$\tilde{T}_{xz} = \tilde{\sigma}_{xz}, \quad (2.39)$$

$$\tilde{T}_{zz} = \tilde{\sigma}_{zz}, \quad (2.40)$$

Here,

$$\tilde{T}_{xz} = d_z \tilde{v}_x + ik\tilde{v}_z,$$

$$\tilde{T}_{zz} = -\tilde{p}_f + 2 d_z \tilde{v}_x,$$

$$\tilde{\sigma}_{zz} = -\tilde{p}_g + 2 \left(\frac{1}{\Gamma} - \eta_r ikc \right) d_z \tilde{u}_z,$$

$$\tilde{\sigma}_{xz} = \left(\frac{1}{\Gamma} - \eta_r ikc \right) [d_z \tilde{u}_x + ik\tilde{u}_z],$$

At rigid solid-deformable wall interface ($z = -H$):

$$\tilde{u}_z = 0, \quad (2.43)$$

$$\tilde{u}_x = 0. \quad (2.44)$$

We solve above equations using a combination of asymptotic and numerical methods. First we would like to do the asymptotic analysis for high Reynolds number (Re) and then we will continue asymptotic results to moderate values of Re using numerical technique.

2.3.2 Numerical method for solving characteristic equations

There are many methods by which Orr-Sommerfeld equation can be solved but the stiffness of the equation at high Reynolds number requires extra care in the solution. The main aim of the numerical solutions for a given basic flow are (1) to find the curve for marginal stability ($c_i = 0$) and the curve of constant growth rate, (2) to find the eigenvalue spectrum for a given pair of positive values of c_i and Re , and (3) to calculate the associated eigenfunctions.

There are three accurate methods to solve Orr-Sommerfeld equation those are Spectral expansion, i.e. expansion of solution as a linear combination of a complete set of orthogonal functions, use of finite differences to integrate the Orr-Sommerfeld equation as initial value problem whereby integration is from one boundary towards the other. We use the principle of expansion of the solution as a linear combination of orthogonal solutions to the governing stability equation which is simple to use as well as accurate.

In our case, we have fourth order ordinary differential equation for both fluid and deformable wall as given in equations 2.33 and 2.35. Hence to know the complete solution of fourth order ODE we must know functional value and their first, second and 3rd derivative. This means we need to choose four orthogonal functions and hence four constants to write general combination of those four functions.

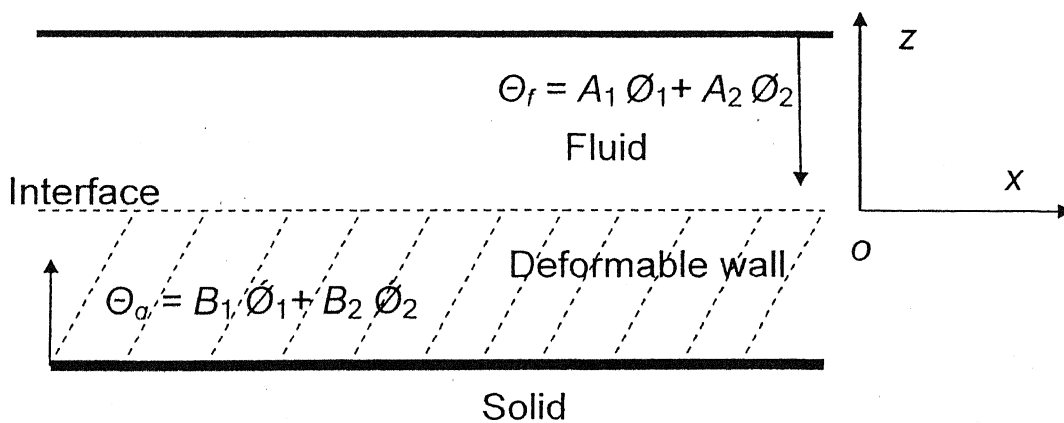


Fig. 2.4 Schematic diagram for numerical calculation

However the boundary conditions at both the rigid walls allow us to take only two orthogonal functions satisfying two given boundary conditions 2.37 and 2.38 at upper rigid wall and conditions 2.43 and 2.44 at lower rigid wall. Thus we need only two constants to write solution set for velocity of fluid and two constants for the deformation field. After that we used fourth order adaptive Runge Kutta as an integrator and marching from the rigid surface to interface of the fluid and deformable wall. We have four interface conditions 2.39, 2.40, 2.41 and 2.42, and after applying interface conditions we are able to get four linear homogenous equations with four constants. As we know for getting non-trivial solutions (i. e. non-zero value of A_1 , A_2 , B_1 and B_2) of homogenous equations, determinant of the coefficient matrix must be zero. Hence by setting determinant equal to zero, we obtained the characteristic equation. This was solved numerically using Newton-Raphson, iteration technique. We used the programming language 'C' for developing code. To compute numerical we must have to know sufficiently close initial guesses and for that we used asymptotic results for high Re (V. Shankar personal communication).

Mathematically the above procedure can be represented as follows:

According to the mentioned procedure two independent orthogonal solutions for the velocity field of fluid consistent with the BC at $z = 1$, can be written as:

$$\begin{array}{llll} \tilde{v}_z = 0 & d_z \tilde{v}_z = 0 & d_z^2 \tilde{v}_z = 1 & d_z^3 \tilde{v}_z = 0 \\ \tilde{v}_z' = 0 & d_z \tilde{v}_z = 0 & d_z^2 \tilde{v}_z = 0 & d_z^3 \tilde{v}_z = 1. \end{array}$$

The velocity field is a linear combination of these two solutions. We can write solutions set in combined form as $\Theta = \{\tilde{v}_z, d_z \tilde{v}_z, d_z^2 \tilde{v}_z, d_z^3 \tilde{v}_z\}$ where $\Theta_1 = \{0, 0, 1, 0\}$ and $\Theta_2 = \{0, 0, 0, 1\}$. Similarly for deformable wall the displacement fields at $z = -H$, consistent with the BC at $z = -H$:

$$\begin{array}{llll} \tilde{u}_z = 0 & d_z \tilde{u}_z = 0 & d_z^2 \tilde{u}_z = 1 & d_z^3 \tilde{u}_z = 0 \\ \tilde{u}_z = 0 & d_z \tilde{u}_z = 0 & d_z^2 \tilde{u}_z = 0 & d_z^3 \tilde{u}_z = 1. \end{array}$$

Here $\mathcal{O}_1 = \{0, 0, 1, 0\}$ and $\mathcal{O}_2 = \{0, 0, 0, 1\}$ and by using matching condition at the interface of fluid and deformable wall, we will be able to get the characteristic equation, which has all the information about the stability of the system of interest.

2.3.3 Validation of numerical method

To check the validity of numerical solution we compare our numerical results with the result of [1999] Kumaran for low Reynolds number flow past a deformable wall and Shankar and Kumaran's wall mode numerical results and asymptotic results. Although our code matches with both the results, I have shown comparison only with Shankar and Kumaran's wall mode results.

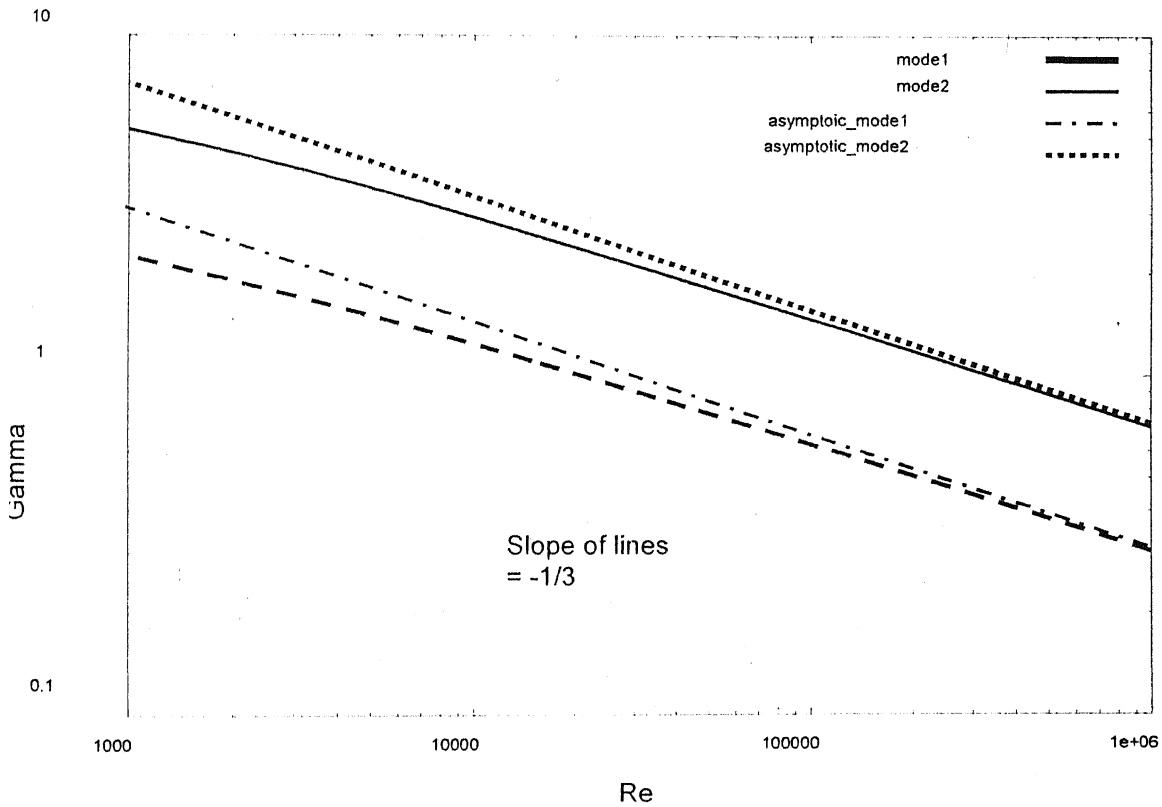


Fig. 2.5 Γ vs. Re in Couette flow past a deformable wall: Data from numerical solution for $H = 2$, $k = 0.5$, $\eta_r = 0$ for first two modes. The two dotted lines are asymptotic results.

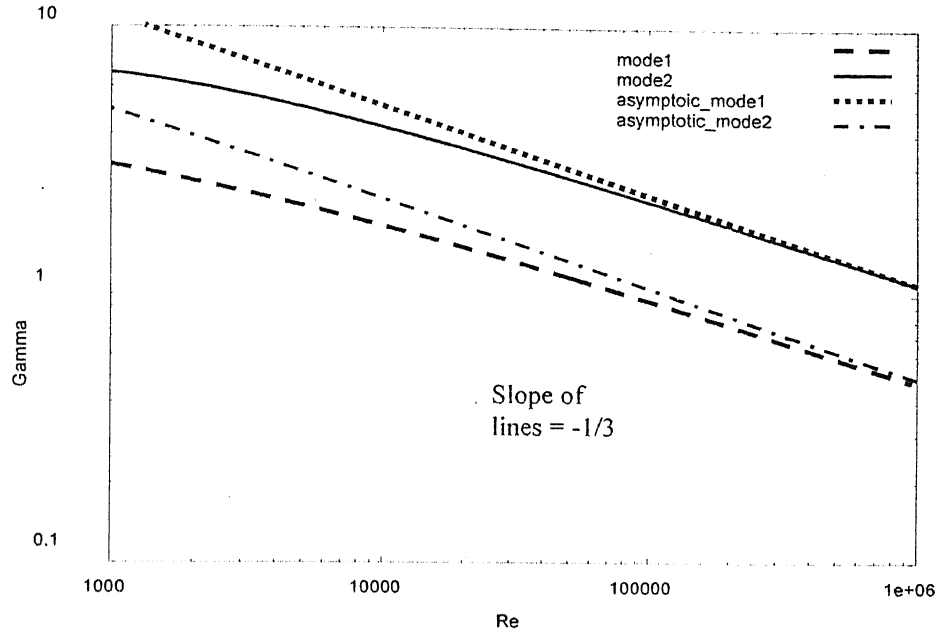


Fig. 2.6 Γ vs. Re in Couette flow past a deformable wall: Data from numerical solution for $H = 1$, $k = 1$, $\eta_r = 0$ for first two modes. The two dotted lines are asymptotic results.

24 Results and Discussions

24.1 Couette flow past a deformable wall

The transition strain rate at which the perturbations become neutrally stable ($c_i = 0$) depends on the wave number k , the wall thickness H , the viscosities ratio η_r and Reynolds number Re . In this section, the behavior of the transition strain rate at $\eta_r = 0$ is analyzed. We already mentioned in introduction that there are several neutral modes in wall mode asymptotic analysis. Hence the corresponding numerical solution also has those modes. Out of that, first mode is viscous mode same as presented by Srivatsan and Kumaran, (1997) with slope $-1/3$ at high Reynolds number; it also gives the results presented by Kumaran (1994) at low Reynolds number. But when we continue the second wall mode, it first has slope $-1/3$, which is expected since it is continuation of wall mode. But at lower Reynolds number it turns back with slope -1 and it continues to intermediate as well as high Reynolds number. This can be observed clearly in Fig. 2.7 and Fig. 2.8.

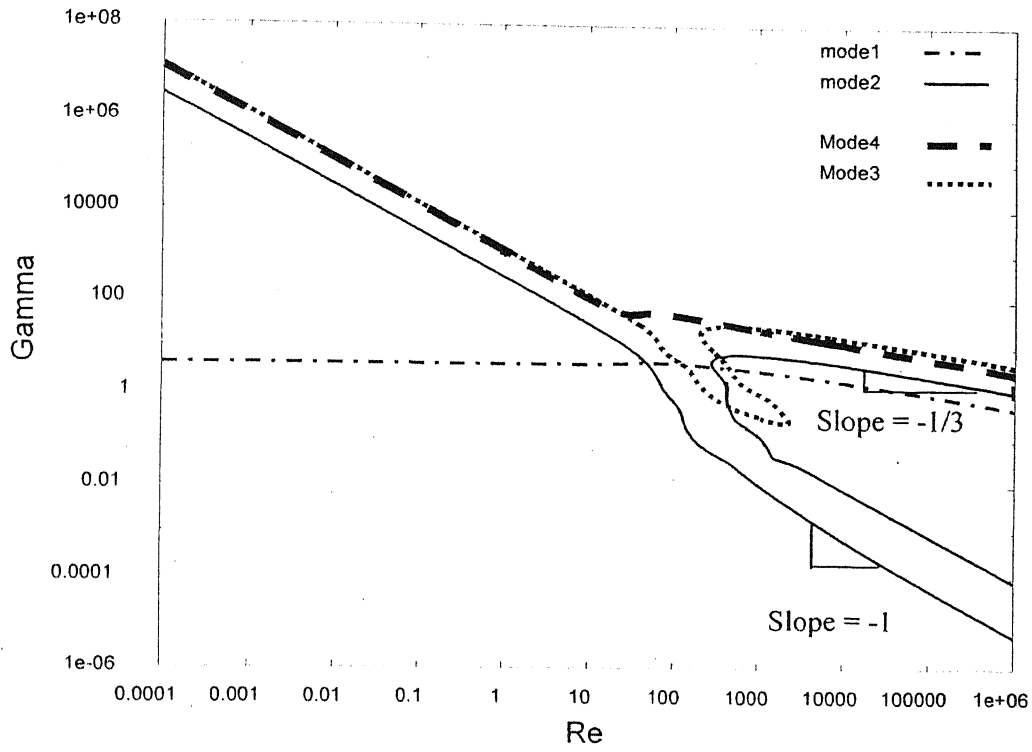


Fig.7 Γ vs. Re for Couette flow past a deformable wall with $H=1$, $k=1$, $\eta_r=0$.

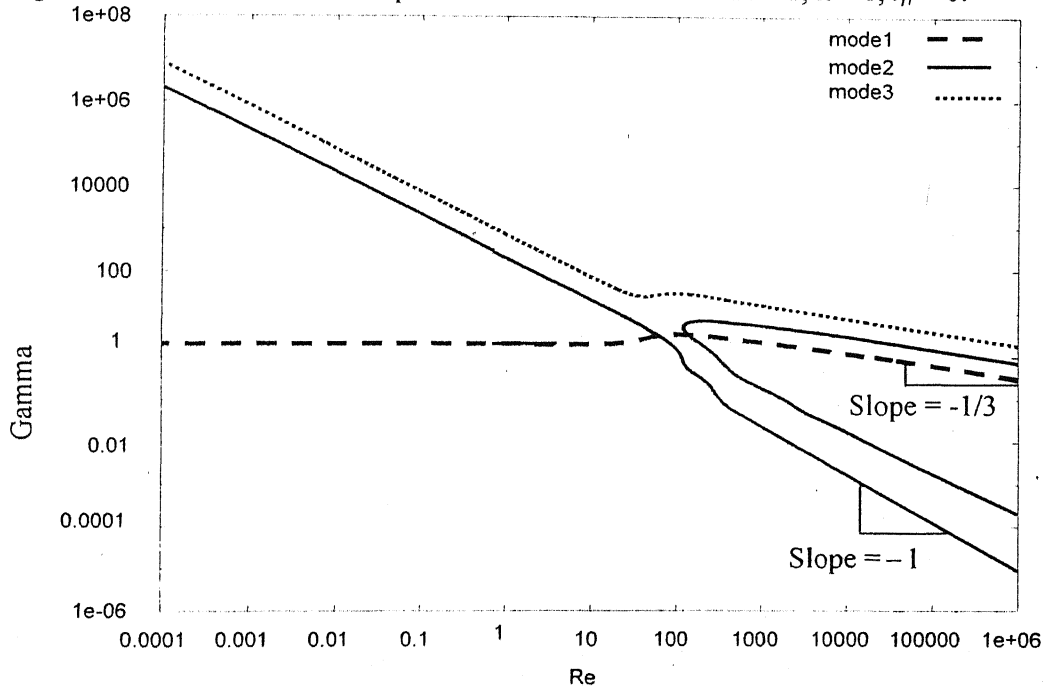


Fig.2.8 Γ vs. Re in case of Couette flow past a deformable wall for $H=2$, $k=0.5$, $\eta_r=0$: Data from full numerical solution.

The transition strain rate Γ_t is shown for $H = 1$, $k = 1$, $\eta_r = 0$ and for $H = 2$, $k = 0.5$, $\eta_r = 0$ as a function of Reynolds number in Fig. 2.7 and 2.8 respectively. Fig. 2.7 and 2.8 reveal that most unstable mode corresponds to scaling $\Gamma \sim Re^{-1}$, which does not have same scaling as wall mode. Thus, it must be a different mode since wall mode has scaling $\Gamma \sim Re^{-1/3}$. Later in this section we will inspect these modes extensively. It can also be observed from Fig. 2.7 and 2.8 that mode-2 has two different curves.

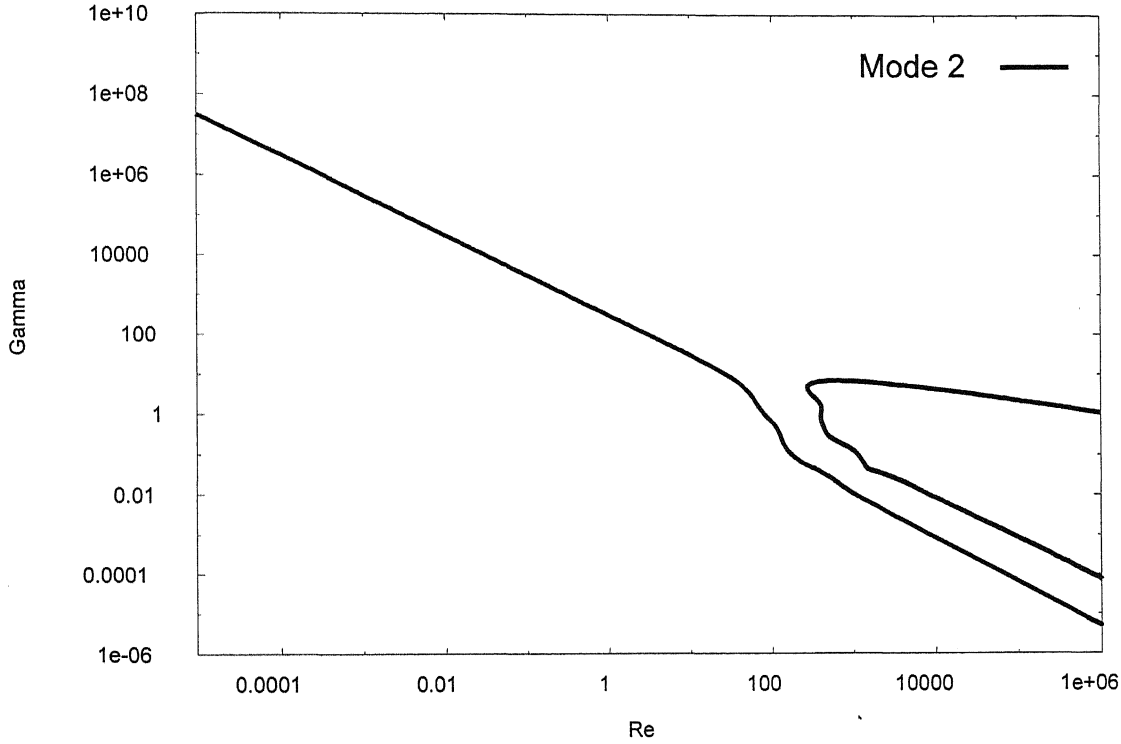


Fig.2.9 Γ vs. Re in case of Couette flow past a deformable wall for $H = 1$, $k = 1$, $\eta_r = 0$ from full numerical solution corresponding to second asymptotic wall mode.

As we have shown in Fig. 2.9 wall mode-2 provides two different curves as compared to all other modes, which have only one. Thus we would like to explain the reason for obtaining two curves for this particular mode. We already had mentioned that when we continued wall mode-2 to lower Reynolds number then it turns back and continues to high Reynolds number unlike wall mode-3 and wall mode-4 in Fig. 2.7 and Fig. 2.10.

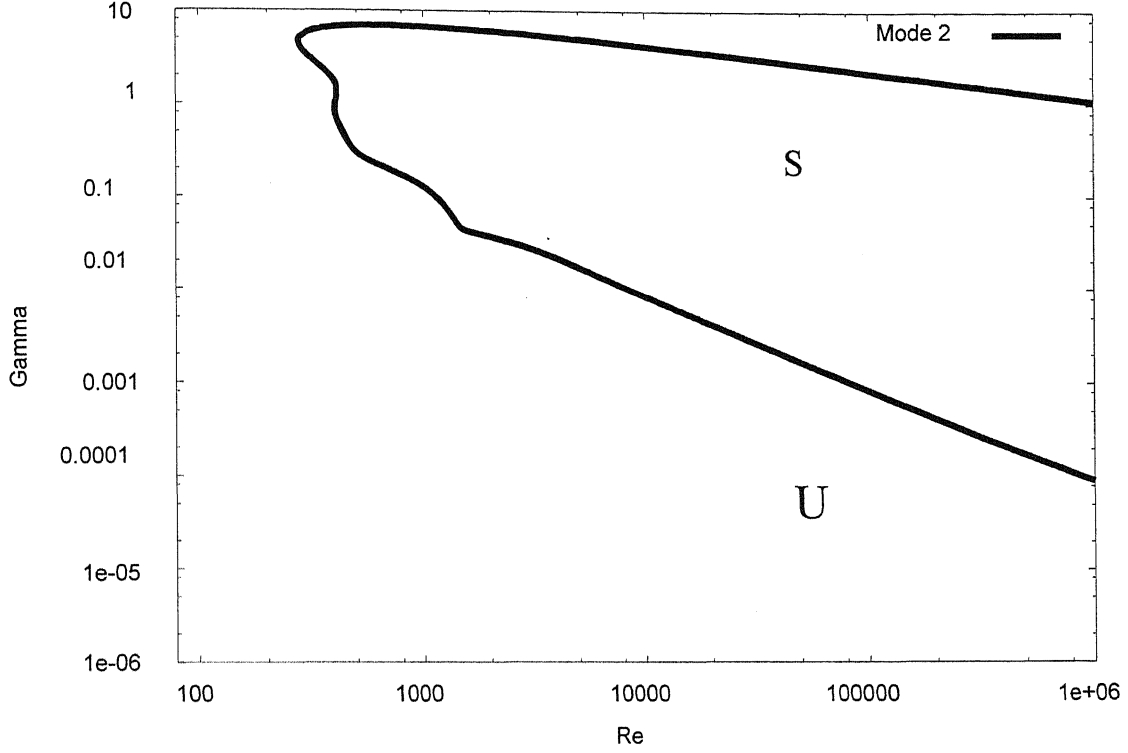


Fig.2.10 Γ vs. Re in case of Couette flow past a deformable wall for $H = 1$, $k = 1$, $\eta_r = 0$ from full numerical solution corresponding to second asymptotic wall mode.

We further analyzed the specific region to check the domain of instability. We found that the region above upper curve is unstable, regime within the U-shape curve is stable and region below the lower curve of Fig. 2.10 is unstable. But we know that wall modes are always stable in the case of flow past a rigid wall. However, the curve in Fig. 2.10 contradicts this expectation since at vanishing Γ deformable wall behaves like rigid wall. This reveals the possibility of an extra curve and therefore we tried to explore the whole lower region of Fig. 2.10 by lowering Γ . We found that after certain values of Γ imaginary part of growth velocity is changing from positive to negative. This indicates the possibility of another neutral curve which appears as the lowest curves which was there in Fig. 2.9 and hence we got stable region as given in Fig. 2.11. We already had mentioned about slope of every part of the figure and also discussed that new part must be a different mode than wall mode.

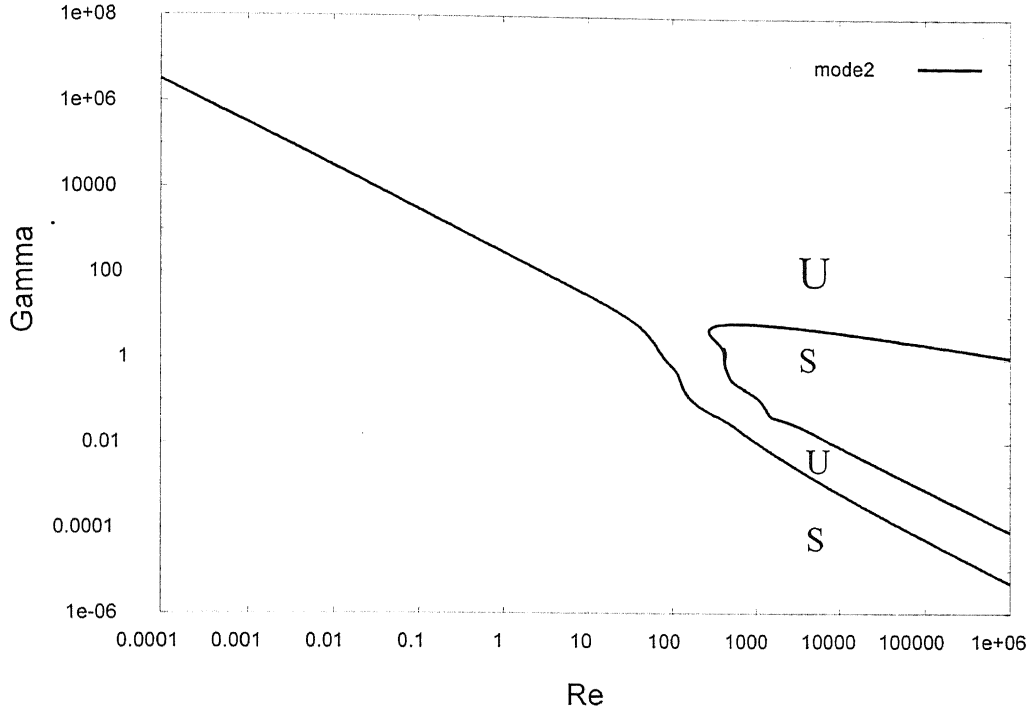


Fig.2.11 Γ vs. Re in case of plane Couette flow past a deformable wall for $H = 1$, $k = 1$, $\eta_r = 0$ for second wall mode and their extension.

When one tries to find the instability experimentally then one will be able to get only the most unstable mode, which is not the wall mode. So it is instructive to examine the eigenfunction of the neutral modes obtained from numerical solution in order to find the validity for wall mode and to find causes for new modes. We find the wall mode has same scaling as my Guide Shankar had used for asymptotic analysis and also Shankar and Kumaran [2002] presented. But when we further analyzed the eigenfunction for lower modes then we found that it has different scaling than wall mode. As mentioned above Γ scales as Re^{-1} as compared to wall mode where Γ scales to $Re^{-1/3}$, and the real part of growth velocity remains constant as compared to wall mode where it varies as $Re^{-1/3}$ and further we can get more idea about the nature of new mode by knowing scaling for all the dynamical quantities with Re as well as velocity distribution as a function of position. Thus we plot velocities and their derivatives as function of Reynolds number on log-log scale as presented in Fig. 2.12-2. 17.

From above mentioned figures we are able to obtain scaling as shown in table 1 for the quantities related to fluids and in table 2 for the deformable wall.

	v_z	v_x	$d_z v_x$	Γ	p_r	c_r
Wall mode	Re^0	$Re^{1/3}$	$Re^{2/3}$	$Re^{-1/3}$	Re^1	$Re^{1/3}$
Lower mode	Re^0	Re^0	$Re^{1/2}$	Re^{-1}	Re^1	Re^0
The lowest mode	Re^0	Re^0	$Re^{1/2}$	Re^{-1}	Re^1	Re^0

Table1. Scaling of different quantities in fluid as a function of Reynolds number for $H = 1$, $k = 1$, $\eta_r = 0$. Obtained from our numerical code.

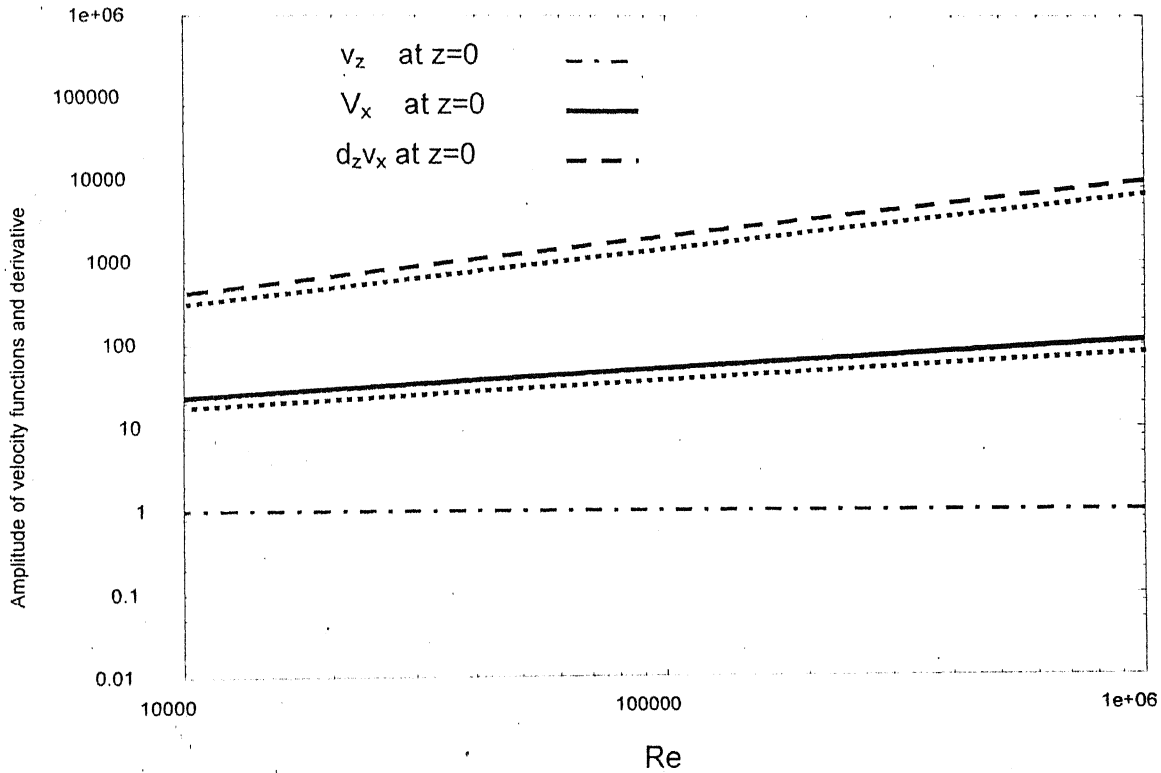


Fig. 2.12 Variation of the absolute value of velocity field and their derivative in the fluid with Reynolds number for wall mode with $H = 1$, $k = 1$, $\eta_r = 0$. The two dotted lines are reference line with slopes 1/3 and 2/3.

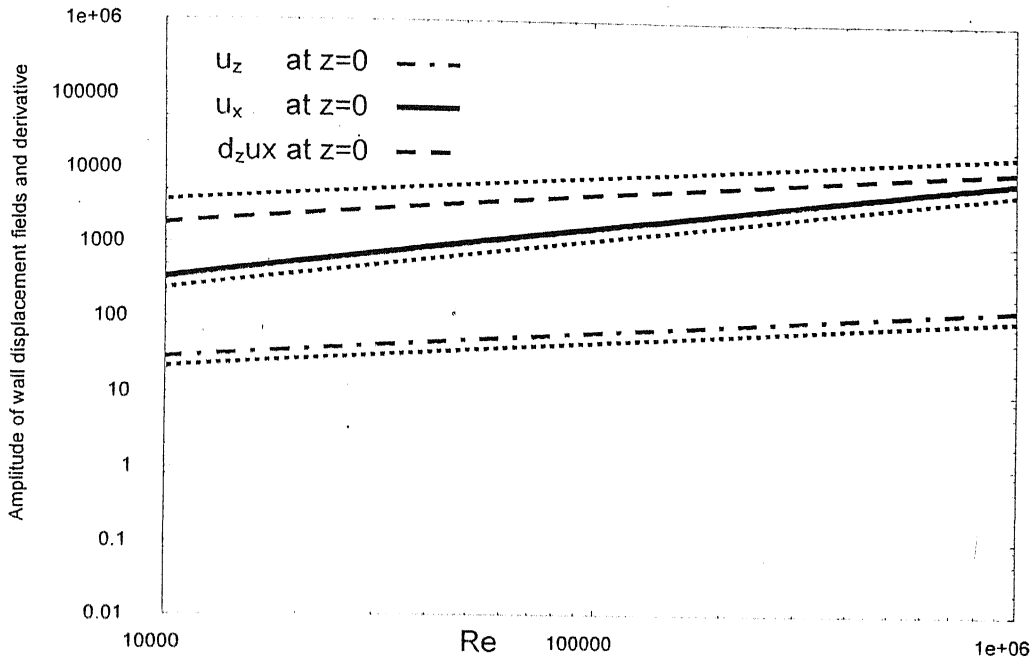


Fig. 2.13 Variation of the absolute value of displacement field and their derivative in the fluid with Reynolds number for wall mode with $H = 1$, $k = 1$, $\eta_r = 0$. The three dotted lines are reference line with slopes $1/3$, $1/2$ and $1/3$.

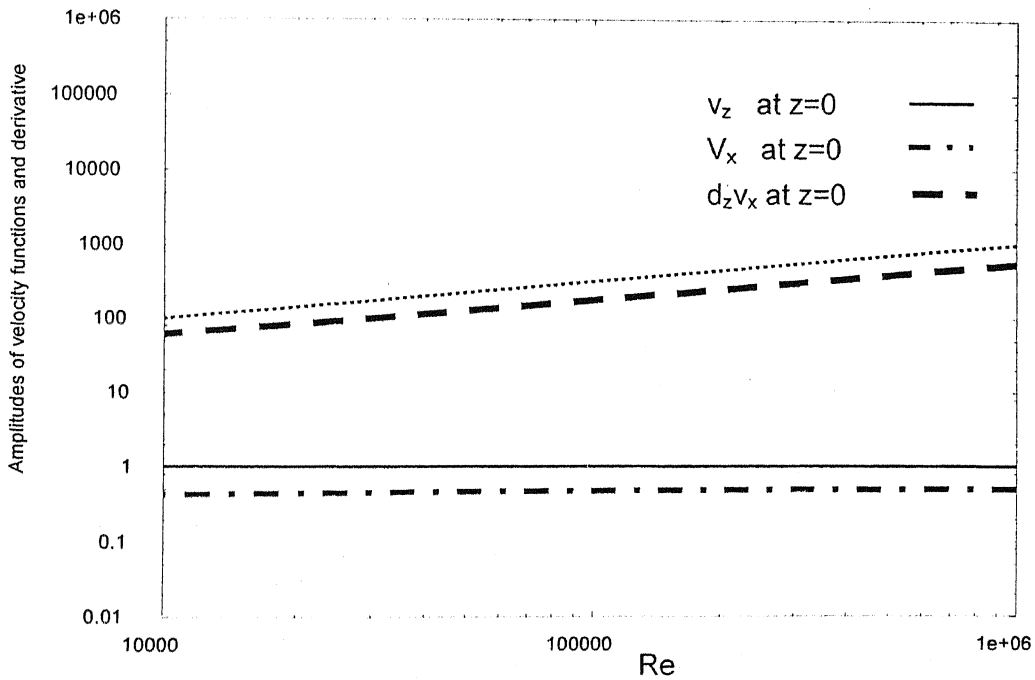


Fig. 2.14 Variation of the absolute value of velocity field and their derivative in the fluid with Reynolds number for lower curve with $H = 1$, $k = 1$, $\eta_r = 0$.

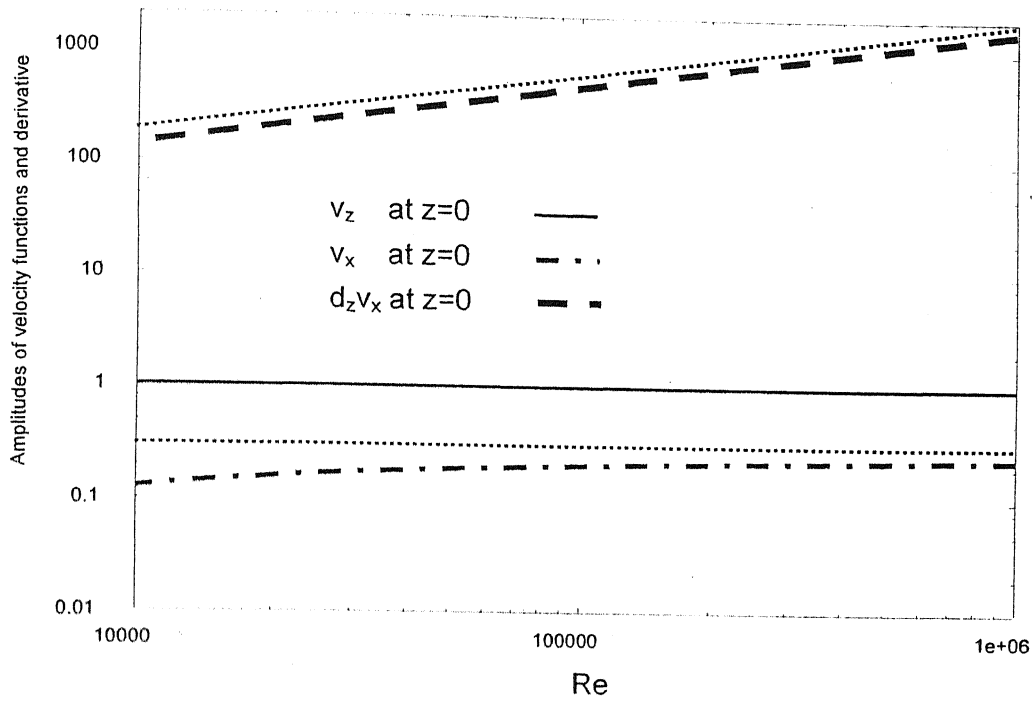


Fig. 2.15 Variation of the absolute value of velocity field and their derivative in the fluid with Reynolds number for the lowest curve with $H=1$, $k=1$, $\eta_r=0$. Dotted line in both Fig. 2.14 and 2.15 is a reference line with slope $1/2$.

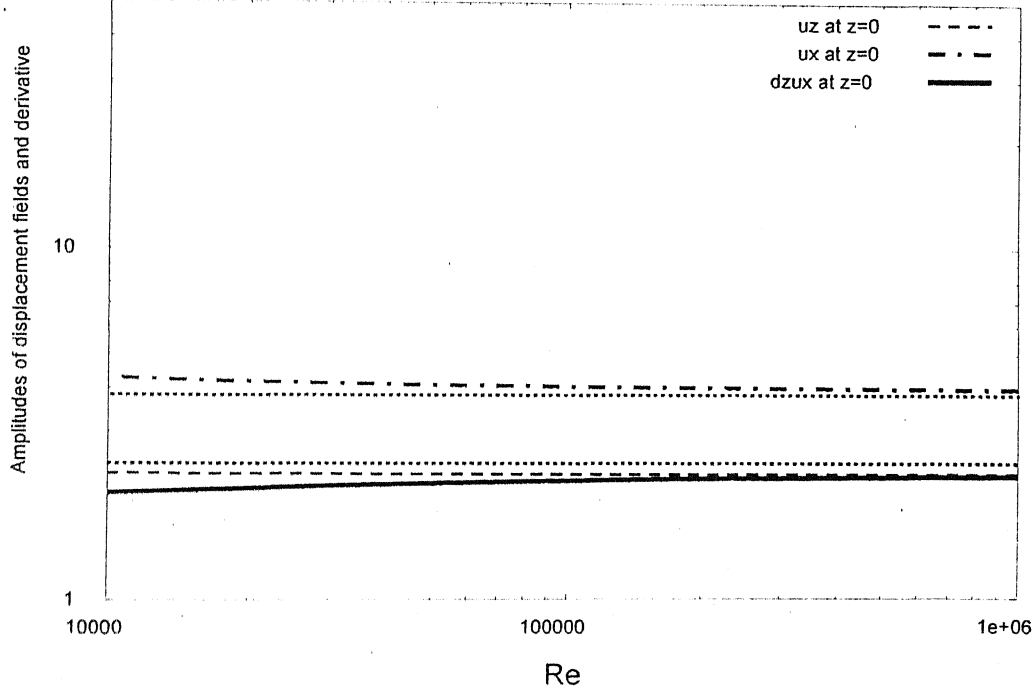


Fig. 2.16 Variation of the absolute value of displacement field and their derivative in the fluid with Reynolds number for lower curve with $H=1$, $k=1$, $\eta_r=0$

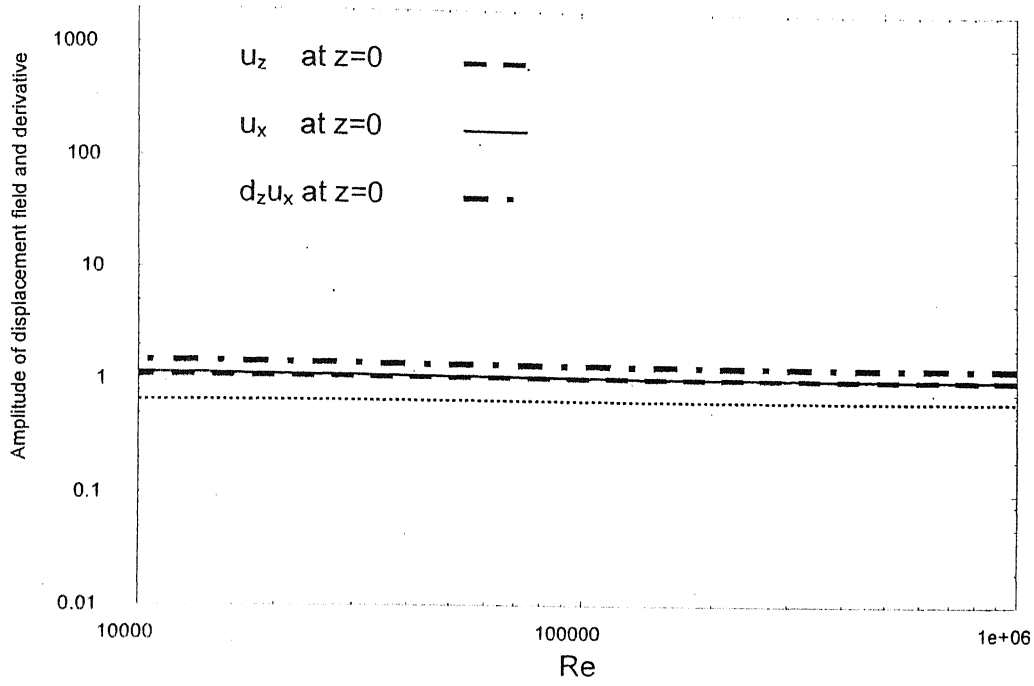


Fig. 2.17 Variation of the absolute value of displacement field and their derivative in the fluid with Reynolds number for the lowest curve with $H = 1$, $k = 1$, $\eta_r = 0$. The three dotted lines in Fig 2.16 and 2.17 are reference line with slope 0.

	u_z	u_x	$d_z u_x$	Γ_t	p_g	c_r
Wall mode	$Re^{1/3}$	$Re^{2/3}$	$Re^{1/3}$	$Re^{-1/3}$	Re^1	$Re^{1/3}$
Lower mode	Re^0	Re^0	Re^0	Re^{-1}	Re^1	Re^0
The lowest mode	Re^0	Re^0	Re^0	Re^{-1}	Re^1	Re^0

Table2. Scaling of different parameters in deformable wall vs Reynolds number for $H = 1$, $k = 1$, $\eta_r = 0$.

We can see from tables the scaling of parameters tells us that lower curve corresponding to mode-2 has exactly same scaling as the lowest curve. This reveals that these two modes have same properties. This scaling is similar to inviscid mode at high Reynolds number mentioned by Shankar and Kumaran [2002]. Further results can be confirmed by the analysis of distribution of velocity field and displacement field (eigenfunctions) as a function of position. Other than this boundary layer thickness vs. Reynolds number graph also reveals that the lower and the lowest modes are inviscid modes.

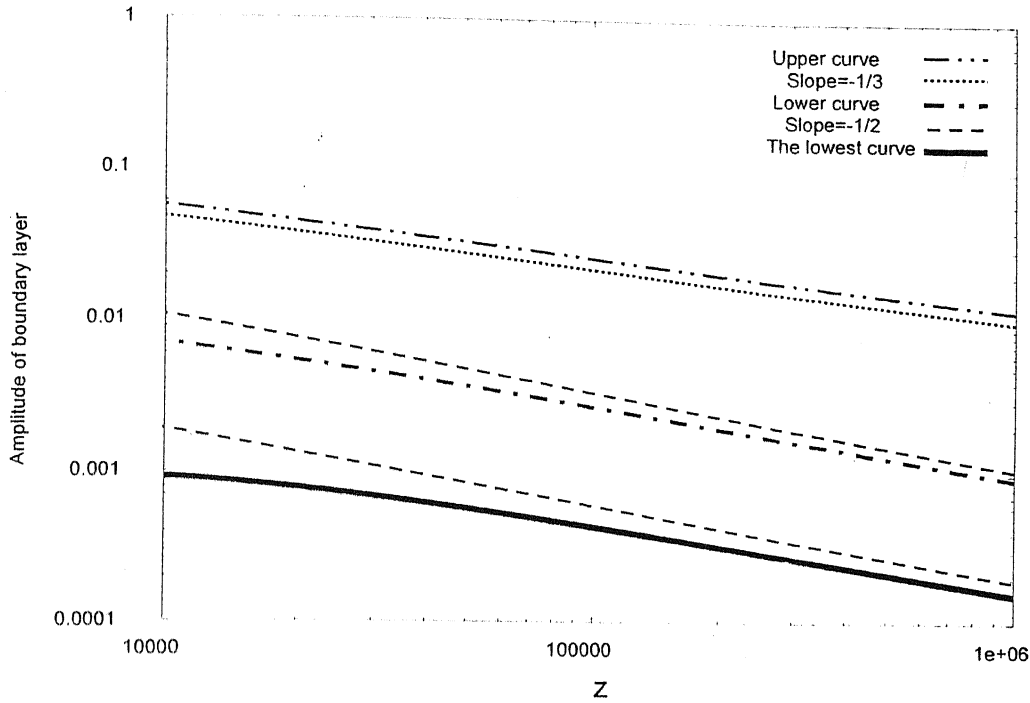


Fig. 2.18 Variation of thickness of wall layer (Boundary layer) with Reynolds number for plane Couette flow with $H = 1$, $k = 1$, $\eta_r = 0$. The three dotted lines have slope $-1/3$, $-1/2$ and $-1/2$.

Figure 2.18 shows the variation of the thickness of the wall layer δ with the Reynolds number. The wall layer thickness may be estimated by computing the ratio $v_x/d_z v_x$ at $z = 0$ from the full numerical solution. As Fig. 2.18 shows, the wall layer thickness δ decreases as $Re^{-1/3}$ for upper curve and as $Re^{-1/2}$ for other two curves in the limit of large Re . Upper curve results matches with the asymptotic analysis for the wall mode case but other two have different scaling which again tells us that these modes are inviscid modes. This shows that the numerically observed upper curves are indeed wall mode and lower curves are inviscid modes. For further conformation we can calculate eigenfunctions.

To calculate eigenfunctions we must know the constants multiplying the linearly independent numerical solutions, which are mentioned in Fig 2.4. But the equations we obtain after substituting in the boundary conditions are homogenous and linearly dependent. So it is not possible to find a unique solution, as the determinant of coefficient

matrix is zero for linearly dependent equations. Thus we change one of the equations with $(\tilde{v}_z)_{z=0} = (1+i)/\sqrt{2}$ and solve for constants. By this, we are fixing the magnitude of fluid velocity. Then we are able to get the distribution of eigenfunctions. We got same behavior for wall mode as presented by Shankar and Kumaran (2002).

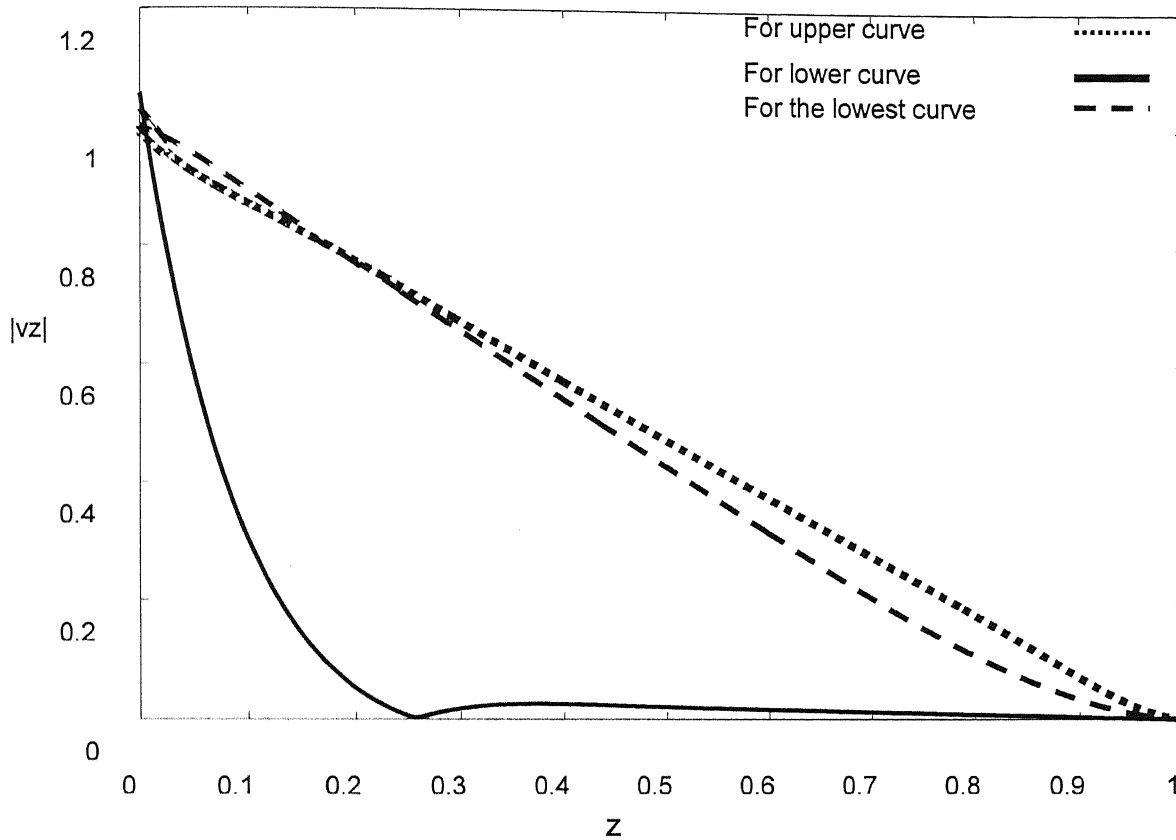


Fig.2.19 The amplitude of velocity $|v_z|$ vs. z in case of Couette flow for $H = 2$, $k = 0.5$, $nr = 0$ at Reynolds number 3000 corresponding to all the curve of mode 2.

Figures 1.19 and 2.20 show the variation $|v_z|$ and $|v_x|$ as a function of z in the fluid, and eigenfunction are calculated subjected to normalized condition mentioned above paragraph. These figures show that corresponding to upper curve behavior is same what Shankar and Kumaran (2002) had presented in their work. But for lower curves velocities are uniformly-distributed through out the channel and there is large variation near the wall. This also confirms that these new modes are inviscid mode.

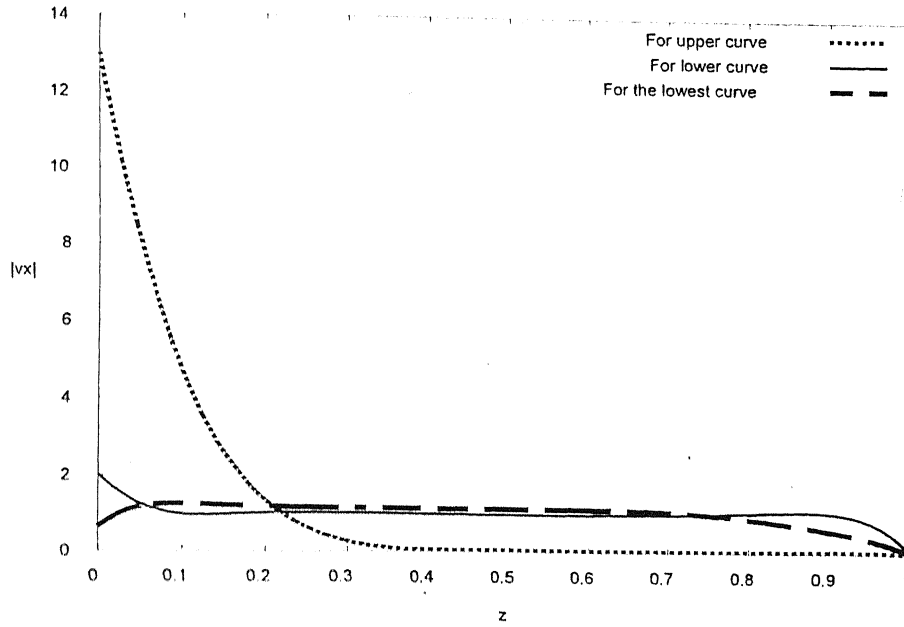


Fig.2.20 The amplitude of velocity $|v_x|$ vs. z in case of Couette flow for $H=2$, $k=0.5$, $nr=0$ at Reynolds number 3000 corresponding to all the curve of mode 2.

Further we can analyze the flow for high Reynolds number limit using the obtained scaling for the new mode which is claimed to be an inviscid mode. When we perform asymptotic analysis by using new scaling, we got equations as follows which further conform that obtained new modes are inviscid mode.

$$ik(\bar{v}_x - c)\bar{v}_x + (d_z \bar{v}_x)\bar{v}_z = -ik \text{Re}^{-1} \tilde{P}_f, \quad (2.45)$$

$$ik(\bar{v}_x - c)\bar{v}_z = -\text{Re}^{-1} d_z \tilde{P}_f. \quad (2.46)$$

$$-k^2 c^2 \tilde{u}_x = -ik \text{Re}^{-1} \tilde{p}_g + \frac{\text{Re}^{-1}}{\Gamma} [d_z^2 - k^2] \tilde{u}_x, \quad (2.47)$$

$$-k^2 c^2 \tilde{u}_z = -\text{Re}^{-1} d_z \tilde{p}_g + \frac{\text{Re}^{-1}}{\Gamma} [d_z^2 - k^2] \tilde{u}_z. \quad (2.48)$$

24.2 Results and discussion for the Poiseuille flow past a deformable wall

We already had discussed about the results of plane Couette flow and their numerical validity. There we confirm that both viscous as well as inviscid modes are present in flow past a deformable wall. For plane Poiseuille flow we just have to change base velocity profile from plane Couette to plane Poiseuille in Orr-Sommerfeld equation in a way mentioned in section 2.3.2. Besides that there must be an extra term in the case of plane Poiseuille flow in Orr-Sommerfeld equation since in this case second derivative of base velocity profile is non zero as compared to plane Couette flow. Other than above changes, all the terms remain same for both the cases since we required only first derivative at $z = 0$ which is same for both the cases. The asymptotic results also agree for high Reynolds number, which is same for both the cases.

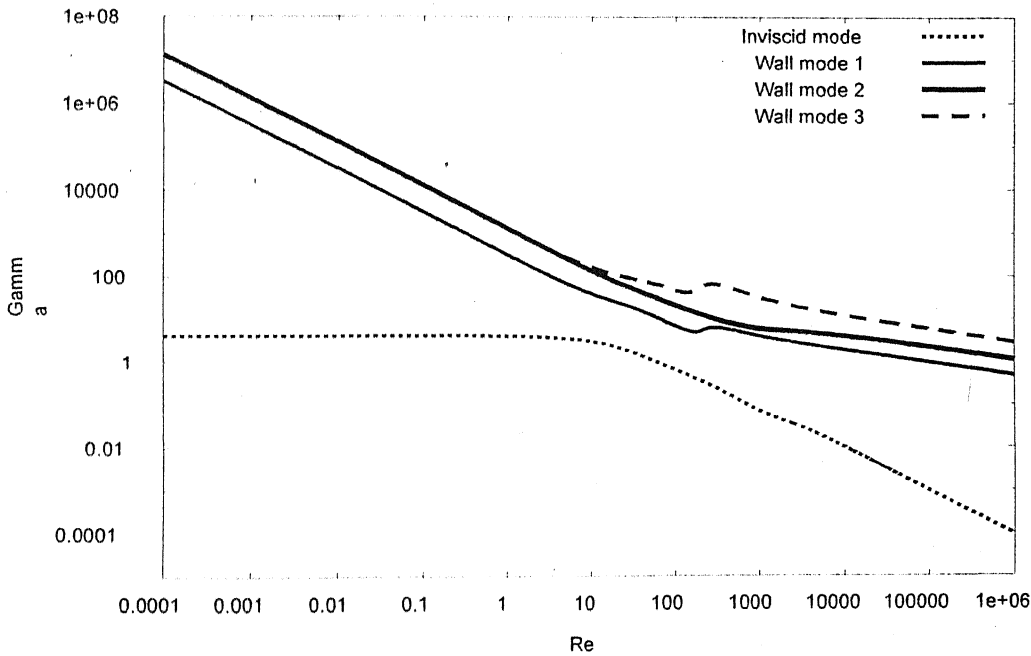


Fig.2.21 Gamma vs. Re in case of Poiseuille flow past a deformable wall for $H = 1$, $k = 1$, $\eta_r = 0$: Data from full numerical solution.

In figure 2.21 we had plotted Γ as a function of Re and the slope of the line at high Reynolds number reveal the existence of wall modes as well as inviscid mode as found in Couette flow. But for intermediate Reynolds number it has very different behavior than Couette flow especially for wall mode 1 and 2. As compared to plane Couette flow in Poiseuille flow first wall mode does not capture low Reynolds number mode and when we extended second wall mode to intermediate as well as low Reynolds number then instead of converging to inviscid mode it continues to low Reynolds number and shows same behavior as other higher modes. When we again tried to understand the behavior of low Reynolds number mode at intermediate and high Reynolds number then it continues to the inviscid mode. To get final confirmation about these modes we determine scaling of various quantities as a function of Reynolds number and presented in tables 3 and 4. From these tables we confirm that these are the same modes what we had anticipated above.

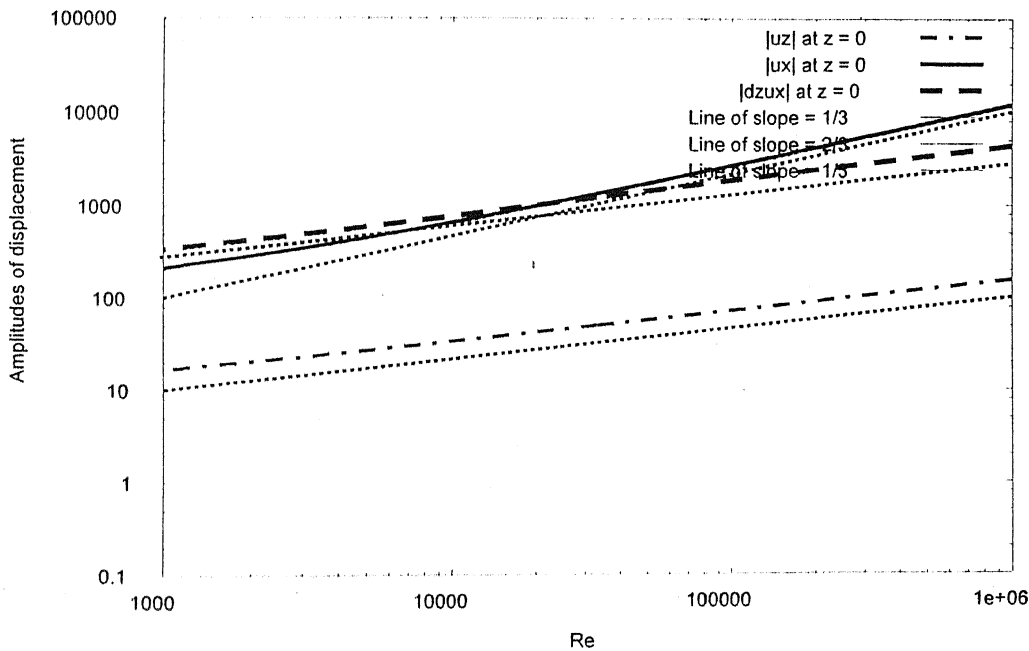


Fig. 2.22 Variation of the absolute value of velocity field and their derivative in the fluid with Reynolds number for the wall mode Poiseuille flow with $H = 1$, $k = 1$, $\eta_r = 0$. The two dotted lines in are reference line with slope $1/3$ and $2/3$.

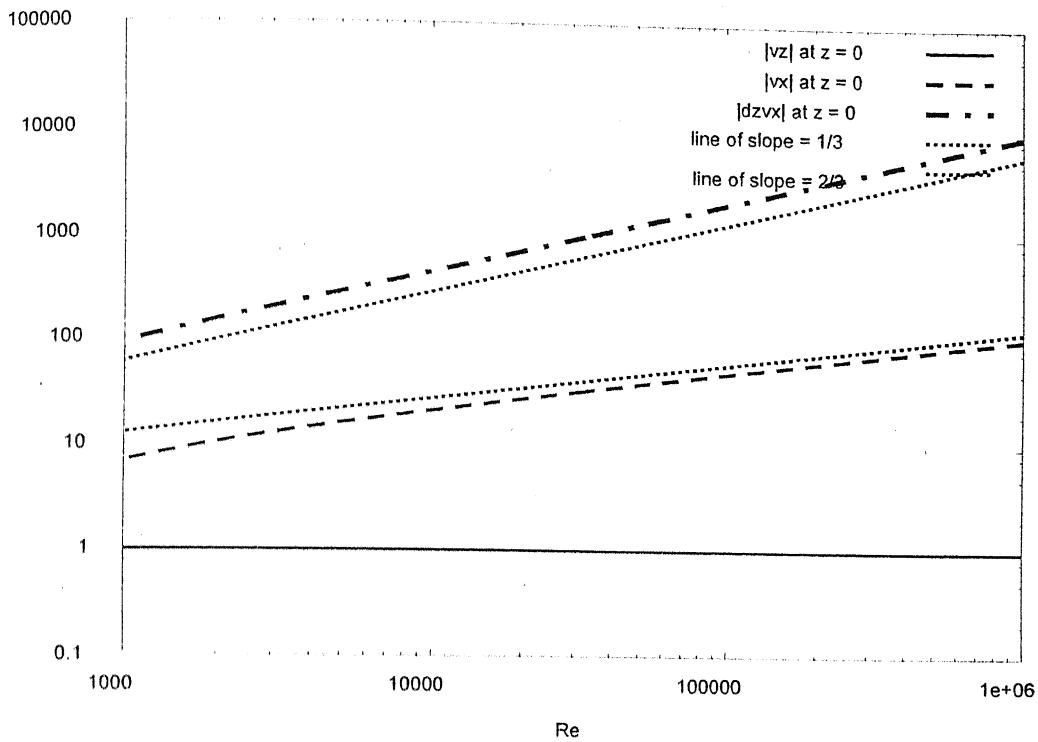


Fig. 2.23 Variation of the absolute value of displacement field and their derivative in the fluid vs. Reynolds number for wall mode Poiseuille flow with $H = 1$, $k = 1$, $\eta_r = 0$.

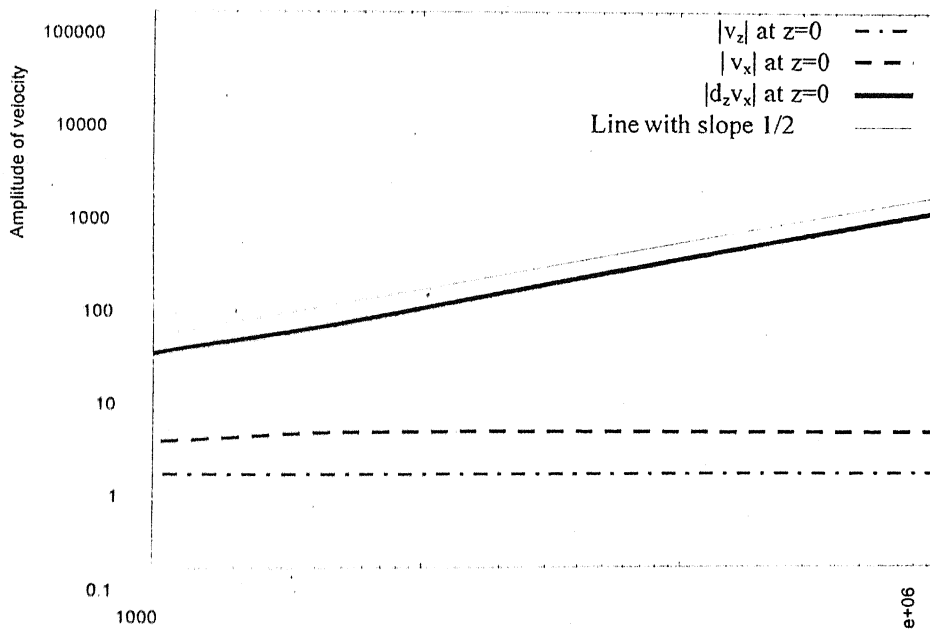


Fig. 2.24 Variation of the absolute value of velocity field and their derivative in the fluid with Reynolds number for inviscid mode Poiseuille flow with $H = 1$, $k = 1$, $\eta_r = 0$.

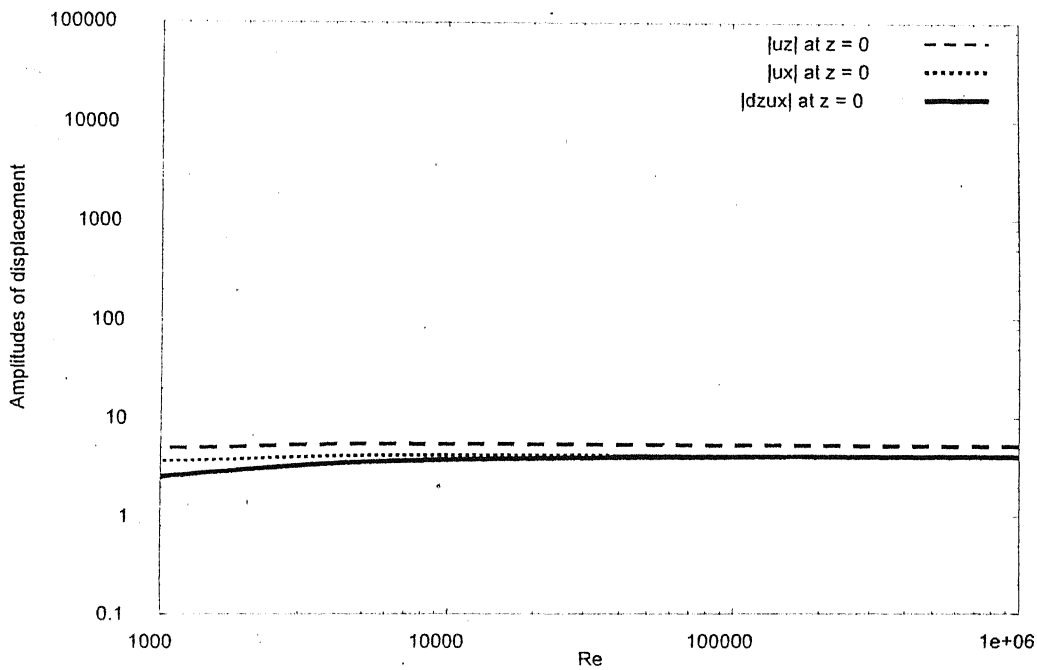


Fig. 2.25 Variation of the absolute value of displacement field and their derivatives vs. Reynolds number for the inviscid mode in Poiseuille flow with $H = 1$, $k = 1$, $\eta_r = 0$.

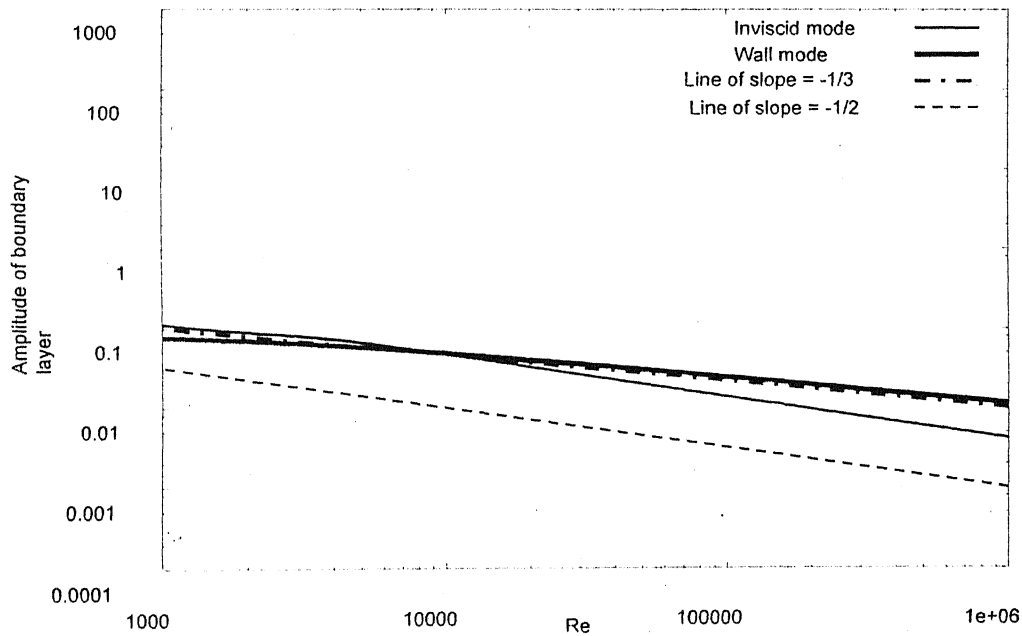


Fig. 2.26 Variation of thickness of wall layer (Boundary layer) with Reynolds number for Poiseuille flow with $H = 1$, $k = 1$, $\eta_r = 0$. The two dotted lines have slope $-1/3$ and $-1/2$.

	v_z	v_x	$d_z v_x$	Γ	p_f	c_r
Wall mode	Re^0	$Re^{1/3}$	$Re^{2/3}$	$Re^{-1/3}$	Re^1	$Re^{1/3}$
Inviscid mode	Re^0	Re^0	$Re^{1/2}$	Re^{-1}	Re^1	Re^0

Table3. Scaling of different parameters in the fluid past a deformable wall with Poiseuille base velocity profile flow vs Reynolds number for $H = 1$, $k = 1$, $\eta_r = 0$.

	u_z	u_x	$d_z u_x$	Γ_t	p_g	c_r
Wall mode	$Re^{1/3}$	$Re^{2/3}$	$Re^{1/3}$	$Re^{-1/3}$	Re^1	$Re^{1/3}$
Inviscid mode	Re^0	Re^0	Re^0	Re^{-1}	Re^1	Re^0

Table4. Scaling of different parameters in the deformable wall with Poiseuille base velocity profile flow vs Reynolds number for $H = 1$, $k = 1$, $\eta_r = 0$.

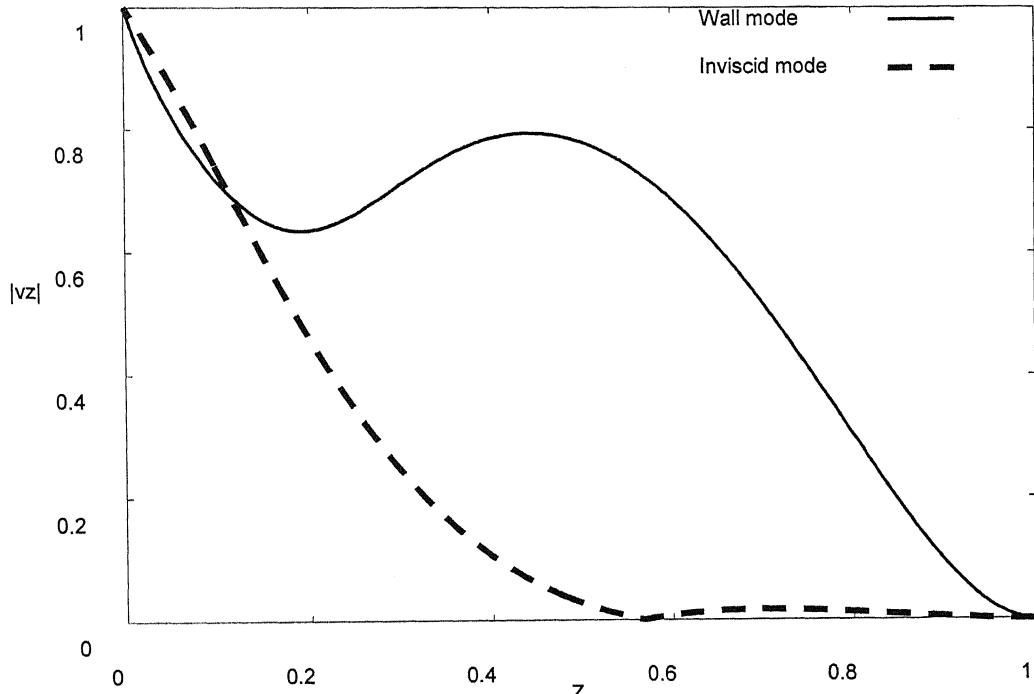


Fig.2.27 The amplitude of velocity $|v_z|$ vs. z in case of Poiseuille flow for $H = 1$, $k = 1$, $\eta_r = 0$ at Reynolds number 1000.

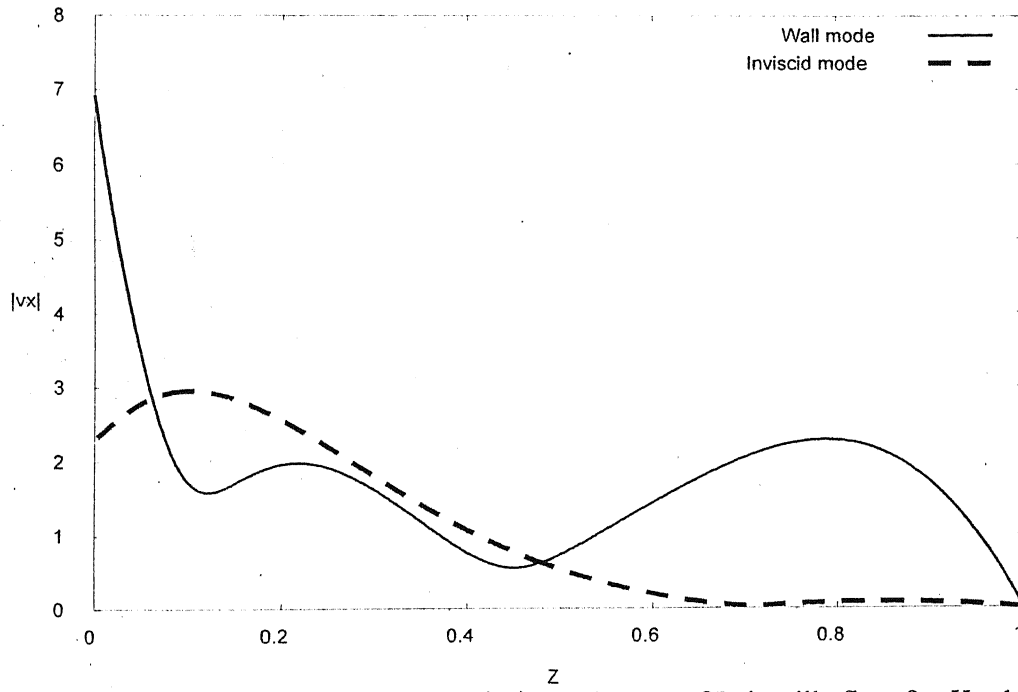


Fig.2.28 The amplitude of velocity $|v_x|$ vs. z in case of Poiseuille flow for $H = 1$, $k = 1$, $\eta_r = 0$ at Reynolds number 1000.

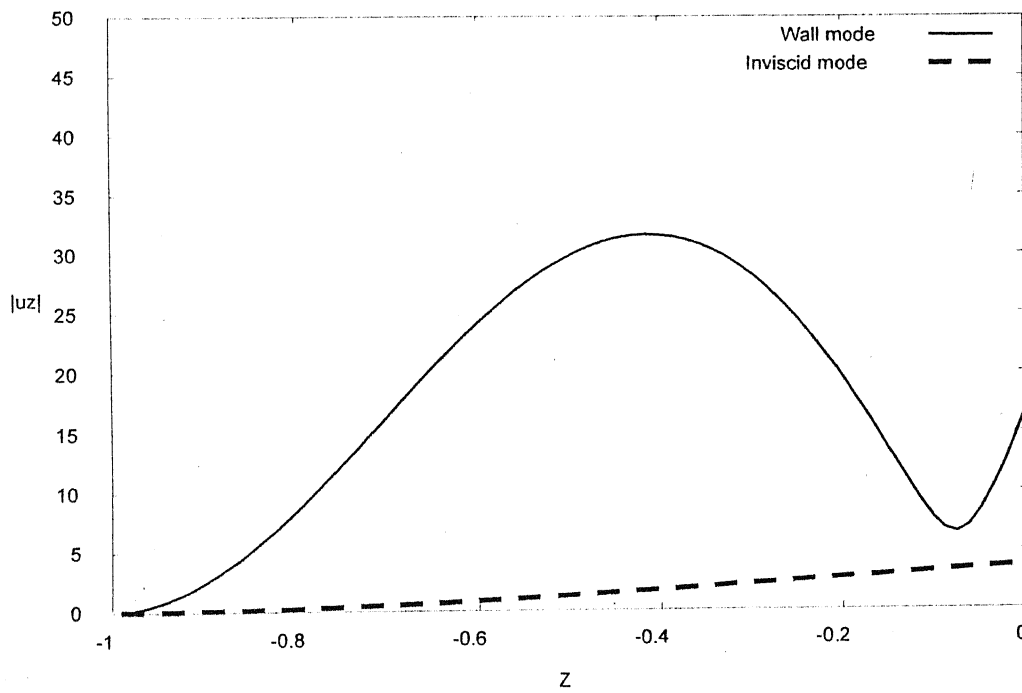


Fig.2.29 The amplitude of velocity $|u_z|$ vs. z in case of Poiseuille flow for $H = 1$, $k = 1$, $\eta_r = 0$ at Reynolds number 1000.

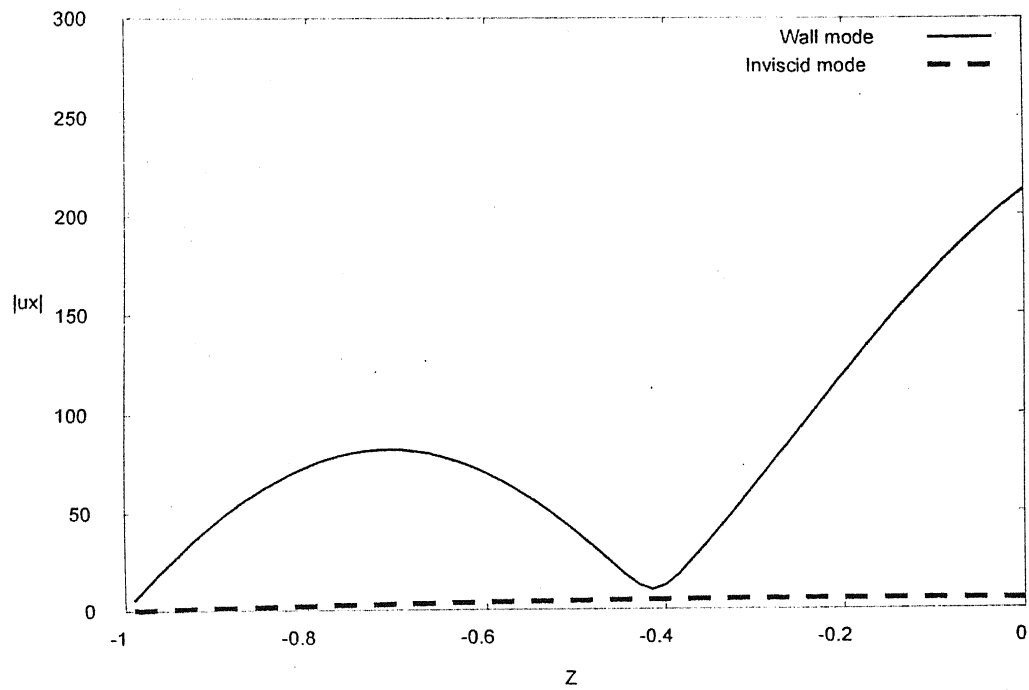


Fig.2.30 The amplitude of velocity $|u_x|$ vs. z in case of Poiseuille flow for $H = 1$, $k = 1$, $\eta_r = 0$ at Reynolds number 1000.

25 Conclusion and future work

The stability of wall modes and inviscid modes in the fluid flow past a deformable wall is analyzed using a combination of asymptotic and numerical method. In order to demonstrate the instability, we used the case of Couette flow as well as Poiseuille flow past a deformable wall. We have shown that wall mode instability predicted by the asymptotic analysis is also captured by numerical methods for both Couette flow as well as Poiseuille flow past a deformable wall. Further we have shown that there exists a mode in Couette flow which has different scaling than that of wall modes and this mode is also present in the Poiseuille flow. But there is a difference between in these two cases. In Couette flow one of the wall modes captures the inviscid mode when we extend wall mode solution numerically. But in Poiseuille flow instead of wall mode, zero Reynolds number modes capture the inviscid mode.

To examine the type of modes, we calculated the scaling of velocities and their derivatives with Reynolds number for the case of Couette flows and we find that new modes are indeed inviscid modes. Further we find the boundary layer thickness as a function of Reynolds number and this also indicates that the new mode is an inviscid mode. Other than these, when we find velocity distribution in the channel and it shows that there is uniform distribution in the channel as compared to wall modes where the velocity field is confined near the wall which confirms that this new mode must be an inviscid mode. But for the case of Poiseuille flow, we got the same scaling as Couette flow but velocity field distributions have a different nature instead of expected critical layer for inviscid modes. This prediction of the present study needs further investigation. Other than this, our numerical results predicted the inviscid modes for both the plane Couette as well as plane Poiseuille flows. The prediction of inviscid modes for plane Couette flow in the present study is in stark contrast with the asymptotic prediction of Kumaran [1994b], who concluded that the inviscid modes are stable in the case of plane Couette flow.

CHAPTER 3

Linear stability analysis of two-layer plane Couette flow past a deformable solid layer

3.0 Introduction

The study of stability of two-layer fluid flow past a deformable wall is important because of its use in multi-layer extrusion, where an accurate understanding of stable and unstable processing conditions can help in preventing interfacial instabilities, which is important to achieve desired product quality. In this chapter, we intend to study the effect of a deformable solid layer on the stability of two-layer plane Couette flow in a channel. We are motivated to study this problem by considering the possibility of coupling between two interfacial waves of the fluid-fluid & fluid-deformable solid wall interfaces. First we analyzed asymptotically for long wave and zero Reynolds number limits and then continued the asymptotic results numerically to intermediate values. Before our study on stability of two-layer fluid flow, first significant study had been done by Yih [1967]. Yih carried out an asymptotic analysis of the interfacial mode for long waves and showed that a jump in viscosity across the interface can lead to long wave instability. Moreover Yih find that long wave instability is present when more viscous fluid is thinner otherwise long wave is stable.

Subsequently Hooper and Boyd (1983) solved the linear stability problem for two-dimensional plane Couette flow using a short wave asymptotic analysis. They showed that this flow is unstable for short waves as well. The asymptotic expression for the growth rate of the interfacial mode for short wave is essentially consists of three terms. Out of that dominant term associated with surface tension, which is always stabilizing. The next term depends on gravity and the ratio of the densities and third term depends on ratio of viscosities: this term is always destabilizing if the density are equal.

In present study, we first analyze for the problem for fluids with equal density then we will examine the effect of density difference on the stability of fluid-fluid interface. Hence out of three-mentioned terms, for short waves as shown by Hooper and

Boyd, only first and third are valid for matched fluid densities. The case of equal densities of the fluid, which is our case there exist some rules of thumb given in text book Fundamental of two-layer Dynamics by Joseph & Renardy, which tells that we can stabilize long wave by placing the less viscous fluid in a thin layer and stabilize the short waves by assuming sufficiently high surface tension. In this chapter, we illustrate the following effects:

- 1) Two-layer flow past a rigid wall is unstable and it is possible to suppress the instability by making the solid layer sufficiently deformable.
- 2) Two layer flow past a rigid wall is stable and it is possible to destabilize the flow with deformable wall and,
- 3) We will examine the effect of various parameters on the stability of both the interfacial modes.

3.1 Problem formulation

Our system consists of two fluid layers of thickness βR and $(1-\beta) R$ respectively and the base is supported by a deformable solid of thickness $H R$ and upper layer is bounded by a rigid wall. The fluids are assumed to be incompressible, Newtonian fluids top rigid wall having shearing tangential velocity equal to U^* . Governing equations for both fluids and deformable solid for mass and momentum transfer in the bulk phases are the continuity equations and the Navier-Stokes equations. Schematic diagram for above situation is shown in Fig. 1.

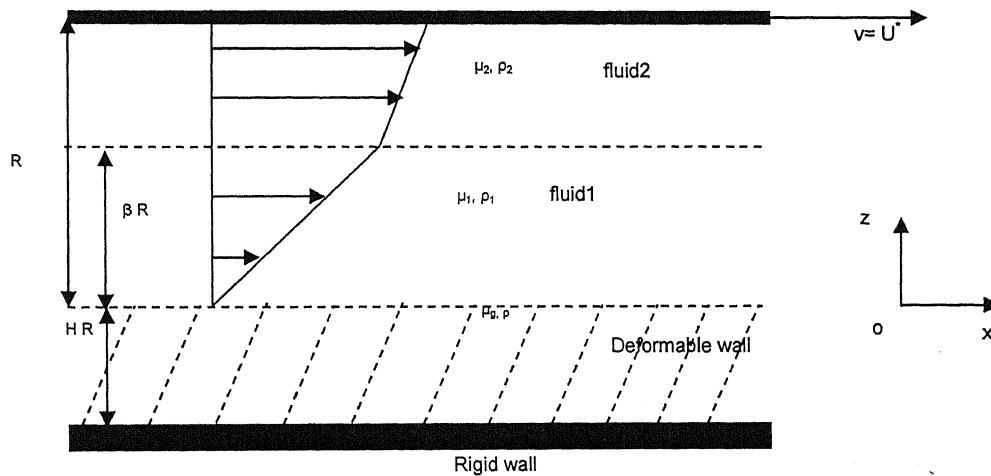


Fig 3.1 Schematic diagram of two-layer plane Couette flow past a deformable wall

3.2 Governing equations

3.2.1 Governing equations in non-Dimensional form

The basic hydrodynamic equations and non-dimensionalisation parameter remains same as in chapter 2 except, for dimensionalisation of viscosities and densities, those are dimensionalised by viscosity of fluid-1 and deformable wall density respectively as follows:

$$\begin{aligned}\eta_r &= \mu_g / \mu_1, & \mu_r^{(2)} &= \mu_2 / \mu_1, \\ \mu_r^{(1)} &= \mu_1 / \mu_1 = 1, & \rho^\alpha &= \rho^{*\alpha} / \rho^*, \\ \gamma &= \gamma^* / (\mu_1^* U^*)\end{aligned}$$

Here $\alpha = 1, 2$. ρ^* , γ^* and γ are dimensional density of deformable solid, dimensional and non-dimensional surface tension between fluid-fluid interface respectively. $\rho^{*\alpha}$ are the dimensional density of two fluids. μ_g , μ_1 and μ_2 are the viscosities of deformable solid, fluid-1 and fluid-2 respectively.

Thus here we can start directly with non-dimensional form of equations.

Mass balance for fluids:

$$\partial_i v_i^\alpha = 0, \quad (3.1)$$

Mass balance for deformable wall:

$$\partial_i u_i = 0, \quad (3.2)$$

Momentum balance for fluid and deformable wall can be written as:

$$\text{Re } \rho^\alpha (\partial_i + v_j^\alpha \partial_j) v_i^\alpha = -\partial_i p_f^\alpha + \mu_r^\alpha \partial_j^2 v_i^\alpha. \quad (3.3)$$

$$\text{Re } (\partial^2 u_i) = -p_g \delta_{ij} + \left(\frac{1}{\Gamma} + \eta_r \partial_i \right) \partial_j^2 u_i. \quad (3.4)$$

Here $\alpha = 1, 2$ represents the fluid index. Here repeated indices are summed over and single index means component of a vector. Here v , u , p_f and p_g represents velocity of fluid, deformation in viscoelastic wall, pressure inside fluid and pressure inside deformable wall respectively.

The no-slip condition at rigid solid and fluid interface is (at $z=1$):

$$v_x^{(2)} = 0, \quad (3.5)$$

The impermeability condition at the solid surface is (at $z = 1$):

$$v_z^{(2)} = 0, \quad (3.6)$$

Continuity of velocity component and stress component can be written as:

$$v_x^{(2)} = v_x^{(1)}, \quad (3.7)$$

$$v_z^{(2)} = v_z^{(1)}, \quad (3.8)$$

$$t_i T_{ij}^{(2)} n_j = t_i T_{ij}^{(1)} n_j + \gamma h_{xx} (1 + h_x^2)^{-3/2}, \quad (3.9)$$

$$n_i T_{ij}^{(2)} n_j = n_i T_{ij}^{(1)} n_j, \quad (3.10)$$

The tangential and normal velocity balance at the fluid-deformable wall interface:

$$v_x^{(1)} = \partial_t u_x, \quad (3.11)$$

$$v_z^{(1)} = \partial_t u_z. \quad (3.12)$$

The shear stress balance at fluid- deformable wall interface:

$$t_i T_{ij}^{(1)} n_j = t_i \sigma_{ij} n_j, \quad (3.13)$$

The normal stress balance at fluid-deformable wall interface:

$$n_i T_{ij}^{(1)} n_j = n_i \sigma_{ij} n_j, \quad (3.14)$$

The no slip-condition at deformable wall-rigid solid surface is (at $z = -H$):

$$u_x = 0, \quad (3.15)$$

The impermeability condition at deformable wall-solid surface is (at $z = -H$):

$$u_z = 0, \quad (3.16)$$

Non-dimensional stresses in liquid and deformable wall can be given respectively as follows:

$$T_{ij}^{\alpha} = -p_f^{\alpha} \delta_{ij} + \mu_r^{\alpha} (\partial_i v_j^{\alpha} + \partial_j v_i^{\alpha}),$$

$$\sigma_{ij} = -\partial_i p_g + \left(\frac{1}{\Gamma} + \eta_r \partial_i\right)(\partial_j u_i + \partial_i u_j).$$

Kinematical equation for fluid-fluid interface can be written as:

$$\partial_t h + v_x^{(1)} \partial_x h = v_z^{(1)}.$$

Where h is the height of the fluid-fluid interface from the x-axis.

3.2.2 Base state calculation for both Poiseuille and Couette flow:

After solving two-dimensional Navier-Stokes equation in non-dimensional form for above situation we obtained the base velocity profile for fluids for the case of equal density are as follows;

$$\bar{v}_{2x} = (z + \beta (\mu_r - 1)) / (1 + \beta (\mu_r - 1));$$

$$\bar{v}_{1x} = z \mu_r / (1 + \beta (\mu_r - 1));$$

$$\bar{v}_{1z} = 0;$$

$$\bar{v}_{2z} = 0;$$

Base state deformation for gel in non-dimensional form is;

$$\bar{u} = \Gamma (z + H) \{ \mu_r / (1 + \beta (\mu_r - 1)) \};$$

3.3 Linear stability analyses

3.3.1 General equation for linear stability analysis

Base state for Couette flow is given in section 3.2.2. We now add perturbation in base profile to find out hydrodynamic equations and boundaries condition in terms of perturbed quantities.

Thus perturbed quantities can be represented as follows;

$$[v_x^{\alpha} - \bar{v}_x^{\alpha}, v_z^{\alpha} - \bar{v}_z^{\alpha}, u - \bar{u}, p_f^{\alpha} - p_0, p_g - p_0, h - h_0] = [\tilde{v}_f^{\alpha}, \tilde{v}_f^{\alpha}, \tilde{u}, \tilde{p}_f^{\alpha}, \tilde{p}_g, \tilde{\varepsilon}] \exp\{ik(x - ct)\}$$

Where, c and k are the growth velocity and the wave number of the instability respectively and base state condition is given in section 3.2.2. ' ε ' represent perturbation amplitude in the height of fluid-fluid interface.

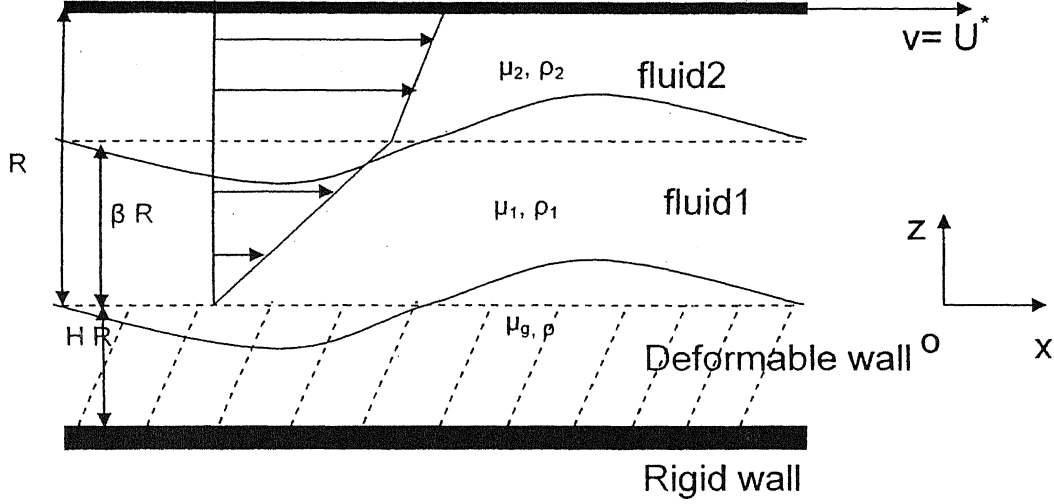


Fig 3.2 Schematic diagram of two layers plane Couette flow past a deformable wall in perturbed state

Applying above perturbation to equation 3.1 to 3.16 and equating linear term on both the sides, we obtain:

$$d_z \tilde{v}_z^\alpha + i k \tilde{v}_x^\alpha = 0, \quad (3.17)$$

$$\text{Re} \rho^\alpha \{ i k (\bar{v}_x^\alpha - c) \tilde{v}_x^\alpha + (d_z \bar{v}_x^\alpha) \tilde{v}_z^\alpha \} = -i k \tilde{p}_f^\alpha + \mu_r^\alpha [d_z^2 - k^2] \tilde{v}_x^\alpha, \quad (3.18)$$

$$\text{Re} \rho^\alpha \{ i k (\bar{v}_x^\alpha - c) \tilde{v}_z^\alpha \} = -d_z \tilde{p}_f^\alpha + \mu_r^\alpha [d_z^2 - k^2] \tilde{v}_z^\alpha. \quad (3.19)$$

For deformable wall continuity equation, x and z component momentum balance for perturbed states are respectively:

$$d_z \tilde{u}_z + i k \tilde{u}_x = 0, \quad (3.20)$$

$$-\text{Re} k^2 c^2 \tilde{u}_x = -i k \tilde{p}_g + \left(\frac{1}{\Gamma} - \eta_r I k c \right) [d_z^2 - k^2] \tilde{u}_x, \quad (3.21)$$

$$-\text{Re} k^2 c^2 \tilde{u}_z = -d_z \tilde{p}_g + \left(\frac{1}{\Gamma} - \eta_r I k c \right) [d_z^2 - k^2] \tilde{u}_z. \quad (3.22)$$

After combining above equations 3.17 to 3.19 for fluid and 3.20 to 3.22 for deformable wall we get a standard equation, which is known as Orr- Sommerfeld equation for fluid and deformable wall respectively.

For deformable wall:

$$-\text{Re } k^2 c^2 [d_z^2 - k^2] \tilde{u}_z = \left(\frac{1}{\Gamma} - \eta_r i k c \right) [d_z^2 - k^2]^2 \tilde{u}_z, \quad (3.23)$$

$$\tilde{p}_g = (1/(i k)) \{ \text{Re } k^2 c^2 \tilde{u}_x + \left(\frac{1}{\Gamma} - \eta_r i k c \right) [d_z^2 - k^2] \tilde{u}_x \}. \quad (3.24)$$

For fluid:

$$\text{Re } \rho^\alpha i k \{ (\bar{v}_x^\alpha - c) [d_z^2 - k^2] + (d_z^2 \bar{v}_x^\alpha) \} \tilde{v}_z^\alpha = \mu_r^\alpha [d_z^2 - k^2]^2 \tilde{v}_z^\alpha, \quad (3.25)$$

$$\tilde{p}_f^\alpha = (1/(i k)) \{ -\text{Re } \rho^\alpha \{ i k (\bar{v}_x^\alpha - c) \tilde{v}_z^\alpha + (d_z^2 \bar{v}_x^\alpha) \tilde{v}_z^\alpha \} + [d_z^2 - k^2] \tilde{v}_z^\alpha \}. \quad (3.26)$$

Boundary conditions in term of perturbed quantities can be written as:

At fluid solid interface (at $z = 1$):

$$\tilde{v}_x^{(2)} = 0, \quad (3.27)$$

$$\tilde{v}_z^{(2)} = 0, \quad (3.28)$$

At fluid-fluid interface (at $z=\beta$):

The second term of left hand side of the tangential velocity condition given below is obtained by linearizing x-component interface velocity about the unperturbed interface at $z = \beta$:

$$\tilde{v}_z^{(2)} = \tilde{v}_z^{(1)} \quad (3.29)$$

$$\tilde{v}_x^{(2)} + (d_z \bar{v}_x^{(2)})_{z=\beta} \varepsilon = \tilde{v}_x^{(1)} + (d_z \bar{v}_x^{(1)})_{z=\beta} \varepsilon \quad (3.30)$$

$$\tilde{T}_{xz}^{(2)} = \tilde{T}_{xz}^{(1)} \quad (3.31)$$

$$\tilde{T}_{zz}^{(2)} = \tilde{T}_{zz}^{(1)} - \gamma k^2 \varepsilon \quad (3.32)$$

At fluid-deformable wall interface (at $z = 0$):

The second term of left hand side of the tangential velocity condition given below is obtained by linearizing x -component interface velocity about the unperturbed interface at $z = 0$:

$$\tilde{v}_z^{(1)} = -ikc\tilde{u}_z, \quad (3.33)$$

$$\tilde{v}_x^{(1)} + (d_z \tilde{v}_x^{(1)})_{z=0} \tilde{u}_z = -ikc\tilde{u}_x, \quad (3.34)$$

$$\tilde{T}_{xz}^{(1)} = \tilde{\sigma}_{xz}, \quad (3.35)$$

$$\tilde{T}_{zz}^{(1)} = \tilde{\sigma}_{zz}, \quad (3.36)$$

At rigid solid-deformable wall interface ($z = -H$):

$$\tilde{u}_z = 0, \quad (3.37)$$

$$\tilde{u}_x = 0. \quad (3.38)$$

Here,

$$\tilde{T}_{xz}^\alpha = \mu_r^\alpha (d_z \tilde{v}_x^\alpha + ik \tilde{v}_z^\alpha),$$

$$\tilde{T}_{zz}^\alpha = -\tilde{p}_f^\alpha + 2 \mu_r d_z \tilde{v}_z^\alpha,$$

$$\tilde{\sigma}_{zz} = -\tilde{p}_g + 2 \left(\frac{1}{\Gamma} - \eta_r ikc \right) d_z \tilde{u}_z,$$

$$\tilde{\sigma}_{xz} = \left(\frac{1}{\Gamma} - \eta_r ikc \right) [d_z \tilde{u}_x + ik \tilde{u}_z],$$

$$-ikc\varepsilon + \tilde{v}_x^{(1)}\varepsilon = \tilde{v}_z^{(1)}.$$

We can solve above equation using a combination of asymptotic and numerical methods. First we would like to solve for some asymptotic cases for long wave and zero Reynolds number limit then we will continue asymptotic results to moderate value using numerical technique.

3.3.2 Numerical method for solving characteristic equations;

In our case we have fourth order ordinary differential equation for both fluids and the deformable wall as given in equations 3.23 and 3.25. Hence to know the complete solution of fourth order ODE we must have to know the function's value and their first, second and 3rd derivatives. This means we need to choose four orthogonal functions and hence four constants to write general combination of those four functions.

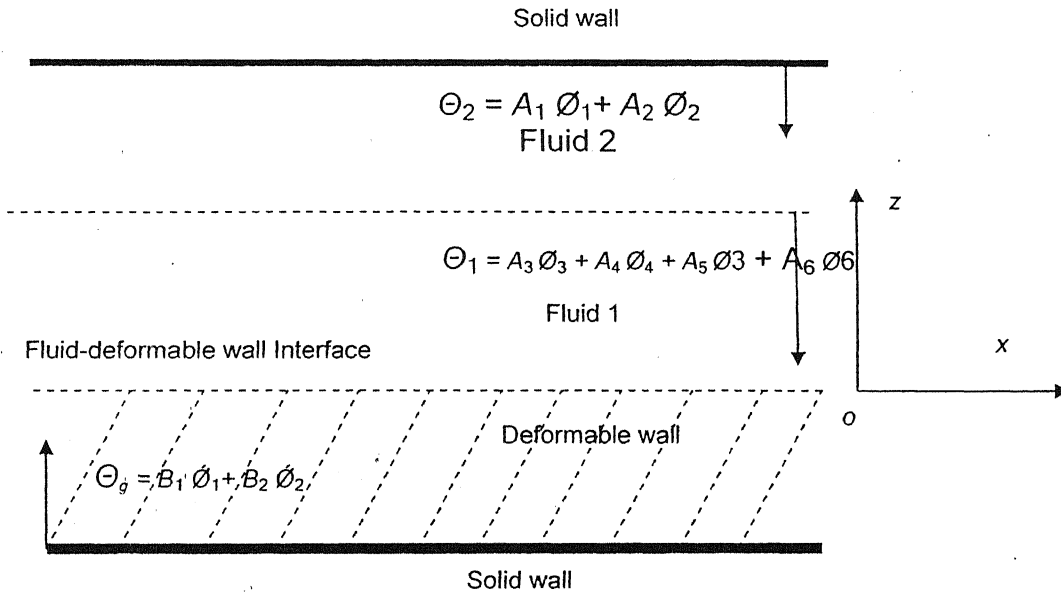


Fig. 3.3 Schematic diagram for numerical calculation

The boundary conditions at both the wall allow us to take only two orthogonal functions which satisfying two given boundary conditions 3.27 and 3.28 at upper rigid wall and conditions 3.37 and 3.38 at lower rigid wall. Thus we need only two constants to write the solution set for velocity of fluid-2 as well as deformation field but we must need four functions to represent complete solution for fluid-1. After that we used fourth order adaptive Runge Kutta as an integrator and marching from the rigid surface to interface of the fluid and gel. We have eight interface conditions 3.29 to 3.36, after applying these interface conditions we are able to get eight linear homogenous equations with eight constants. As we know for getting non trivial solutions (i. e. non-zero value of $A_1, A_2, A_3, A_4, A_5, A_6, B_1$ and B_2) of homogenous equations, determinant of coefficient matrix must be zero. Hence by setting determinant equal to zero, we obtained the characteristic

equation. This was solved numerically using Newton-Raphson, iteration technique. We used programming language 'C' for developing code.

Mathematically above statement can be represented as:

According to mentioned procedure two independent orthogonal solutions for the velocity field of fluid-2 can be written as:

$$\tilde{v}_z = 0 \quad d_z \tilde{v}_z = 0 \quad d_z^2 \tilde{v}_z = 1 \quad d_z^3 \tilde{v}_z = 0$$

$$\tilde{v}_z = 0 \quad d_z \tilde{v}_z = 0 \quad d_z^2 \tilde{v}_z = 0 \quad d_z^3 \tilde{v}_z = 1.$$

For fluid-1:

$$\tilde{v}_z = 1 \quad d_z \tilde{v}_z = 0 \quad d_z^2 \tilde{v}_z = 0 \quad d_z^3 \tilde{v}_z = 0$$

$$\tilde{v}_z = 0 \quad d_z \tilde{v}_z = 1 \quad d_z^2 \tilde{v}_z = 0 \quad d_z^3 \tilde{v}_z = 0$$

$$\tilde{v}_z = 0 \quad d_z \tilde{v}_z = 0 \quad d_z^2 \tilde{v}_z = 1 \quad d_z^3 \tilde{v}_z = 0$$

$$\tilde{v}_z = 0 \quad d_z \tilde{v}_z = 0 \quad d_z^2 \tilde{v}_z = 0 \quad d_z^3 \tilde{v}_z = 1.$$

The velocity field is a linear combination of these four solutions. We can write solutions set in combined form as $\Theta = \{\tilde{v}_z, d_z \tilde{v}_z, d_z^2 \tilde{v}_z, d_z^3 \tilde{v}_z\}$ where $\emptyset_1 = \{0, 0, 1, 0\}$, $\emptyset_2 = \{0, 0, 0, 1\}$, $\emptyset_3 = \{1, 0, 0, 0\}$, $\emptyset_4 = \{0, 1, 0, 0\}$, $\emptyset_5 = \{0, 0, 1, 0\}$ and $\emptyset_6 = \{0, 0, 0, 1\}$.

Similarly for deformable wall the displacement fields are:

$$\tilde{u}_z = 0 \quad d_z \tilde{u}_z = 0 \quad d_z^2 \tilde{u}_z = 1 \quad d_z^3 \tilde{u}_z = 0$$

$$\tilde{u}_z = 0 \quad d_z \tilde{u}_z = 0 \quad d_z^2 \tilde{u}_z = 0 \quad d_z^3 \tilde{u}_z = 1.$$

Here $\emptyset_1 = \{0, 0, 1, 0\}$ and $\emptyset_2 = \{0, 0, 0, 1\}$ and by using matching condition at the interface of fluid and deformable wall. We will able to get characteristic equation which has all the information about the stability of the system.

3.4 Results and discussions

3.4.1 Numerical validation and results for Rigid channel

To check the validity of numerical solution we need to put the value of $\mu_r = 1$ and surface tension zero in current numerical code. By putting these values two-fluid problem becomes single layer flow past a deformable wall, which is rightly able to capture all the results presented in Chapter-2. First it is instructive to briefly recapitulate the results for the stability of two-layer Couette flow past in a rigid channel and this has been the subject of earlier study of Yih [1967] and Hooper and Boyd [1983]. Yih carried out asymptotic analysis for long wave using a formal power series in the wave number $k \ll 1$ for $k Re \ll 1$, where Re is Reynolds number and k is wave number. Yih show that jump in viscosity across the interface can lead to long wave instability which can be observed from Fig. 3.4 and 3.6 which is computed numerically taking asymptotic results as a initial guess.

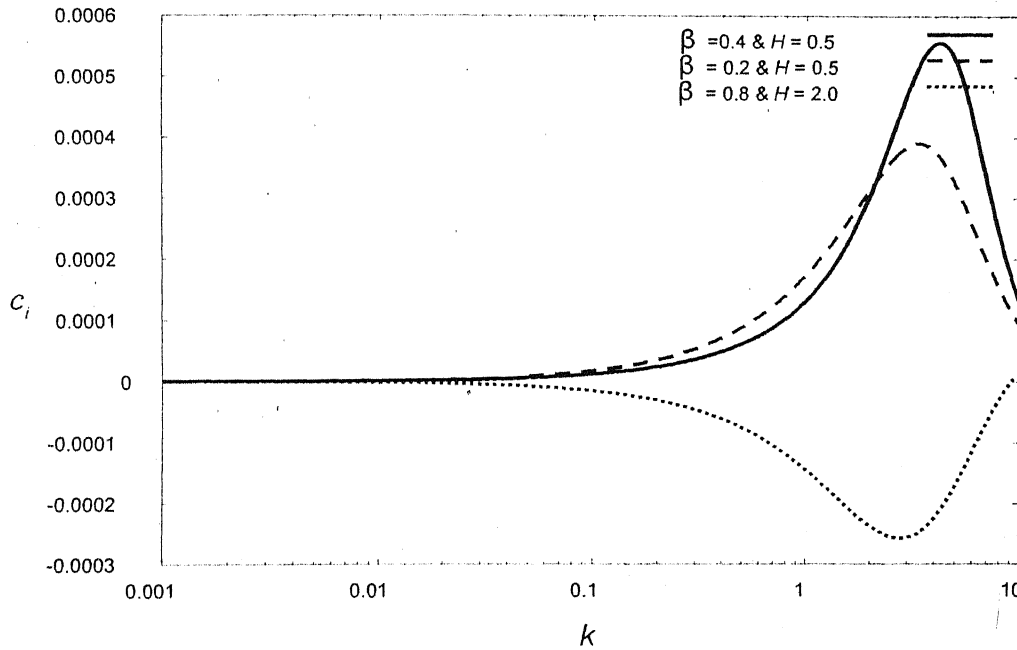


Fig. 3.4 Fluid-fluid interface instability in rigid channel ($\Gamma = 0$): variation of the imaginary parts of the wave speed c with the wave number k for different values of thickness ratio β , interfacial tension = 0, viscosity ratio $\mu_r = 0.5$ and Reynolds number $Re = 1$.

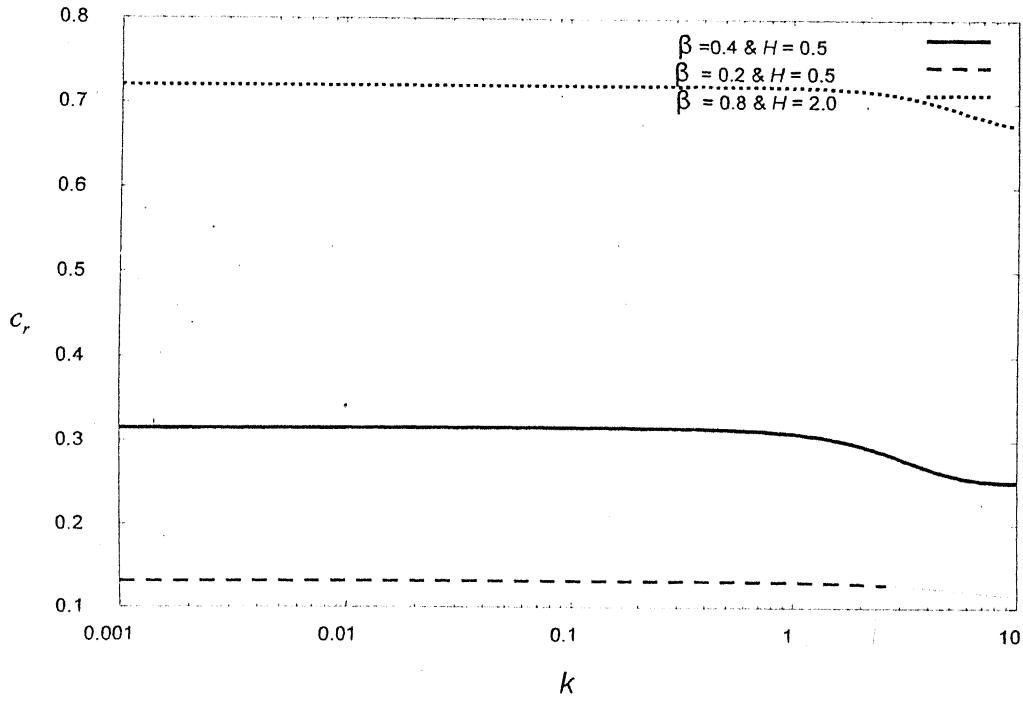


Fig. 3.5 Fluid-fluid interface instability in rigid channel ($\Gamma = 0$): variation of the real parts of the wave speed c with the wave number k for different values of thickness ratio β , interfacial tension = 0, viscosity ratio $\mu_r = 0.5$ and Reynolds number $Re = 1$.

Further Hooper and Boyd [1983] performed an asymptotic analysis for short waves and showed that short waves are unstable and surface tension has ability to stabilize the instability associated with short waves, which can be easily observed by seeing the difference between Fig 3.4 and Fig 3.6 is plot between c_r vs. k with surface tension zero thus it is unstable for all ranges of wave number similar to what Yih and Hooper & Boyd found in their work. But in Fig 3.6 flow is unstable for small wave number and gets stabilized for long wave number due to presence of surface tension as mentioned by Hooper and Boyd [1983]. Although these authors talk of short and long wave number, the most unstable mode has finite wave numbers as observed in Fig. 3.4 and 3.6. Thus we must need full a numerical solution to analyze the stability for whole range of wave number including intermediate wave numbers.

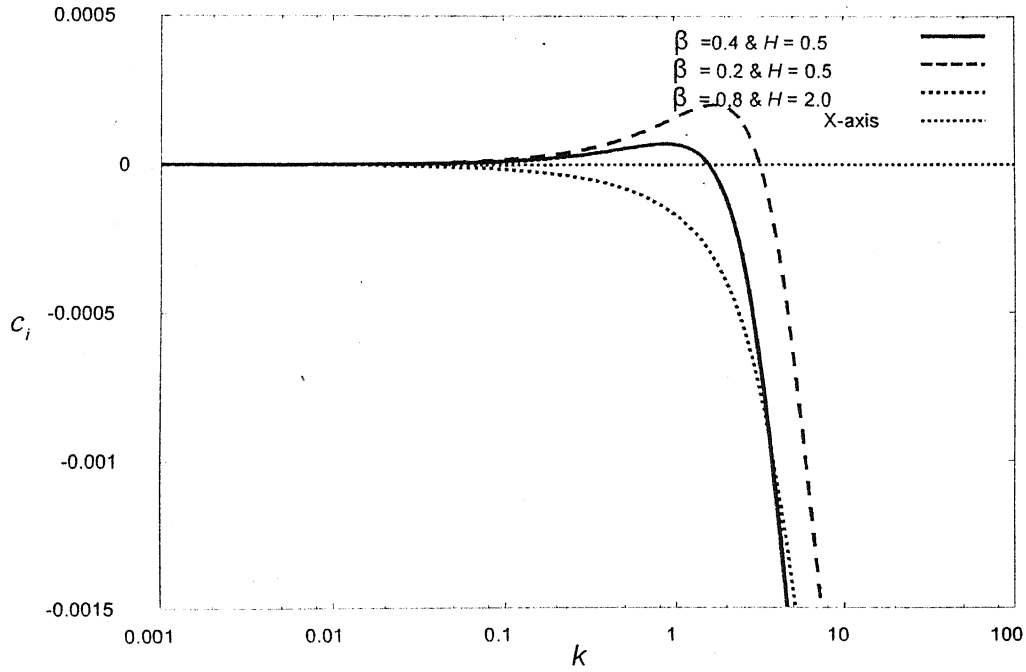


Fig. 3.6 Fluid-fluid interface instability in rigid channel ($\Gamma = 0$): variation of c_i with k for different value of β , interfacial tension = 0.01, $\mu_r = 0.5$ and $Re = 1$.

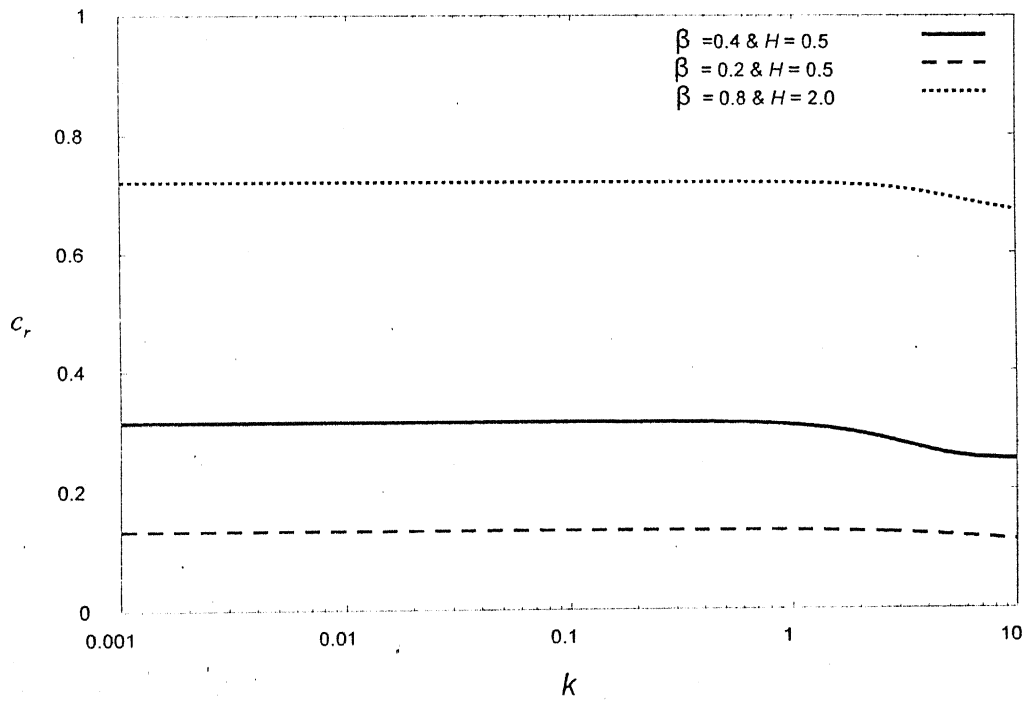


Fig. 3.7 Fluid-fluid interface instability in rigid channel ($\Gamma = 0$): variation of c_r with k for different value of β , interfacial tension = 0.01, $\mu_r = 0.5$ and $Re = 1$.

गुरुपुष्पलाल काशीनाथ केलकर पुस्तकालय
भारतीय प्रौद्योगिकी संस्थान कानपुर
अवधि क्र० A... 148883

3.4.2 Asymptotic results

Before proceeding further we want to summarize the asymptotic results (V. Shankar, personal communication) showing the effect of Γ on the stability of our system of flow for the case of long waves where analytical results are available. Analytical results for the long waves are obtained as follows:

$$c = c_0 + i k c_1, \quad (a)$$

Where c_0 is a real number does not depends on Γ & Re and c_1 is also a real quantity know as first correction factor which is responsible for the stability and instability of flow is a function of Γ as well as Re (*when $c_1 > 0$ flow is unstable and $c_1 < 0$ flow is stable*). We first had presented an analytical results for interfacial tension = 0.1, $\mu_r = 0.5$ and $H = 0.5$ as in equation (b) for the case when two-layer flow is unstable in rigid channel and deformable wall has stabilizing effect. This can be observed by equation (b) that $\Gamma = \mu U^*/G R$ always be non-negative hence it has always stabilizing effect other than the case of rigid wall for which Γ is zero (elasticity of the solid layer is very high).

$$c = 0.767023 + i (-0.00527865 * \Gamma + 0.000124662 * Re) \quad (b)$$

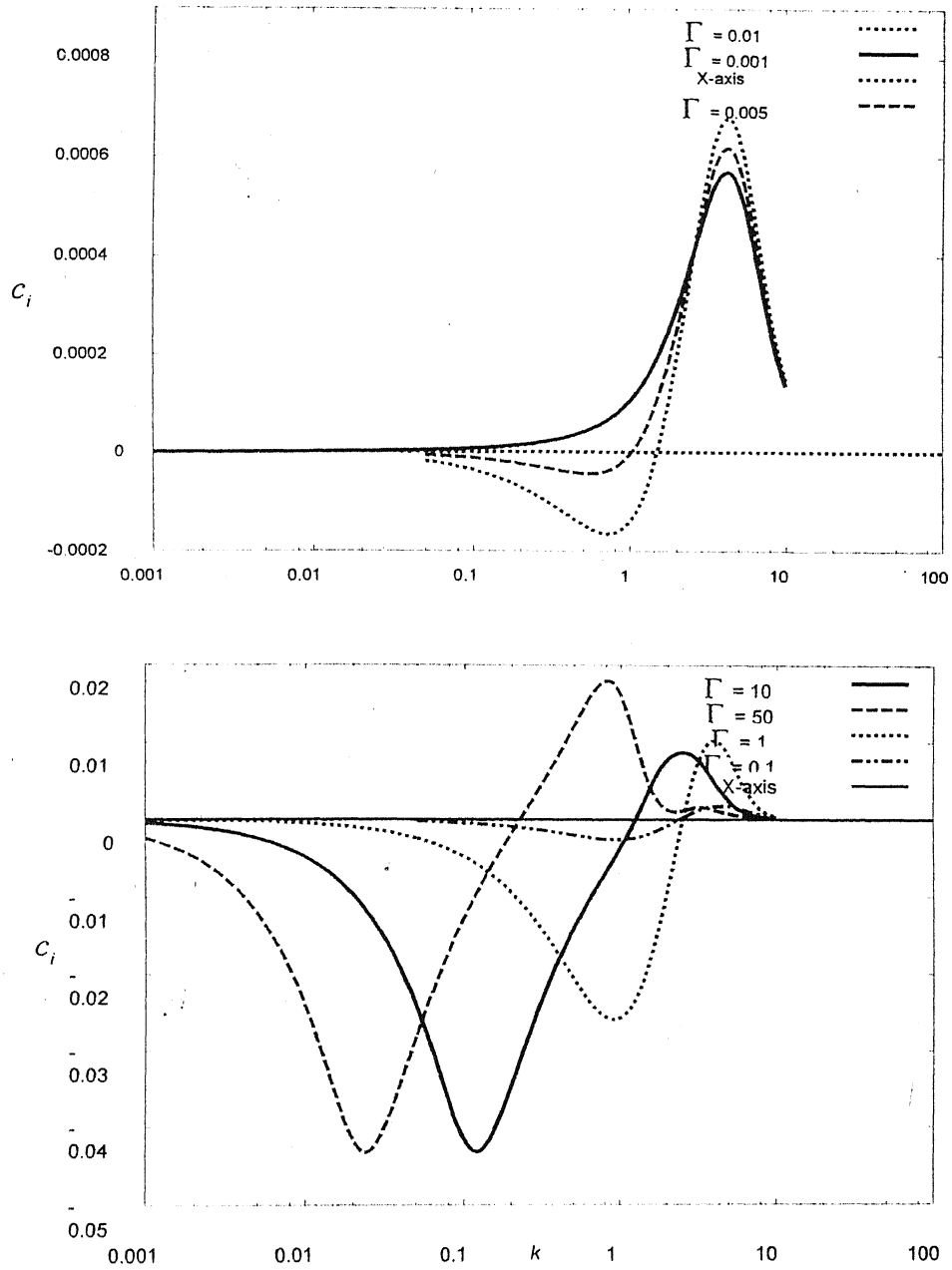
Again we would like to discuss an analytical result for the case when two-layer flow in a rigid channel is stable and deformable wall has destabilizing effect. This is possible for the case of thin layer effect (i.e. thinner fluid has higher viscosity). For obtaining analytical results for this case we used the variable quantities $\beta = 0.8$, interfacial tension = 0.0, $\mu_r = 0.25$ and $H = 2.0$ and will able to get expression given in equation (c). From equation (c) it is obvious that for this case Γ has a destabilizing effect and flow remains stable for the particular value of Γ know as transitional value but if we will further increase the value of Γ than our system becomes unstable as suggested by equation (c). In proceeding parts of the thesis we intended to examine the effect of deformable wall on the stability of flow for moderate and high values of wave numbers.

$$c = 0.720214 + i (0.44450 * \Gamma - 0.000155329 * Re) \quad (c)$$

3.4.3 Fluid flow past a rigid wall is unstable and deformable wall has stabilizing effect ($\mu_r > 1$ & $\beta > 1/2$ or $\mu_r < 1$ & $\beta < 1/2$)

In this section we intended to analyze the arrangement of the two-layer flows, which is unstable in rigid channel and deformable wall has stabilizing effect. From Fig 3.8 it is clear that it is possible to stabilize low wave number instability by changing rigid wall to deformable wall as presented in equation (b). This can be explained by considering the interference between two interfacial perturbations namely fluid-fluid and fluid deformable wall. Further it is clear that it is not possible to stabilize short wave length instability irrespective of Γ value. This is because; there is no possibility of coupling between two interfacial perturbations for short wave lengths (high wave number perturbations) as they are confined near the interface only. Other thing we can observe from the same Fig. is first stability increases as elasticity of deformable wall (Γ value) increases but after certain limiting value of Γ , if we further increase the value of Γ flow becomes unstable. But we know from the Hooper and Boyd [1983] asymptotic analysis that short wave (long wave number) instability could be stabilized by surface tension. Thus we plot c_i vs. k as in Fig 3.6 with non dimensional surface tension 0.01 keeping all other parameters same. Then we find that for sufficiently high value of Γ and given value of surface tension, the high wave number modes are stabilized but some of the intermediate wave numbers are still unstable and very low Γ value does not have capability to stabilize the flow for all wave number. We further increased the value of surface tension to 0.05 and plotted in Fig. 3.8. From these Figs it is clear that for complete stability, we need to choose combinations of intermediate value of Γ and sufficiently high value of surface tension as presented in Fig 3.6 and 3.8. But the flow is still not completely stable for very low as well as very high value of Γ (very high or very low value of elasticity constant of deformable wall). Thus this needs further explanation why even a very high value of Γ is not able to stabilize flow as compared to intermediate values where flow is stable. For this purpose it is useful to plot neutral stability curve for Γ vs. k . Thus we plotted Γ vs. k in Fig. 3.17-3.24 by which it is clear that there are two modes of instability for the two layers Couette flow past a deformable wall. First one is associated with fluid-fluid interface which we call Mode-1 and other

and other one is associated with fluid-deformable wall interface which we named as Mode-2. This will be discussed in 3.4.4.



(a) For low value of Γ : c_i vs. k (above) (b) For high value of Γ : c_i vs. k (below)

Fig. 3.8 Variation of c_i with k for different value of Γ , $\beta = 0.4$, interfacial tension = 0.0, $\mu_r = 0.5$, $H = 0.5$ and $Re = 1$.

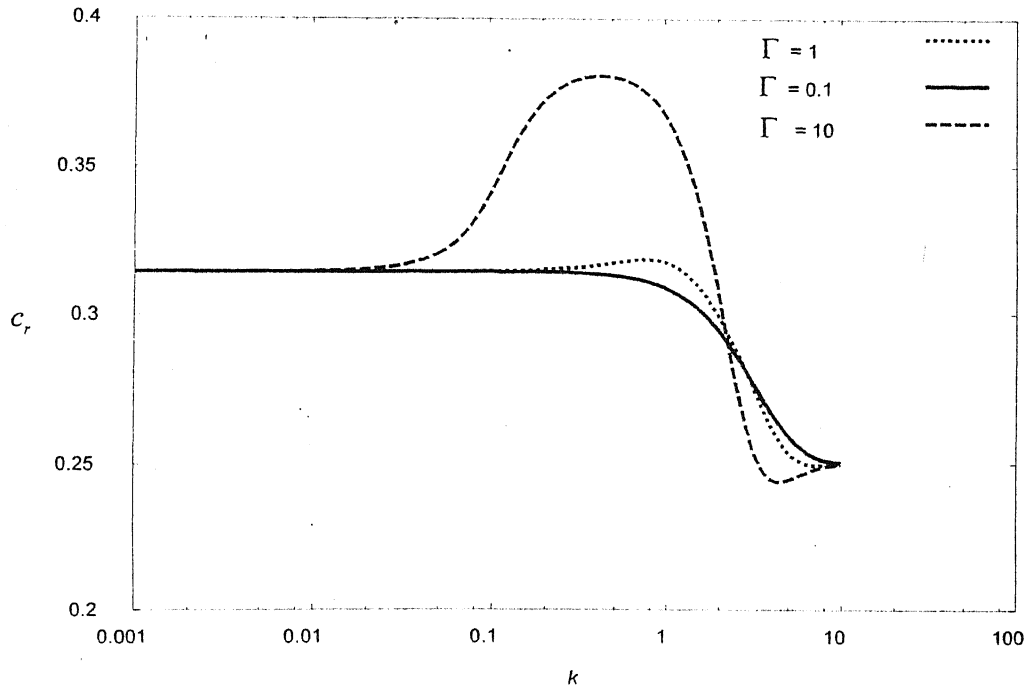
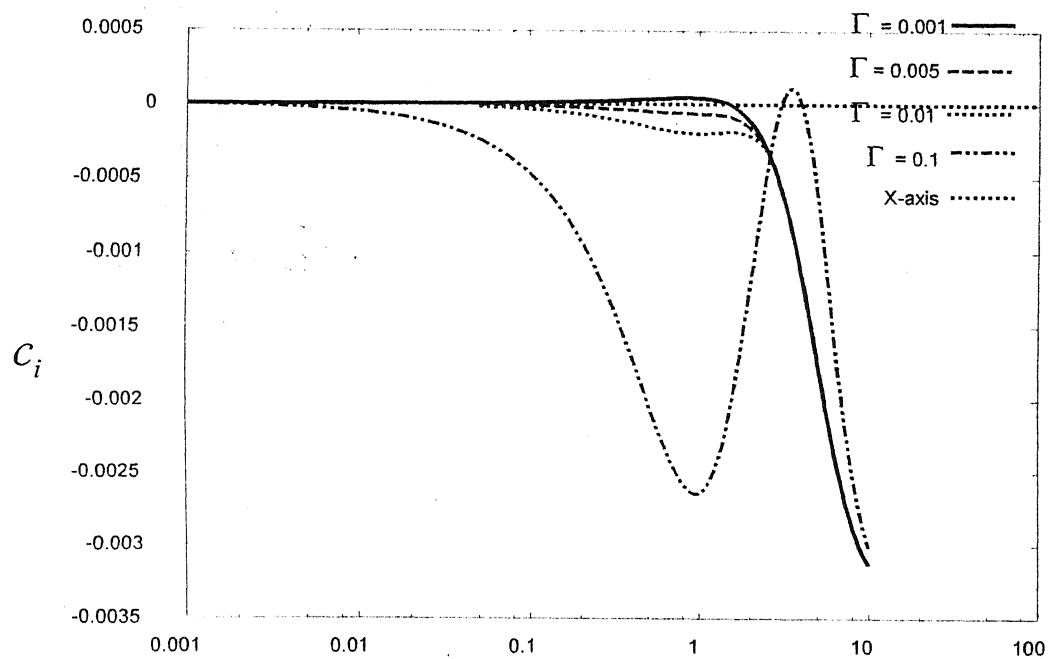
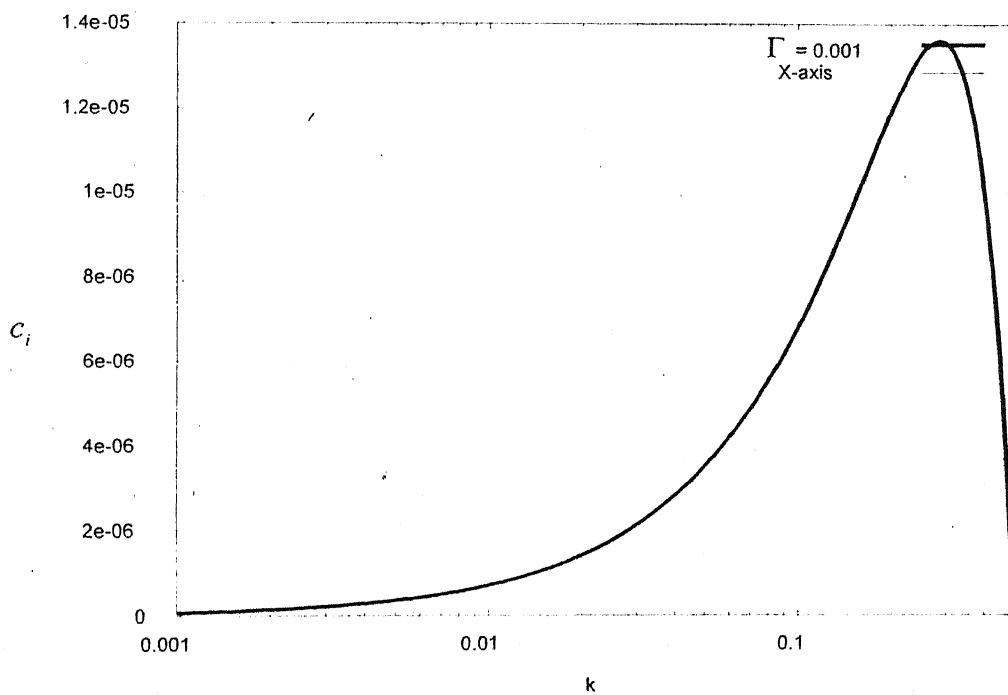


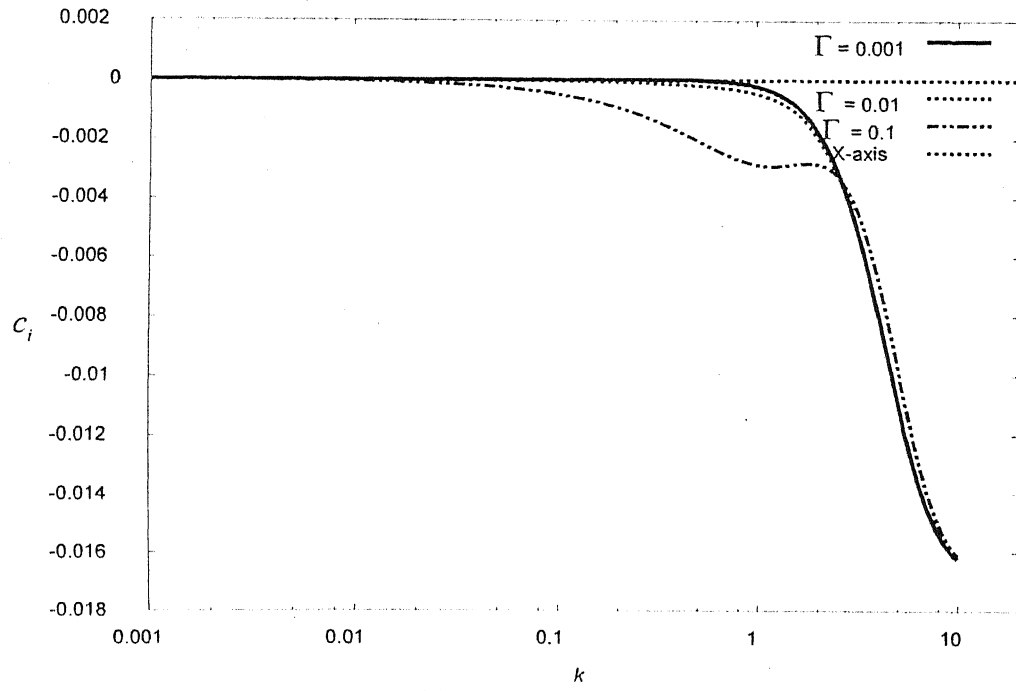
Fig. 3.9 Variation of c_r with k for different value of Γ , $\beta = 0.4$, interfacial tension = 0.0, $\mu_r = 0.5$, $H = 0.5$ and $Re = 1$.



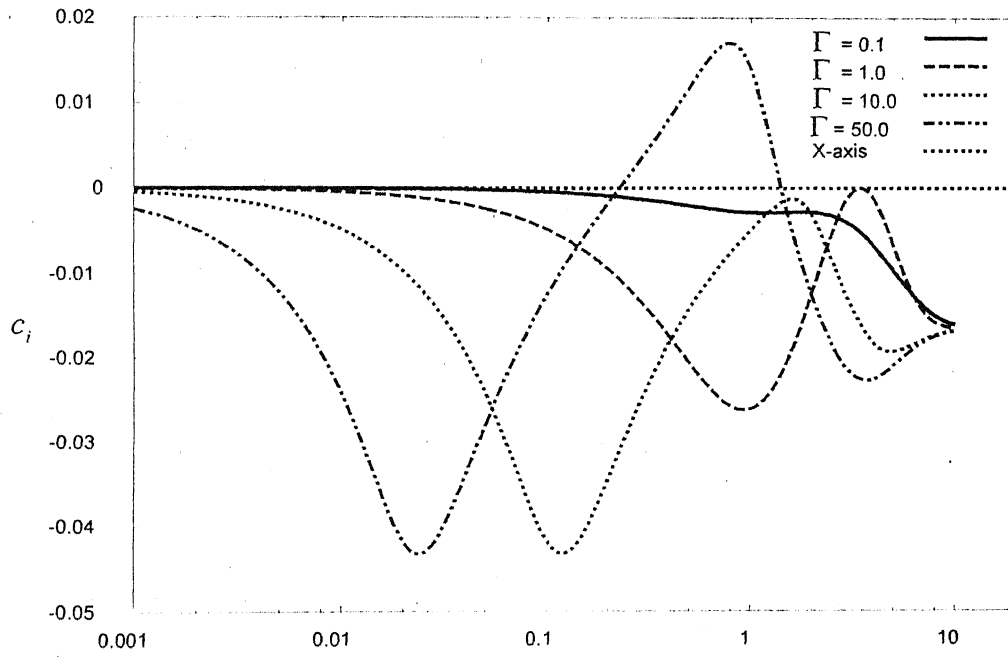
(a) For low value of Γ : c_i vs. k



(b) Zoom of the above curve for low values of k and $\Gamma = 0.001$



(a) For low value of Γ : c_i vs. k



(b) For high value of Γ : c_i vs. k

Fig. 3.12 Variation of c_i with k for different value of Γ , $\beta = 0.4$, interfacial tension = 0.05, $\mu_r = 0.5$, $H = 0.5$ and $Re = 1$.

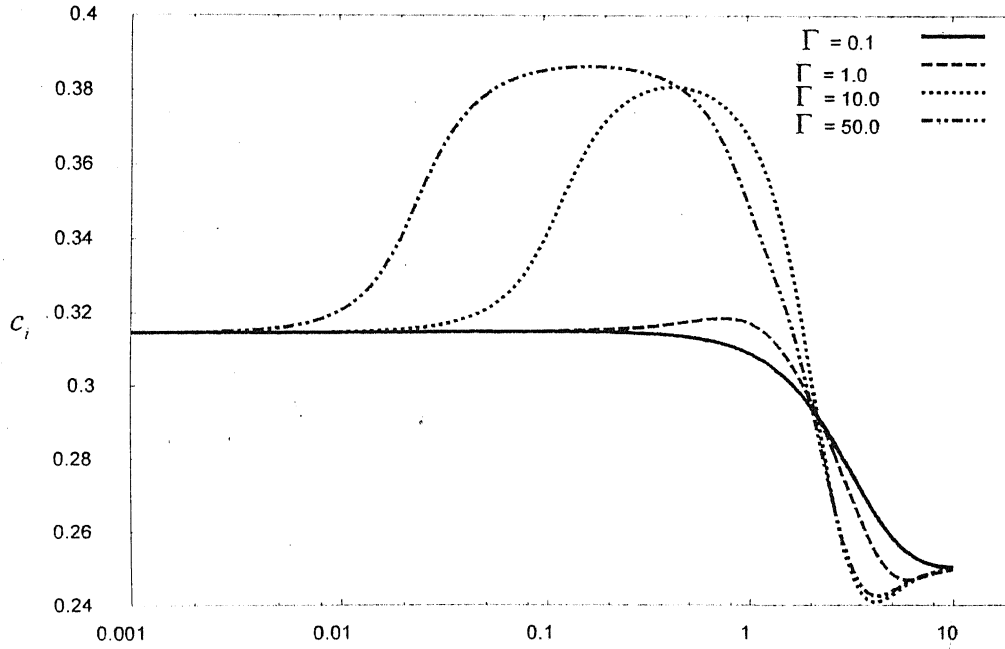
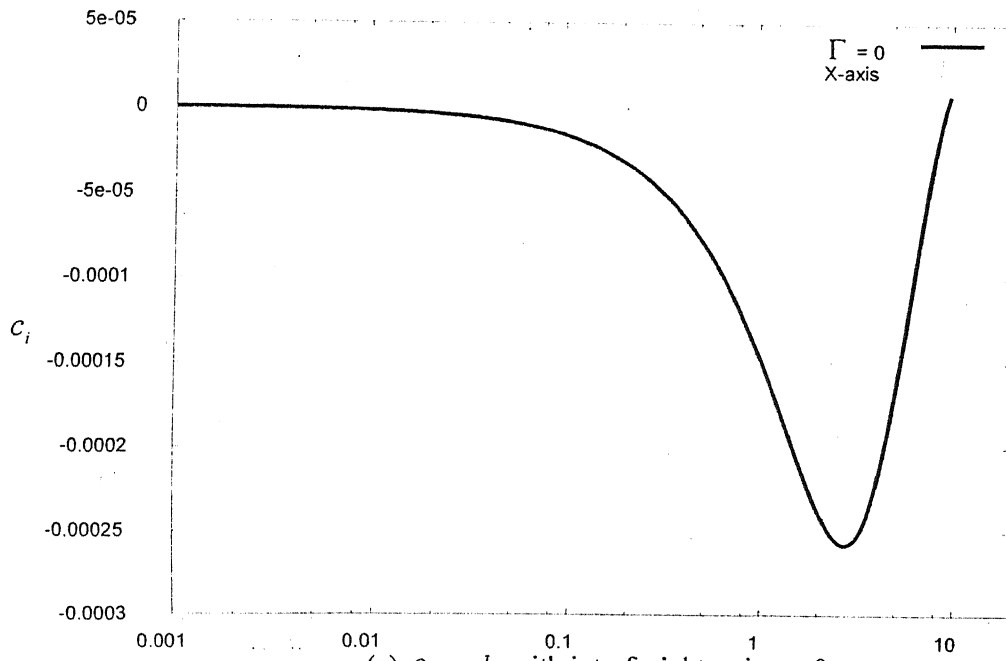


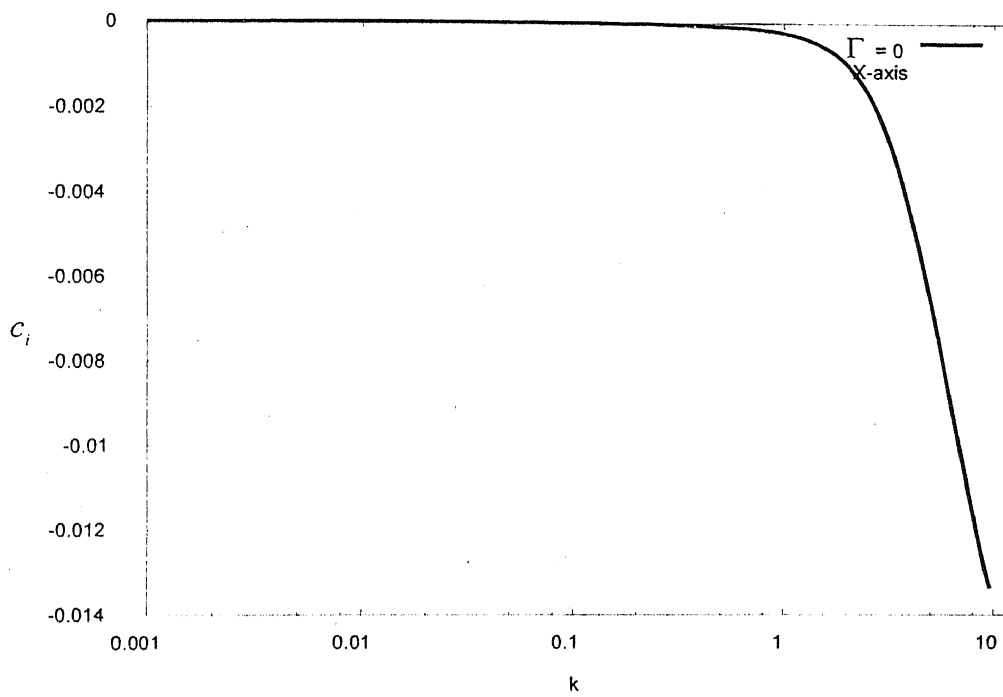
Fig. 3.13 Variation of c_i with k for different value of Γ , $\beta = 0.4$, interfacial tension = 0.05, $\mu_r = 0.5$, $H = 0.5$ and $Re = 1$.

3.4.4 Fluid flow past a rigid wall is stable and deformable wall has destabilizing effect ($\mu_r > 1$ & $\beta < 1/2$ or $\mu_r < 1$ & $\beta > 1/2$)

In this section we will discuss those cases where two-layer Couette flow past a rigid wall is stable (known as the thin layer effect) and deformable wall causes destabilization in the low k limit consistent to the equation (c). As shown in Fig. 3.14(a) flow is stable for $\Gamma = 0$ except very high wave number where it becomes unstable but from Fig. 3.14(b) it is clear that if we put non zero value of surface tension it becomes stable for all values of k . But further from Fig. 3.15 reveal that low wave number perturbations are unstable when Γ value is non-zero and extent of instability further increases as Γ value increases. But for higher wave number perturbation Γ has no effect on the stability of flow as the perturbations are confined near the fluid-fluid interface. Again in Fig. 3.15, we plotted c_i vs. k which reveals that presence of surface tension would stabilize high wave number perturbation but small wave number perturbation can not any effect of surface tension and it is unstable for non-zero value of Γ .

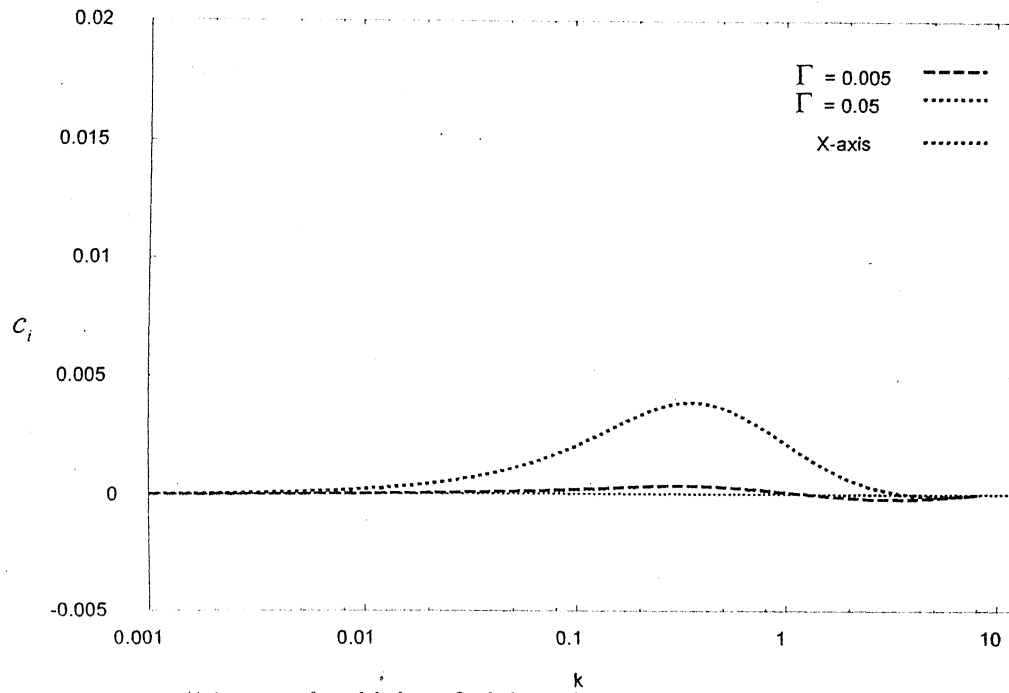


(a) c_i vs. k : with interfacial tension = 0.

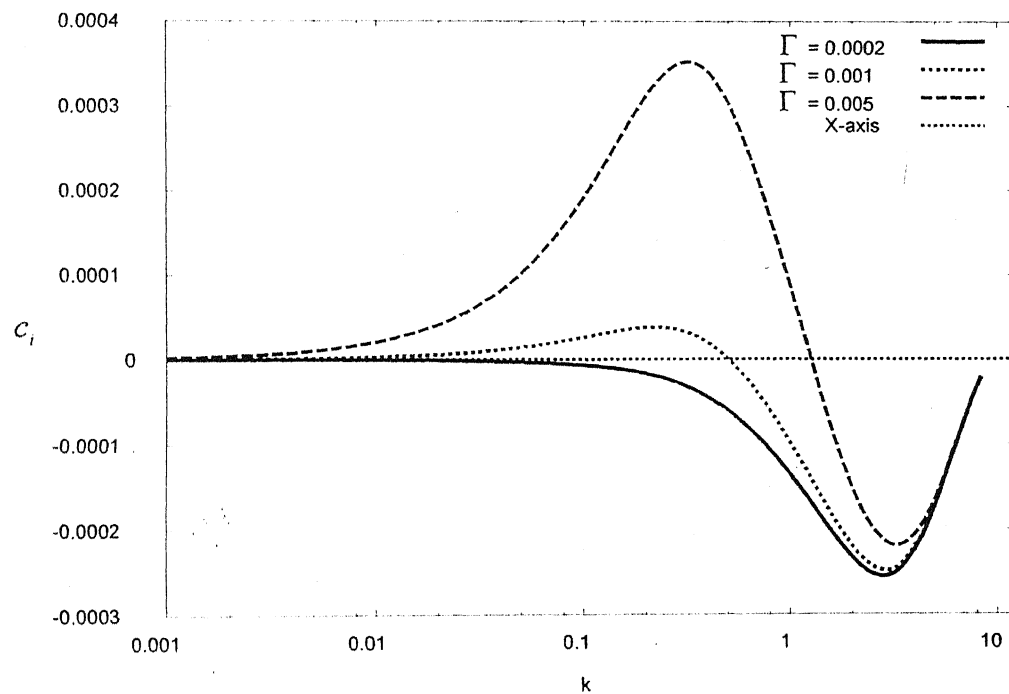


(b) c_i vs. k : with interfacial tension = 0.05.

Fig. 3.14 Variation of c_i vs. k for $\Gamma = 0.0$, $\beta = 0.8$, $\mu_r = 0.5$, $H = 2.0$ and $Re = 1$.

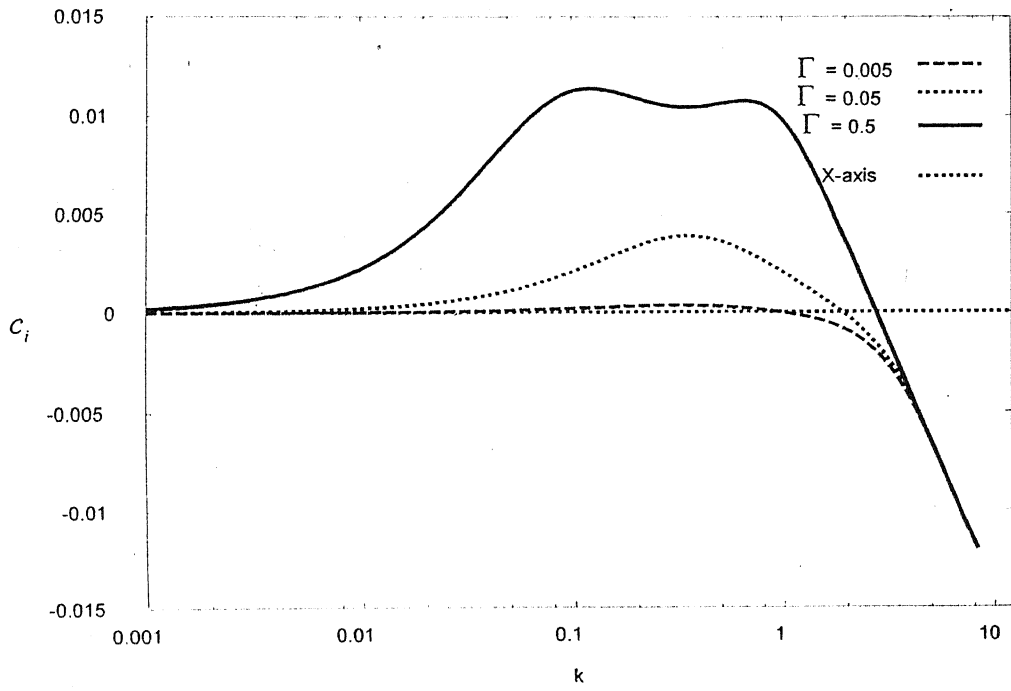


(a) c_i vs. k : with interfacial tension = 0.0 and different values of Γ .

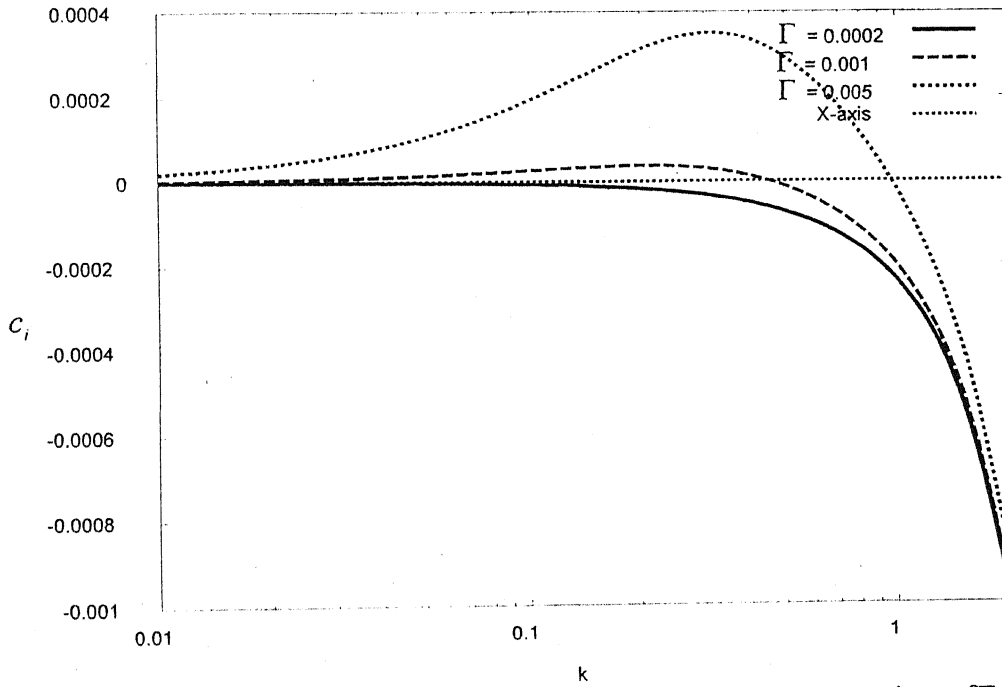


(b) c_i vs. k : with interfacial tension = 0.0 and different lower values of Γ .

Fig. 3.15 Variation of c_i vs. k for different values of Γ , $\beta = 0.8$, interfacial tension = 0.0, $\mu_r = 0.5$, $H = 2.0$ and $Re = 1$.



(a) c_i vs. k : with interfacial tension = 0.05 and different values of Γ .



(b) c_i vs. k : with interfacial tension = 0.05 and different lower values of Γ .

Fig. 3.16 Variation of c_i vs. k for different values of Γ , $\beta = 0.8$, interfacial tension = 0.05, $\mu_r = 0.5$, $H = 2.0$ and $Re = 1$.

3.4.5 Neutral stability curves (Γ vs. k)

In this section, we intended to find the range of Γ and surface tension where our system of flow is stable. From fig 3.17, which is a neutral stability curve for parameter $\beta = 0.4$, interfacial tension = 0.00, $\mu_r = 0.5$, $H = 0.5$ and $Re = 1$, it is clear that flow is unstable for any value of Γ . It is expected since without surface tension we can not stabilize short wave as discussed above. Further in fig 3.17-3.24 we have two mode of instability first mode is associated with fluid-fluid interface instability, which requires a minimum value of Γ to stabilize this mode and if we choose more than this value then mode-1 is always stable. That also reveals the reason for instability in fig. 3.9 when we choose gamma 0.001 which is lower than the require value to stabilize mode-1. Further the upper curve corresponds to mode-2 i.e. fluid-deformable wall instability, which is stable up to a maximum value of Γ beyond that flow become unstable. That's why when

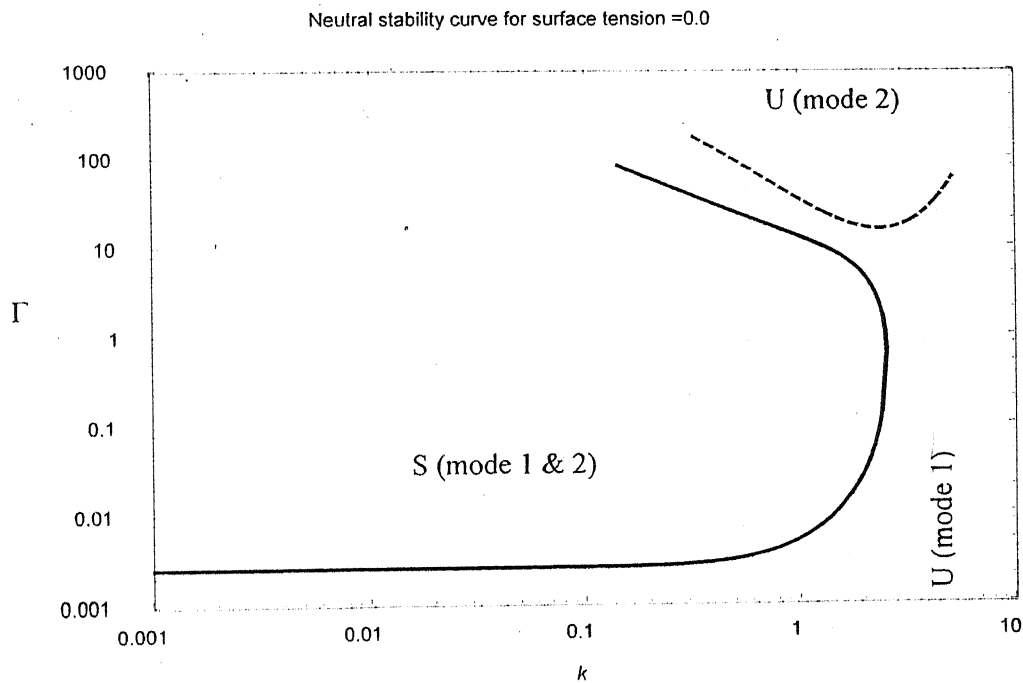


Fig. 3.17 Neutral stability curves (Γ vs. k) for fluid-fluid interfacial mode (Model 1) and Fluid- deformable wall mode (Mode 2) for parameter $\beta = 0.4$, interfacial tension = 0.00, $\mu_r = 0.5$, $H = 0.5$ and $Re = 1$.

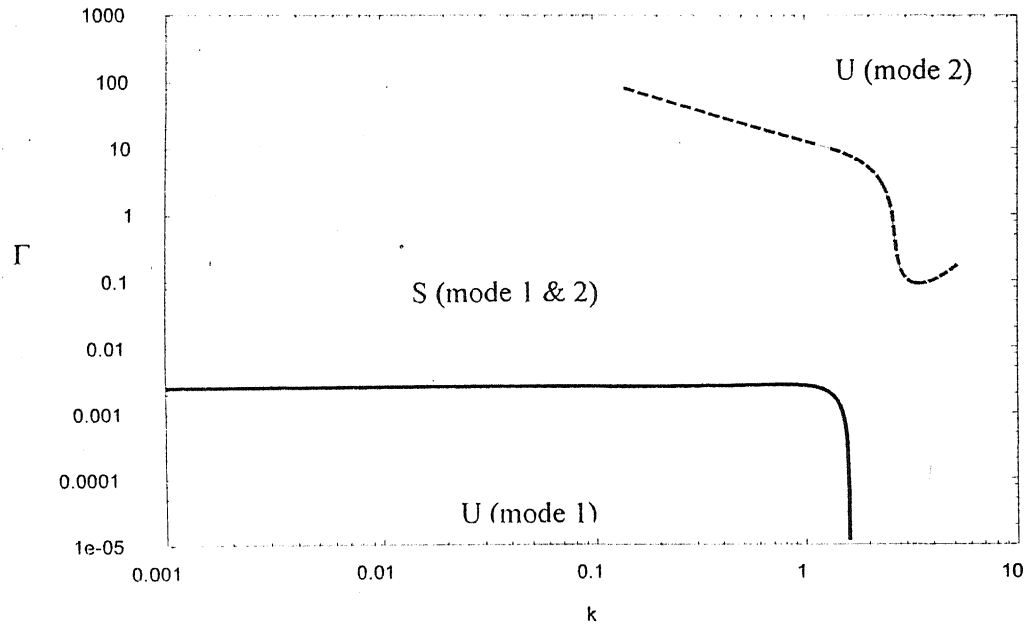


Fig. 3.18 Neutral stability curves (Γ vs. k) for Model 1 and Mode 2 for parameter $\beta = 0.4$, interfacial tension = 0.01, $\mu_r = 0.5$, $H = 0.5$ and $Re = 1$.

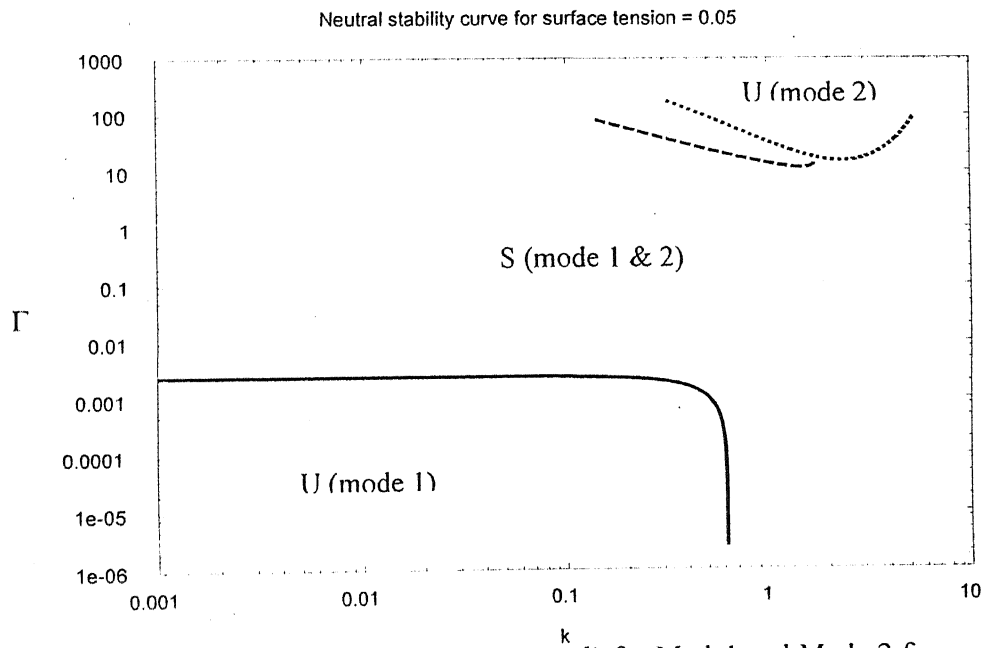


Fig. 3.19 Neutral stability curves (Γ vs. k) for Model 1 and Mode 2 for parameter $\beta = 0.4$, interfacial tension = 0.05, $\mu_r = 0.5$, $H = 0.5$ and $Re = 1$.

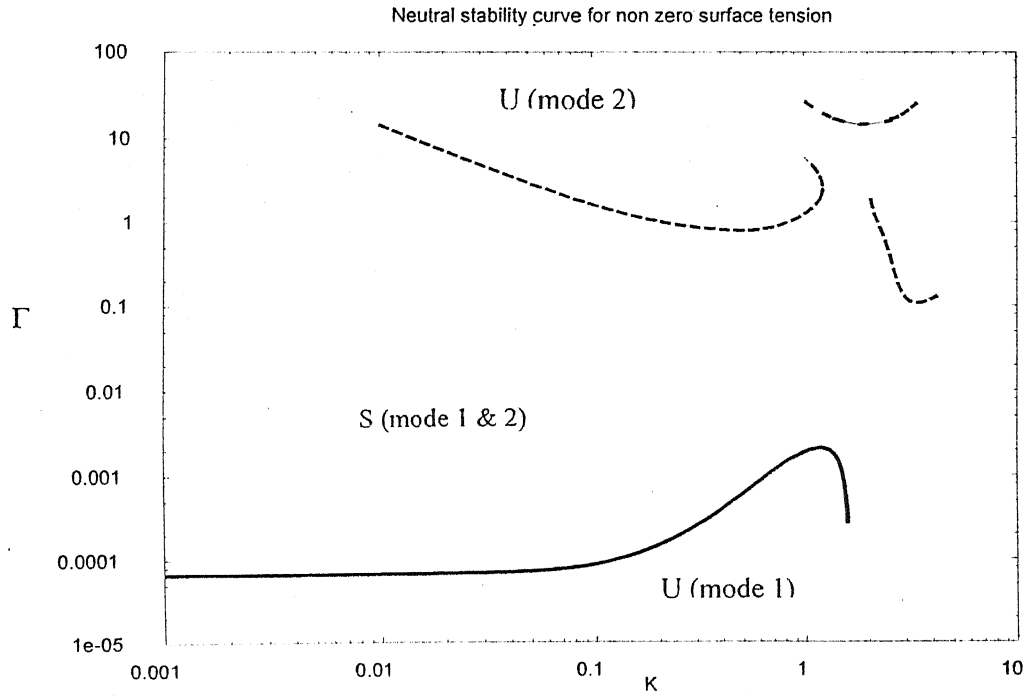


Fig. 3.20 Neutral stability curves (Γ vs. k) for Mode1 and Mode 2 for parameter $\beta = 0.4$, interfacial tension = 0.01, $\mu_r = 0.5$, $H = 4$ and $Re = 1$.

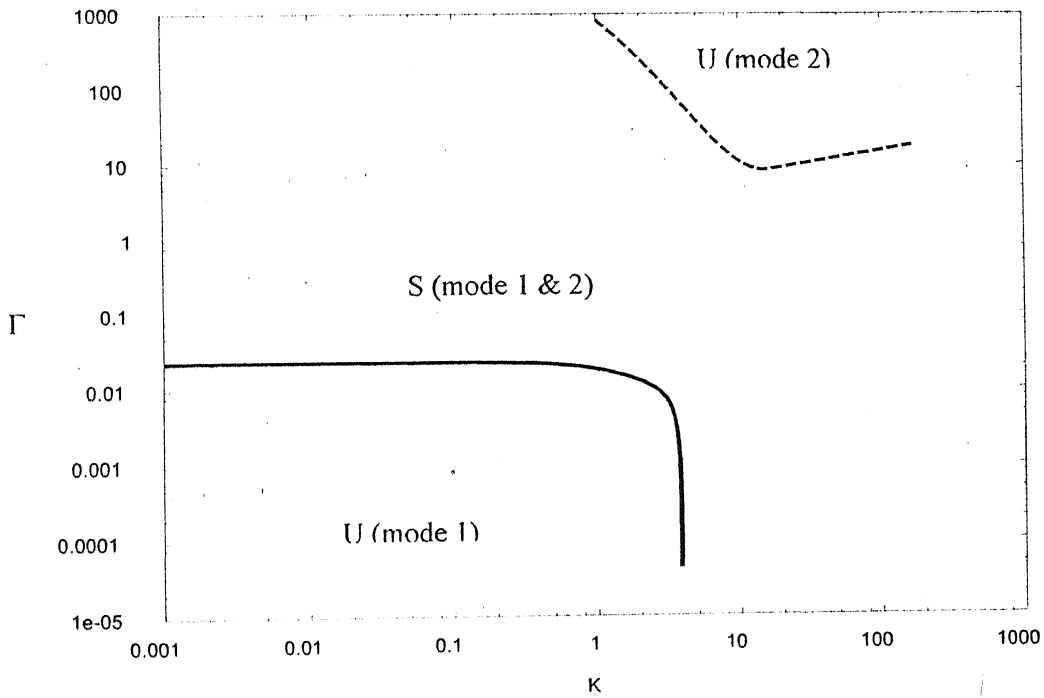


Fig. 3.21 Neutral stability curves (Γ vs. k) for Mode1 and Mode 2 for parameter $\beta = 0.6$, interfacial tension = 0.01, $\mu_r = 2.0$, $H = 0.1$ and $Re = 1$.

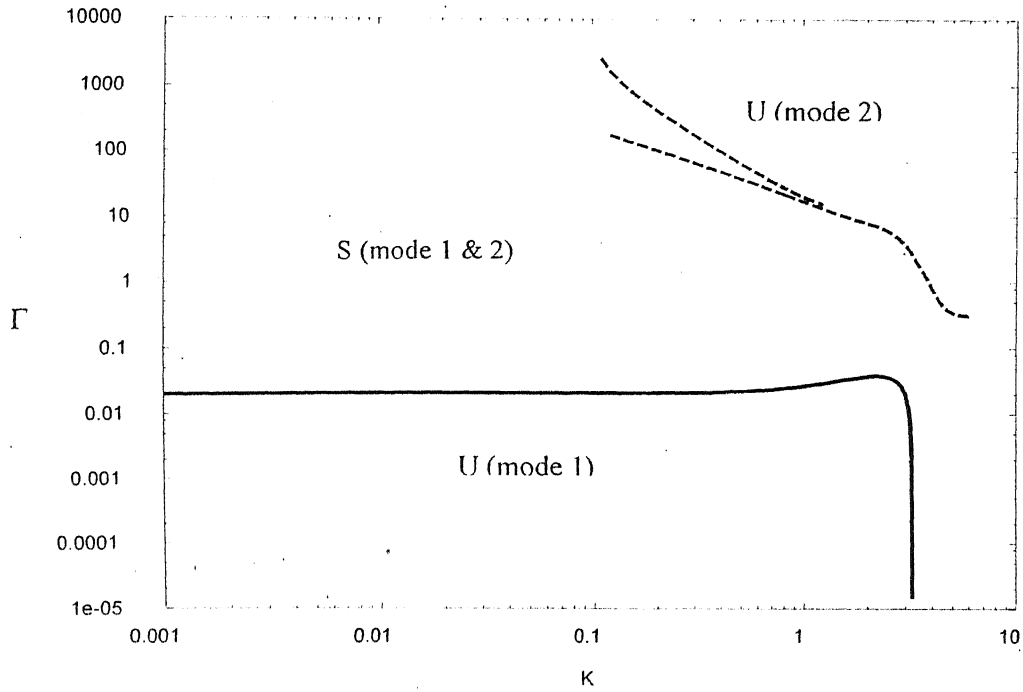


Fig. 3.22 Neutral stability curves (Γ vs. k) for Model 1 and Mode 2 for parameter $\beta = 0.2$, interfacial tension = 0.01, $\mu_r = 0.5$, $H = 0.5$ and $Re = 1$.

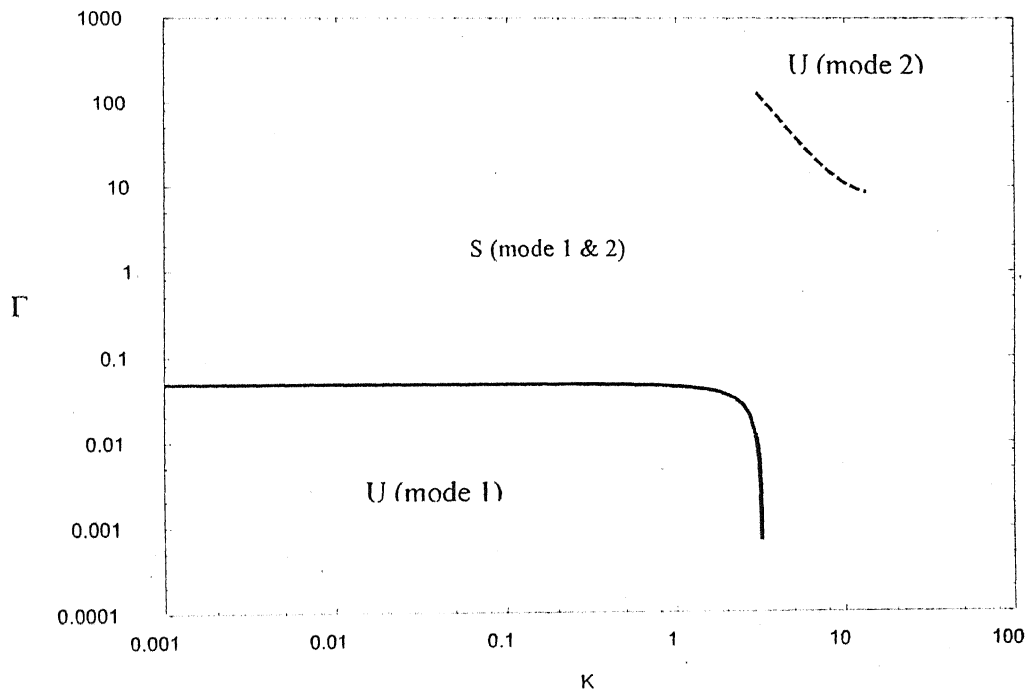


Fig. 3.23 Neutral stability curves (Γ vs. k) for Model 1 and Mode 2 for parameter $\beta = 0.8$, interfacial tension = 0.01, $\mu_r = 2.0$, $H = 0.1$ and $Re = 1$.

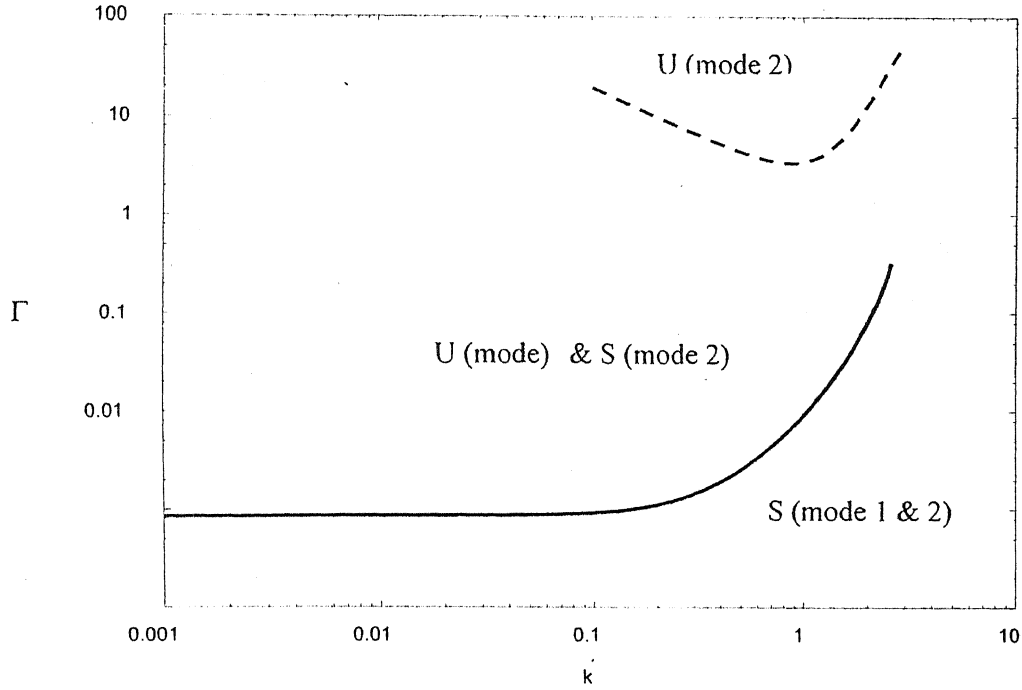


Fig. 3.24 Neutral stability curves (Γ vs. k) for Model 1 and Mode 2 for parameter $\beta = 0.8$, interfacial tension = 0.01, $\mu_r = 0.25$, $H = 2.0$ and $Re = 1$.

we plotted c_i vs. k then stability of fluid firstly increases with Γ but after a maximum Γ limit flow becomes unstable. It is clear that high value of Γ certainly has ability to stabilize fluid-fluid interface instability but mean time it destabilizes fluid-deformable wall instability. Thus we need to choose an intermediate value of Γ and surface tension for which both the modes become stable.

Above explanation is only valid for the case where flow is unstable in a rigid channel and deformable solid wall has stabilizing effect. Now we like to explain the case when flow is stable in rigid channel and we intended to destabilize with the help of deformable solid wall. From Fig 3.24 it is clear that low wave number perturbations at the fluid-fluid interface are unstable if we increase the Γ value beyond the maximum limit and Fig 3.14 and 3.15 reveals that surface tension has stabilizing effect on the short waves.

3.4.6 Effect of various parameters on the stability

(a) Effect of viscosity ratio on the stability of flow system:

First of all we want to know the effect of viscosity ratio (μ_r) on the stability of two-layer fluid flow past a deformable wall for that purpose we plotted Γ vs. k in Fig. 3.25, which reveals that as the value of μ_r increases system needs lesser value of Γ for flow to become unstable. We can explain this observation by considering that the non-dimensional velocity gradient at the solid-deformable wall interface, which is given by $\mu_r / (1 + \beta (\mu_r - 1))$, and for a given value of Γ , this quantity increases with increase in ratio of viscosities, thus having a destabilizing effect on the fluid-solid interfacial mode. Similarly, for decreasing ratio of viscosities, the non-dimensional velocity gradient at the fluid-solid interface decreases, thus having a stabilizing effect.

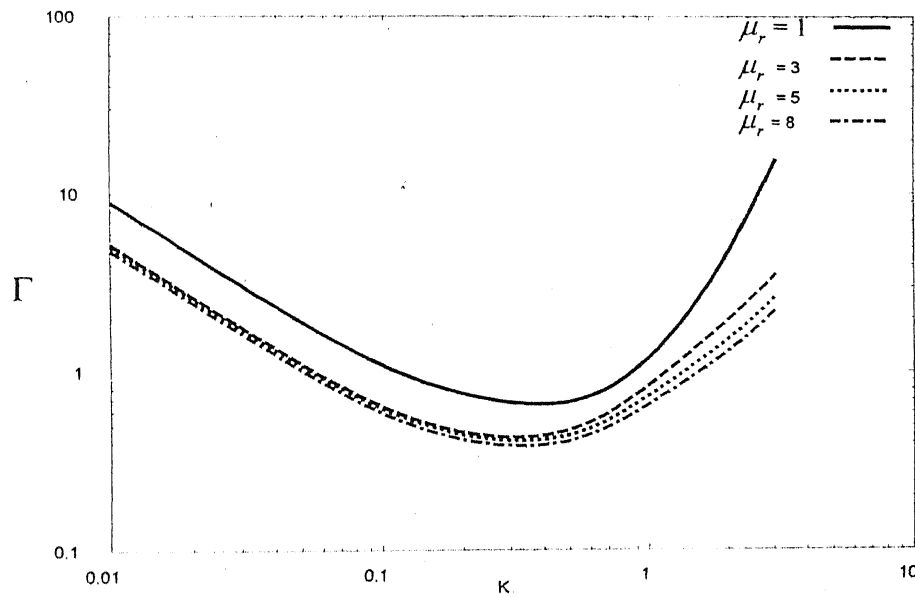


Fig. 3.25 Neutral stability curves (Γ vs. k) for Mode 2 for the parameter $\beta = 0.4$, interfacial tension = 0.0, $H = 5.0$ and $Re = 1$.

(b). Effect of density of upper fluid on the stability of system of flow:

Although density difference itself has instability modes (density stratification modes) but here we intended to examine the effect of density difference on stability of fluid-fluid interface. From Fig. 3.28 it is clear that as density of upper fluid increases as compare to density of lower fluid, flow become more and more unstable.

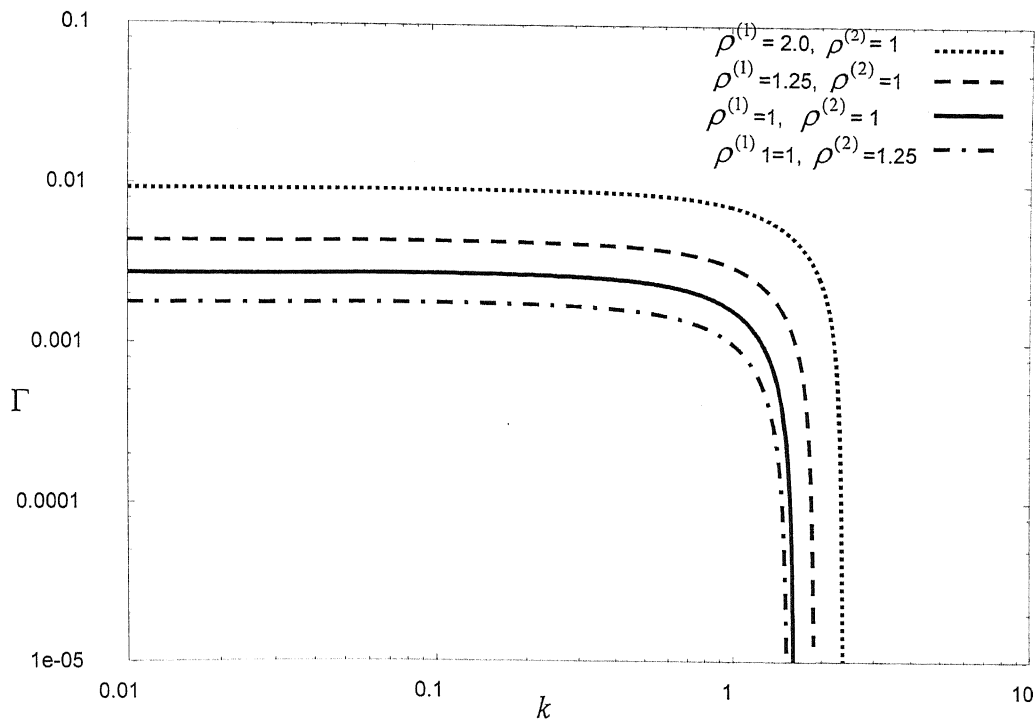


Fig. 3.26 Variation of Γ vs. k for different values of densities ratio, $\beta = 0.6$, interfacial tension = 0.01, $\mu_r = 0.5$, $H = 2.0$ and $Re = 1$.

(c) Effect of height of deformable wall on the stability of system of flow:

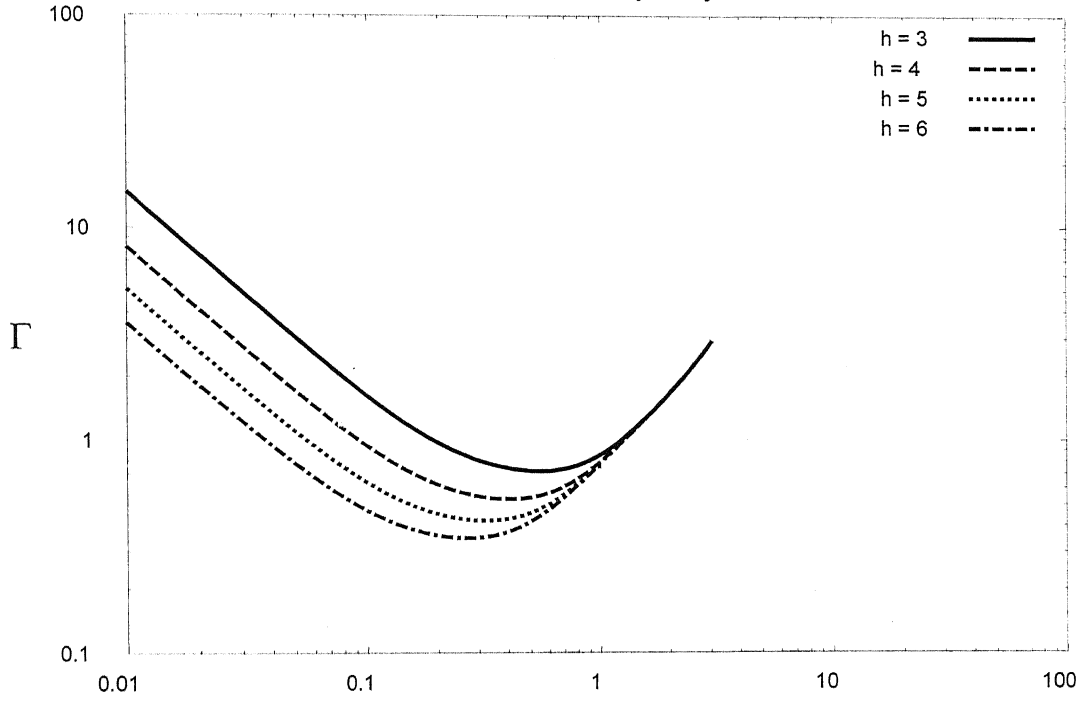


Fig. 3.27 Neutral stability curves (Γ vs. k) for Mode 2 for the parameter $\beta = 0.4$, interfacial tension = 0.0, $H = 5.0$ and $Re = 1$.

3.5 Conclusion and future work

We have shown in this chapter that the deformable wall plays an important role in the stability of two-layer fluid flows. This can be explained on the basis of coupling between two interfacial perturbations. But it has certain limitations, as it is only able to affect long waves and finite waves, since coupling between two interfacial perturbations is not possible for short waves. This is because, the velocity perturbations are confined near the interfaces only. Further short waves are stabilized by the interfacial tension between the two fluids.

Here we intended to analyze the instability due to viscosity stratification. For this purpose we first considered the case where the interface is unstable in a rigid channel and deformable wall has stabilizing effect. But we had shown that it is not possible to stabilize the two-layer flow by using any deformable wall rather it depends of the coefficient of elasticity of deformable wall. We found a region of Γ for which our system of flow becomes stable. But if we have a system such that the Γ value is less than of minimum transition value Γ then fluid-fluid interface becomes unstable and simultaneously when we have Γ value more than maximum transition value then fluid-deformable wall interface becomes unstable. Next we consider a case where two-layer flows are stable (thin layer effect) and deformable wall has destabilizing effect. Similar to the above case in this case also there is a region of Γ which deformable wall is able to destabilize the system of flow. Finally, we had shown the effect of various parameters on the stability of fluid flow. For this, first we choose a case in which fluid-fluid interface is stable and fluid-deformable wall stability increases as μ_r increases. Then we had shown that as Reynolds increases and height of deformable wall have destabilizing and stabilizing effect as their values increases. Finally we had shown that the density difference also has effect on the both fluid-fluid mode as well as fluid deformable wall modes.

Although we talk about the coupling between two interfacial perturbations, we never got any information that how actually they are coupled with each other for that purpose we must need to know the perturbation growth for this system of flow. Other than that in present analysis we predicted stability and instability based on linear stability

analysis but we can further confirm the results by doing non-linear stability analysis. We also showed that density difference has effect on instability caused by viscosity stratifications. There is also the effect of viscosity difference on the stability caused by density stratification. In fact these things are already available in literature for rigid wall case but now it is possible to study these effects for the case of deformable wall. This present study is associated with finite thick fluid layers so if we reduce the thickness of fluid layers to the range of thin layer where vander waals force are significant. Then our analysis is also valid for the case of thin film but we have to incorporate the vander waals forces.

CHAPTER 4

Conclusion and future work

We found that Couette flow past a deformable wall has an inviscid mode, which is very important for these types of flows. If one tries to study flow past a deformable wall experimentally then one will encounter inviscid modes, because they require lower value of Γ . Further we confirmed that Poiseuille flow also have both wall modes, as well as inviscid modes. However there is a difference between these two cases. In Couette flow one of the wall modes captures the inviscid mode when we extend wall mode solution numerically. But in Poiseuille flow, instead of wall modes, zero Reynolds number modes capture the inviscid mode. In case of Poiseuille flow, we got the same scaling as Couette flow but velocity field distributions have different nature instead of expected critical layer for inviscid modes. The present study needs further investigation of velocity distribution in the case of Poiseuille flow. Other than this, our study numerically predicted inviscid modes for both the plane Couette as well as plane Poiseuille flow. The prediction of inviscid modes for plane Couette flow is in stark contrast with the asymptotic prediction of Kumaran [1995], who concluded that the inviscid modes are stable in the case of plane Couette flow. Hence we further need asymptotic explanation for the inviscid cases.

We have shown in Chapter 3 that the deformable wall plays an important role in the stability of two-layer fluid flows. This can be explained on the basis of coupling between two interfacial perturbations. First we have shown that deformable wall is able to stabilize those flows, which are unstable in rigid channels. In the other case where flow is stable in rigid channel, deformable wall has destabilizing effect on the two-layer interfacial modes. Finally, even different density fluid flow can be stabilized by the deformable wall.

Although we talk about the coupling between two interfacial perturbations, we never obtained any information that how actually they are coupled with each other for that purpose we must need to know the perturbation growth for this system of flow. Other than that in present analysis we predicted stability and instability based on linear stability analysis but we can further confirm the results by doing non-linear stability analysis. We also showed that density difference has an effect on instability caused by viscosity

stratifications. There is also the effect of viscosity difference on the in the stability caused by density stratification. In fact these things are already available in literature for rigid wall case but now it is possible to study these effects for the case of deformable wall. This present study is associated with finite thick fluid layers so if we reduce the thickness of fluid layers to the range of thin layer where van der Waals force are significant. Then our analysis is also valid for the case of thin film but we have to incorporate the van der Waals forces.

Bibliography

- [1] Krindel, P. & Silberberg, A. 1979 Flow through get-walled tube. *J. colloid Interface Sci.* **71**, 39.
- [2] Karmer, M. O. 1957 Boundary-layer stabilization by distributed damping. *J. Aero. Sci.* **24**, 459.
- [3] Karmer, M. O. 1960 Boundary-layer stabilization by distributed damping. *J. Am. Soc. Naval Engrs.* **74**, 25.
- [4] V. Kumaran, Effect of fluid flow on the fluctuations at the surface of an elastic medium. *J. Chem. Phys.*, **102** , 3452 - 3460, (1995).
- [5] V. Kumaran, G. H. Fredrickson and P. Pincus, Flow induced instability at the interface between a fluid and a gel at low Reynolds number, *J. Phys. France II*, **4**, 893 - 911, (1994).
- [6] L. Srivatsan and V. Kumaran, Flow induced instability of the interface between a fluid and a gel, *J. Phys. II (France)* , **7** , 947 - 963, (1997).
- [7] V. Shankar and V. Kumaran, Stability of non - parabolic flows in a flexible tube, *J. Fluid Mech.*, **395**, 211 - 236, (1999).
- [8] V. Shankar and V. Kumaran, Stability of fluid flow in a flexible tube to nonaxisymmetric disturbances, *Journal of Fluid Mechanics*, **407**, 291-314 (2000).
- [9] C. Davies and P. W. Carpenter, Instabilities in a plane channel flow between complaint wall, *J. Fluid Mech.* **352**, 205, (1997)

- [10] V. Shankar and V. Kumaran, Stability of wall modes in fluid flow past a flexible surface, *Physics of Fluids*, **14**, 2324-2338 (2002)
- [11] V. Kumaran, Stability of fluid flow in a flexible tube at intermediate Reynolds number, *J. Fluid Mech.*, **357**, 123 - 140, (1998).
- [12] V. Kumaran and R.Muralikrishnan, Spontaneous growth of fluctuations in the viscous flow of a fluid past a soft interface, *Phys. Rev. Lett.* **84**, 3310 (2000).
- [13] R. Muralikrishnan and V. Kumaran, Experimental study of the instability of viscous flow past a flexible surface, *Phys. Fluids*. **14**, 775 (2002).
- [14] C. S. Yih, Instability due to viscosity stratification, *J. Fluid. Mech.* **27**, 337 (1967).
- [15] D. Joseph and Y. Renardy, Fundamentals of Two-Fluid Dynamics: Part 1, Mathematical theory and applications, (*Springer-Verlag, New York*, 1993).
- [16] A. P. Hooper and W. G. C. Boyd, Shear flow instability at the interface between two viscous fluids, *J. Fluid. Mech.* **128**, 507 (1984).
- [17] C.-H. Li, Instability of three-layer viscous stratified flow, *Phys. Fluids*. **12**, 2473 (1969).
- [18] P. Drazin and W. Reid, Hydrodynamic Stability (*Cambridge University Press, Cambridge*, 1981).